Bipolar Junction Transistors (BJTs)

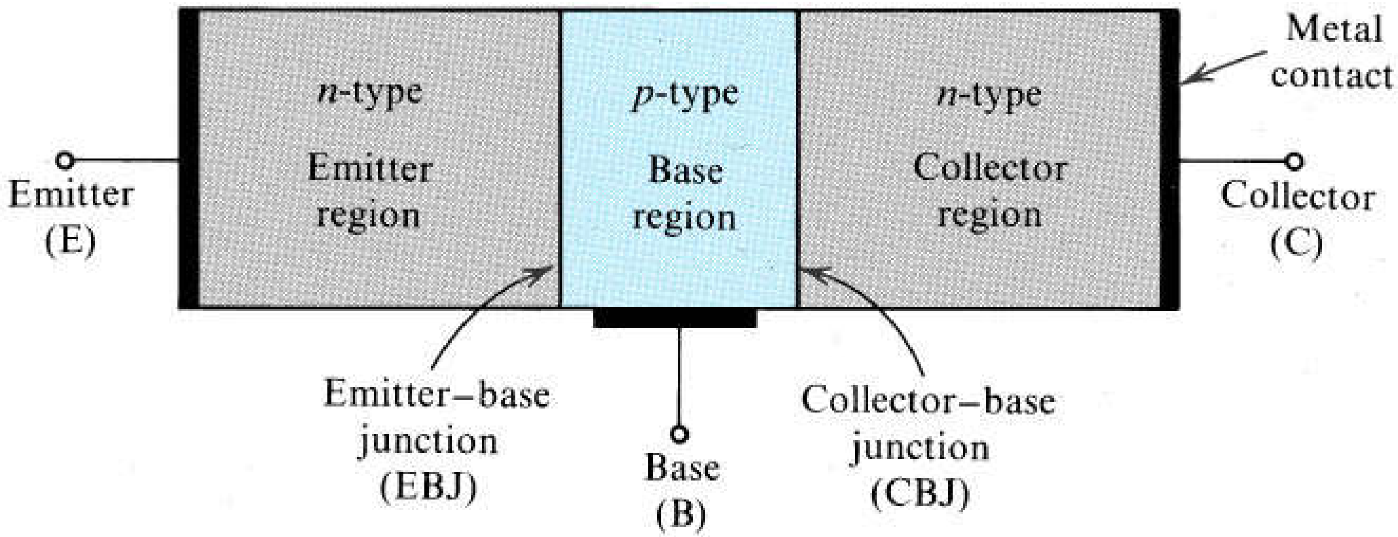

Figure 5.1 A simplified structure of the *npn* transistor.

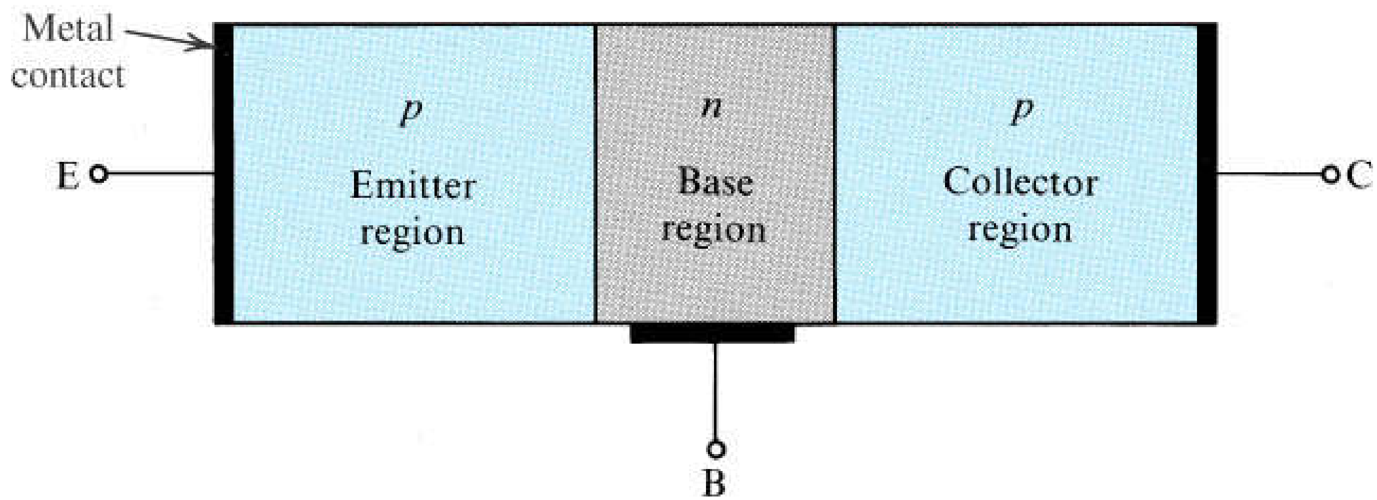

Figure 5.2 A simplified structure of the *pnp* transistor.

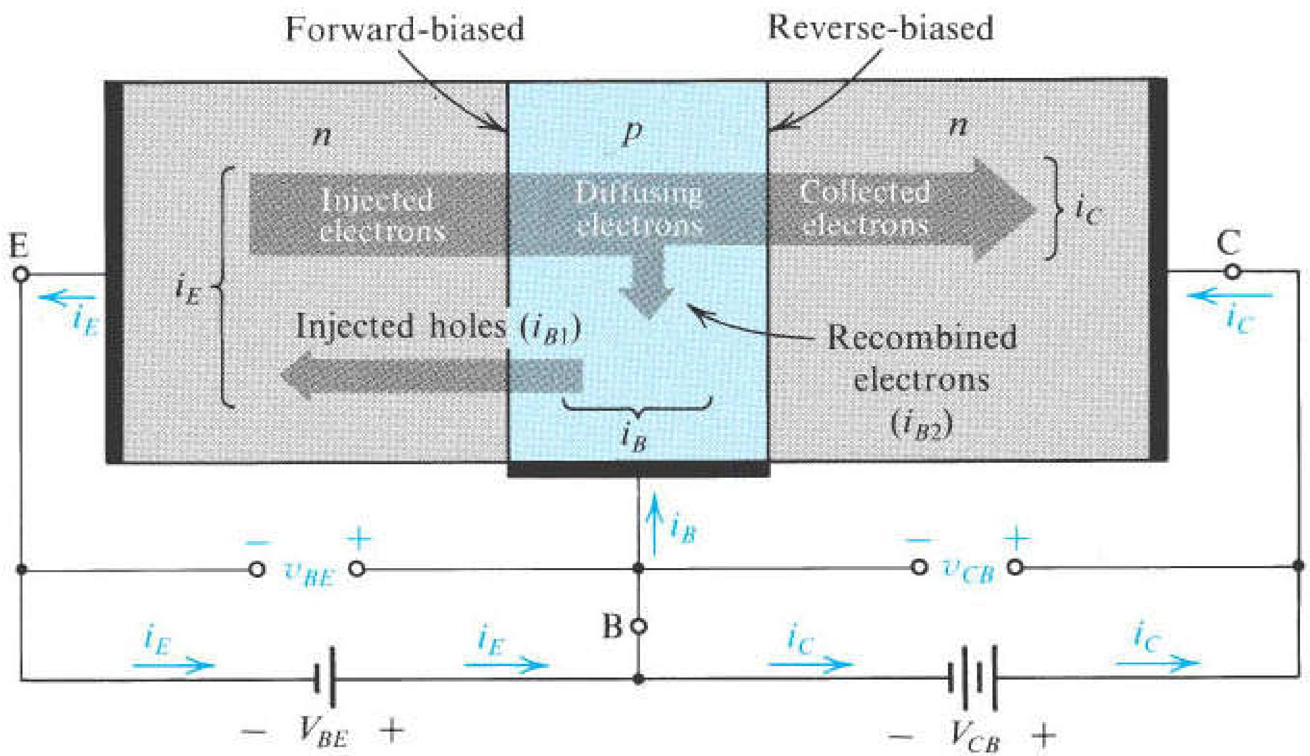

Figure 5.3 Current flow in an *npn* transistor biased to operate in the active mode. (Reverse current components due to drift of thermally generated minority carriers are not shown.)

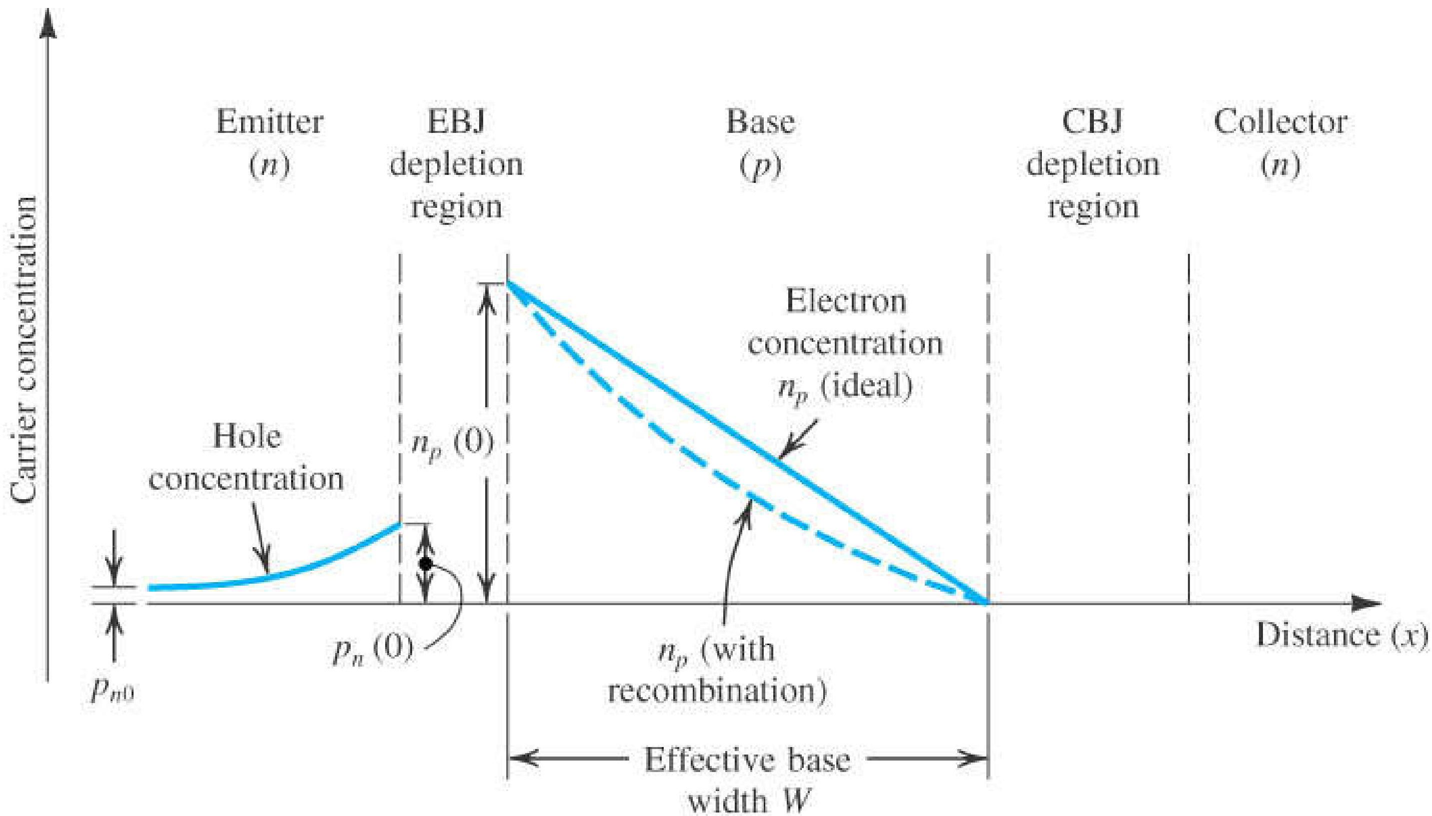

Figure 5.4 Profiles of minority-carrier concentrations in the base and in the emitter of an *npn* transistor operating in the active mode: $v_{BE} > 0$ and $v_{CB} \geq 0$.

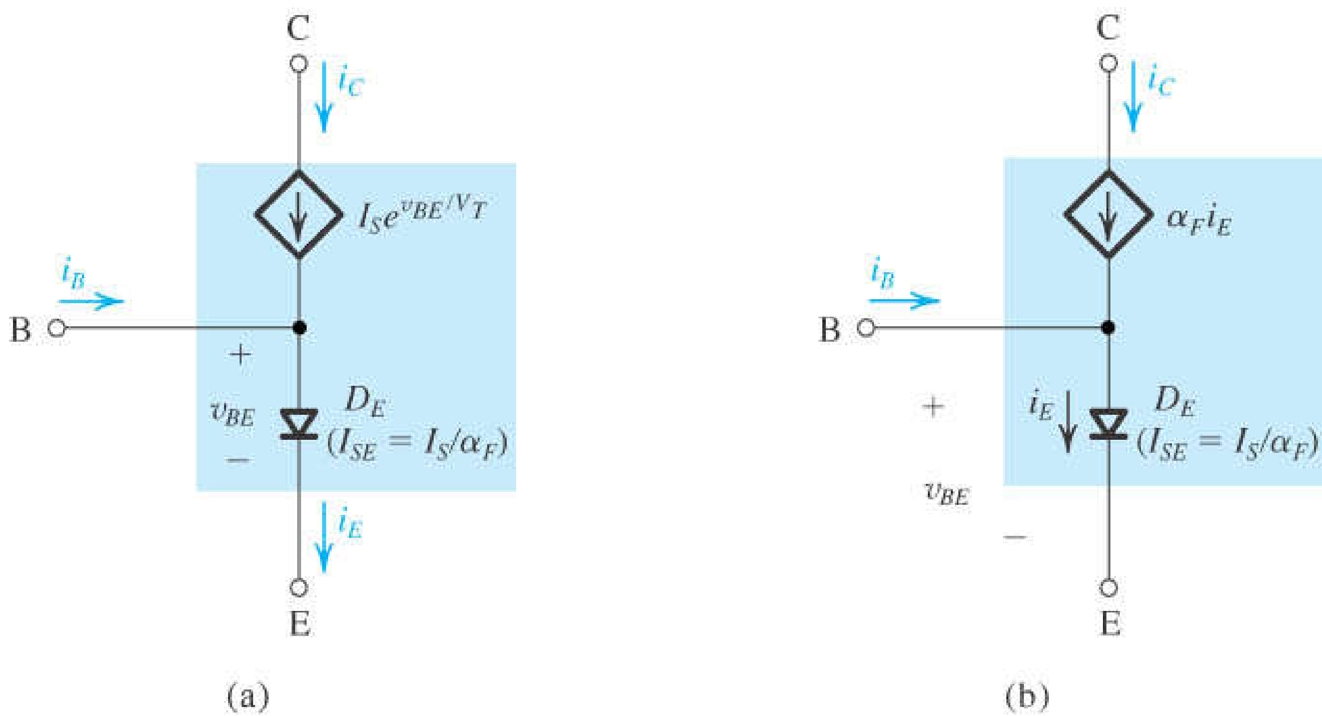

Figure 5.5 Large-signal equivalent-circuit models of the *npn* BJT operating in the forward active mode.

iccuser:

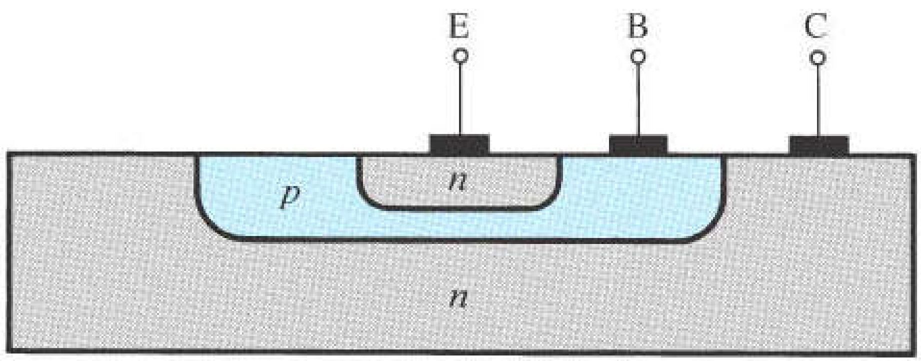

Figure 5.6 Cross-section of an *npn* BJT.

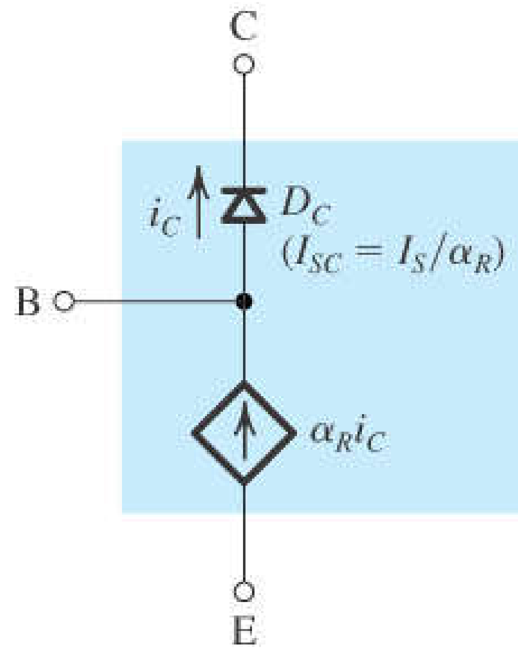

Figure 5.7 Model for the *npn* transistor when operated in the reverse active mode (i.e., with the CBJ forward biased and the EBJ reverse biased).

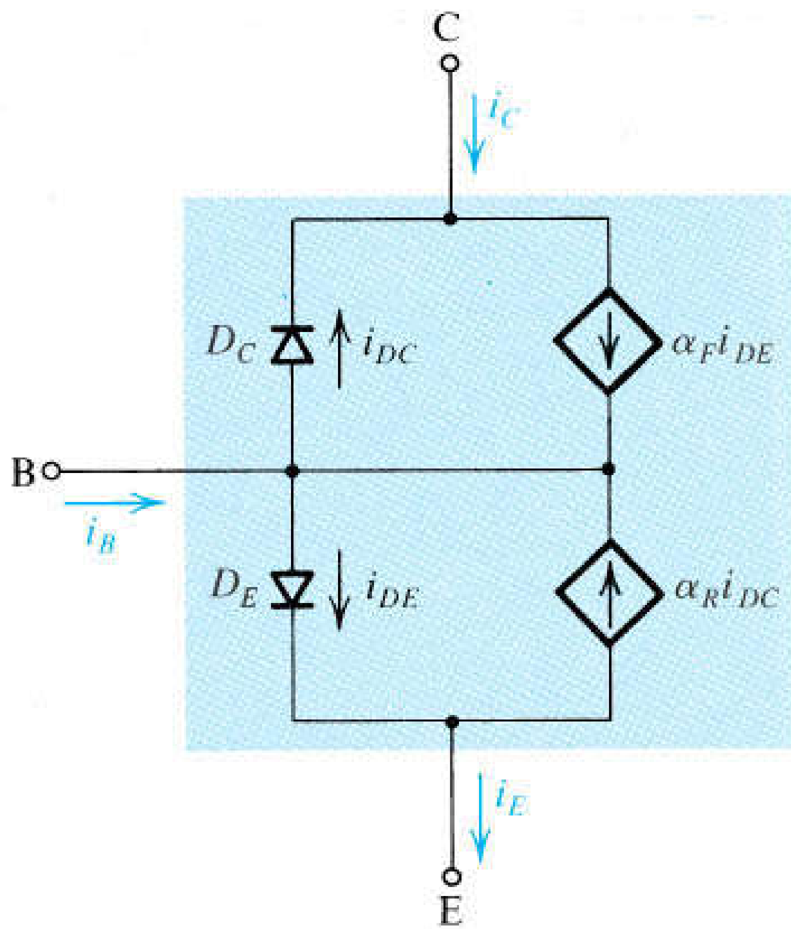

Figure 5.8 The Ebers-Moll (EM) model of the *npn* transistor.

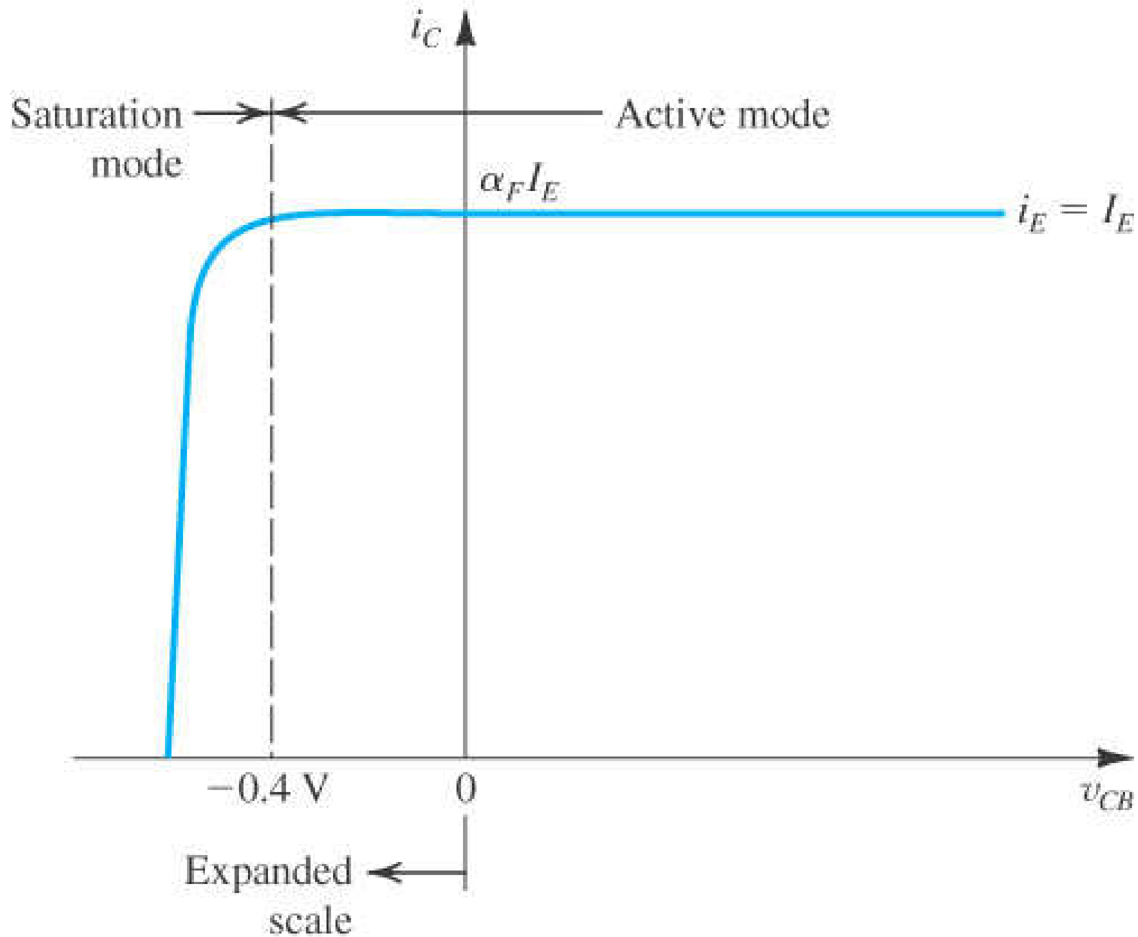

Figure 5.9 The i_C–v_{CB} characteristic of an *npn* transistor fed with a constant emitter current I_E. The transistor enters the saturation mode of operation for $v_{CB} < -0.4$ V, and the collector current diminishes.

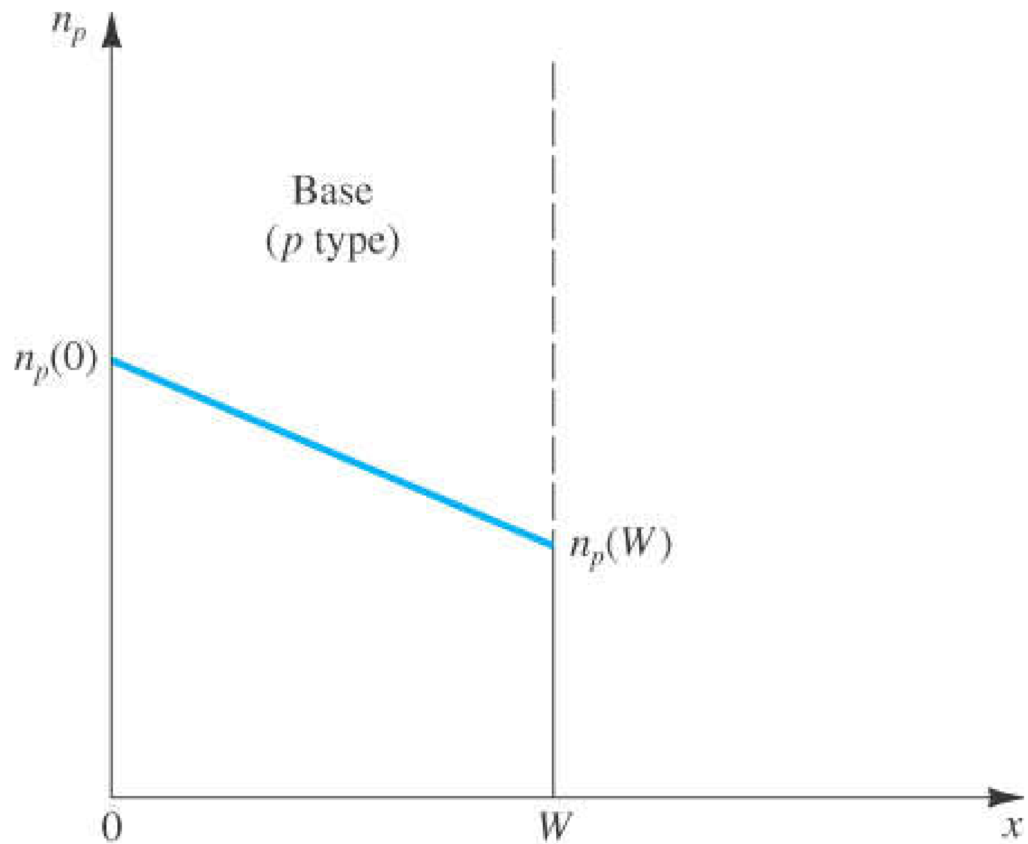

Figure 5.10 Concentration profile of the minority carriers (electrons) in the base of an *npn* transistor operating in the saturation mode.

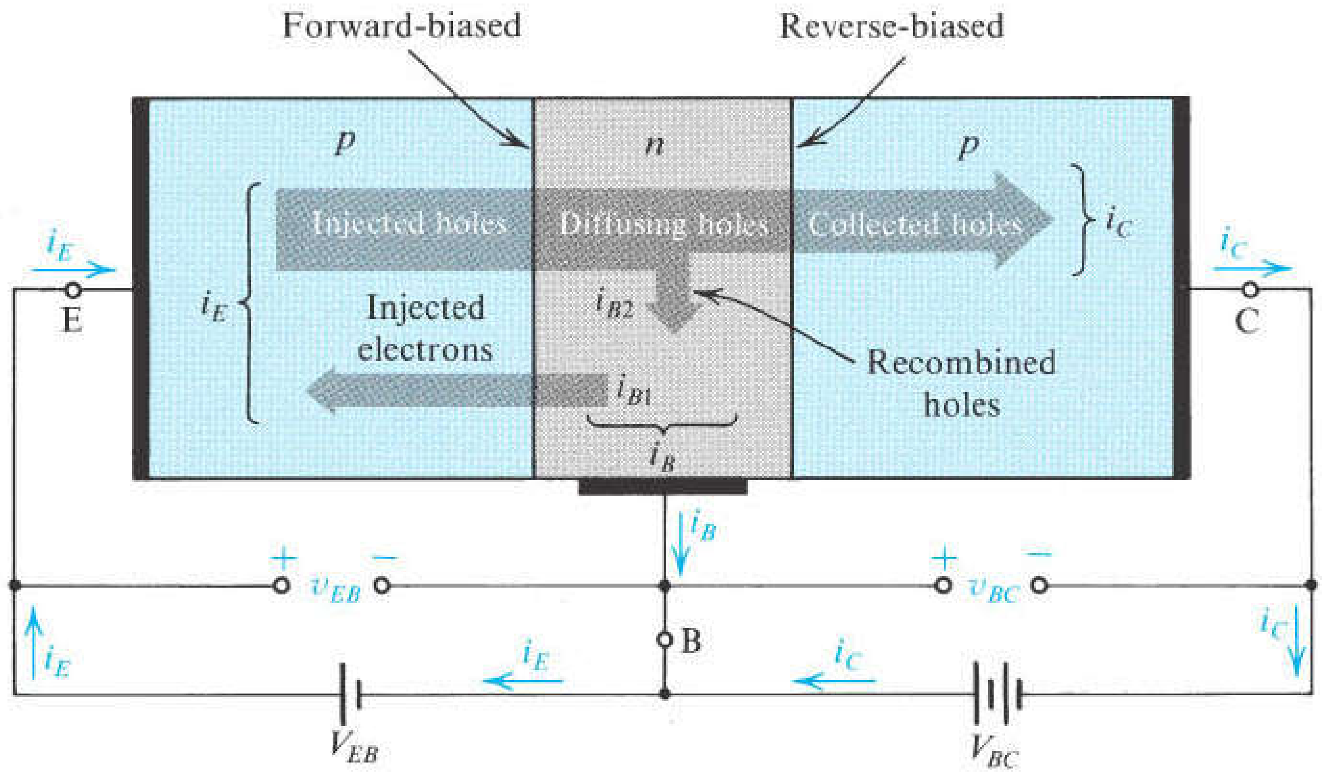

Figure 5.11 Current flow in a *pnp* transistor biased to operate in the active mode.

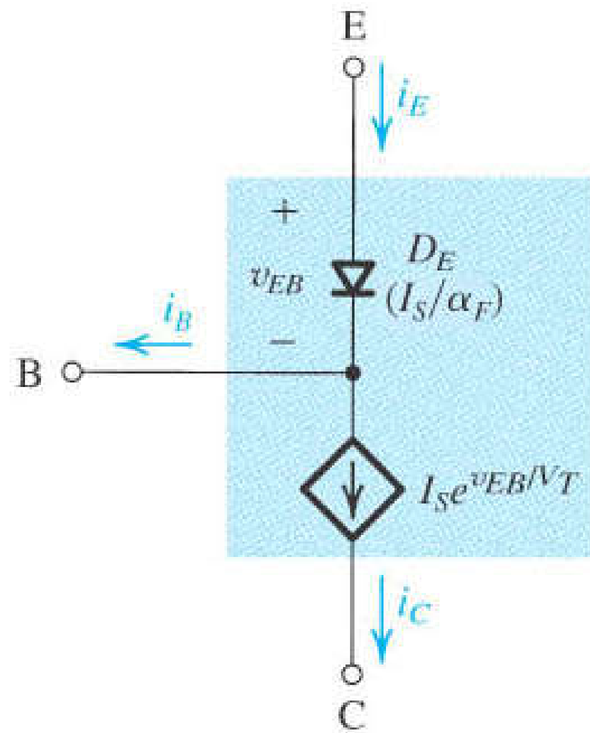

Figure 5.12 Large-signal model for the *pnp* transistor operating in the active mode.

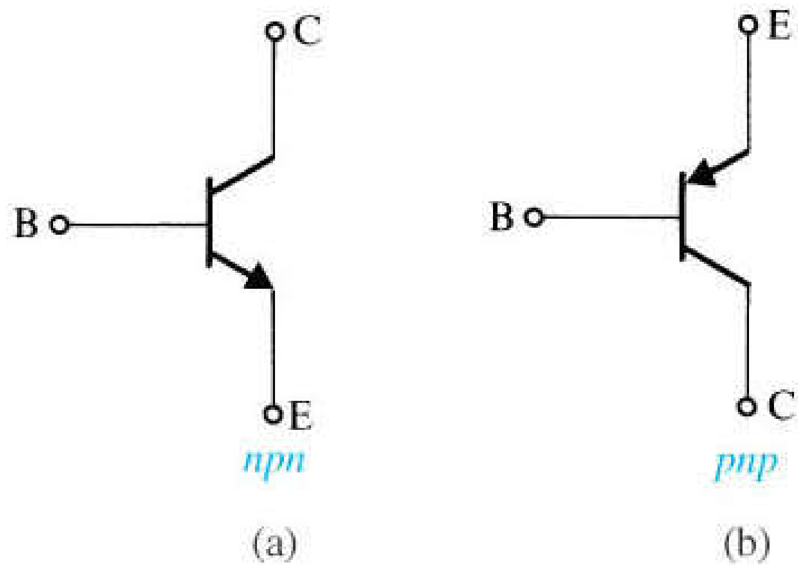

Figure 5.13 Circuit symbols for BJTs.

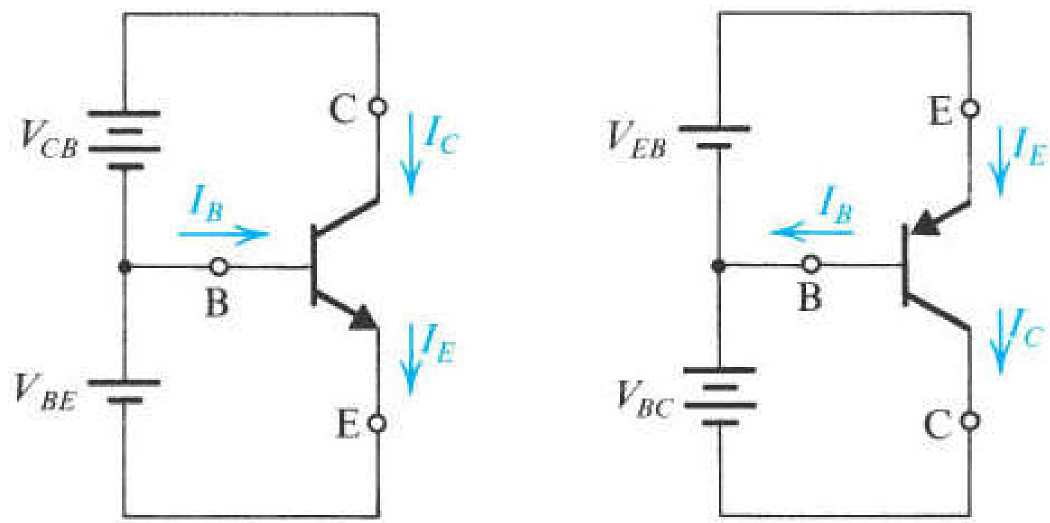

Figure 5.14 Voltage polarities and current flow in transistors biased in the active mode.

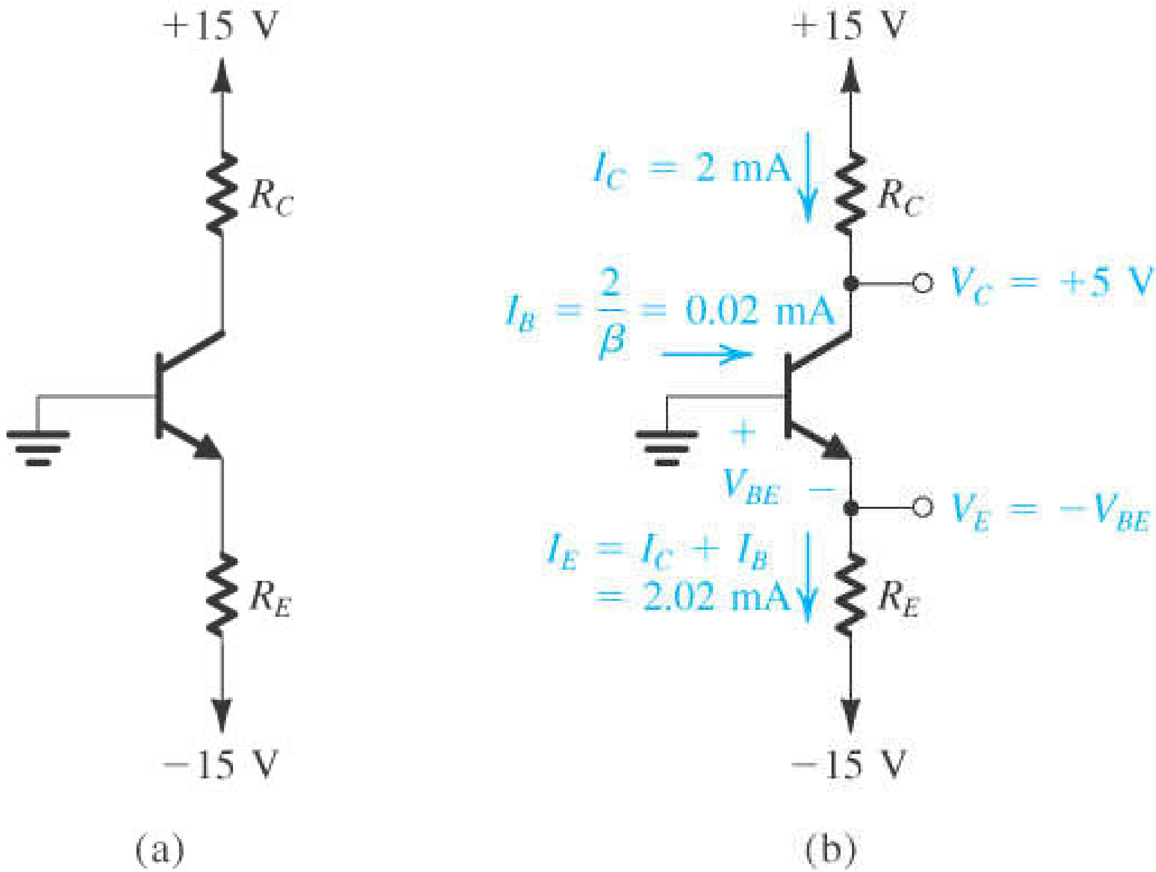

Figure 5.15 Circuit for Example 5.1.

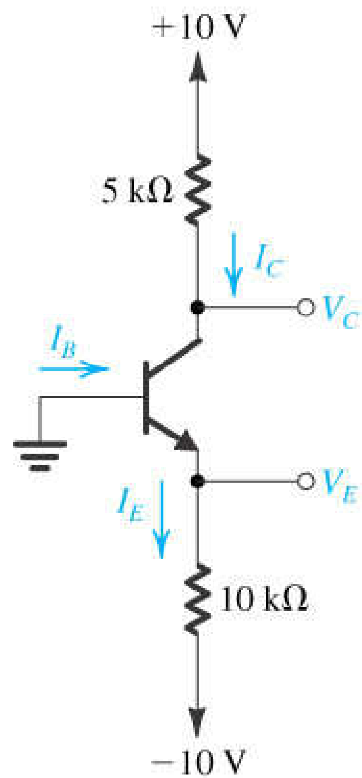

Figure E5.10

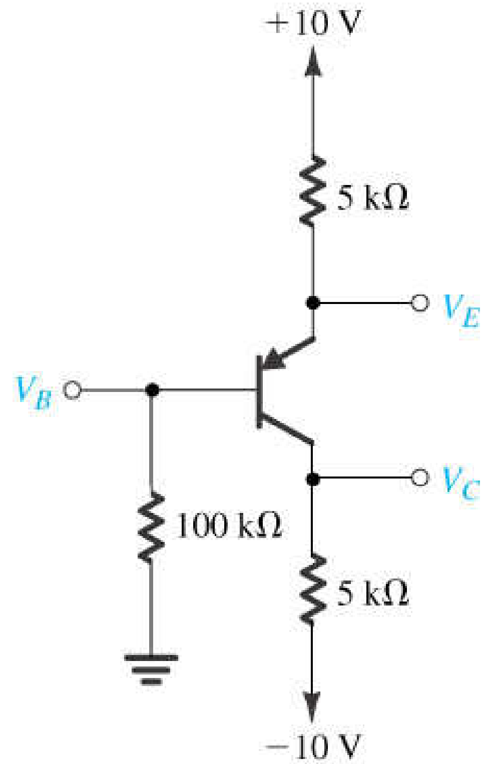

Figure E5.11

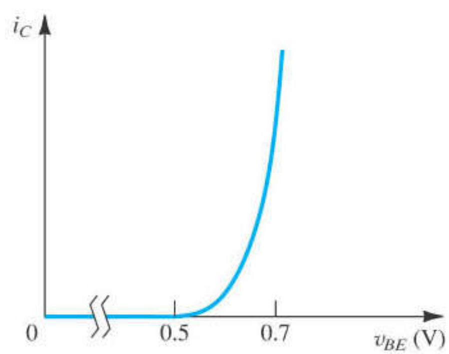

Figure 5.16 The i_C–v_{BE} characteristic for an *npn* transistor.

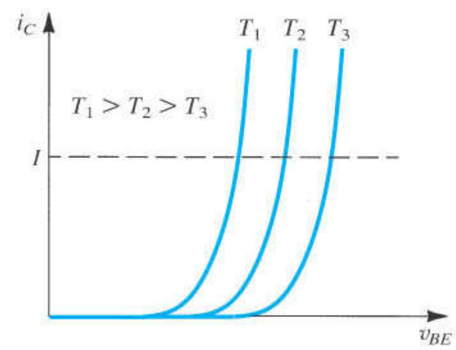

Figure 5.17 Effect of temperature on the i_C–v_{BE} characteristic. At a constant emitter current (broken line), v_{BE} changes by –2 mV/°C.

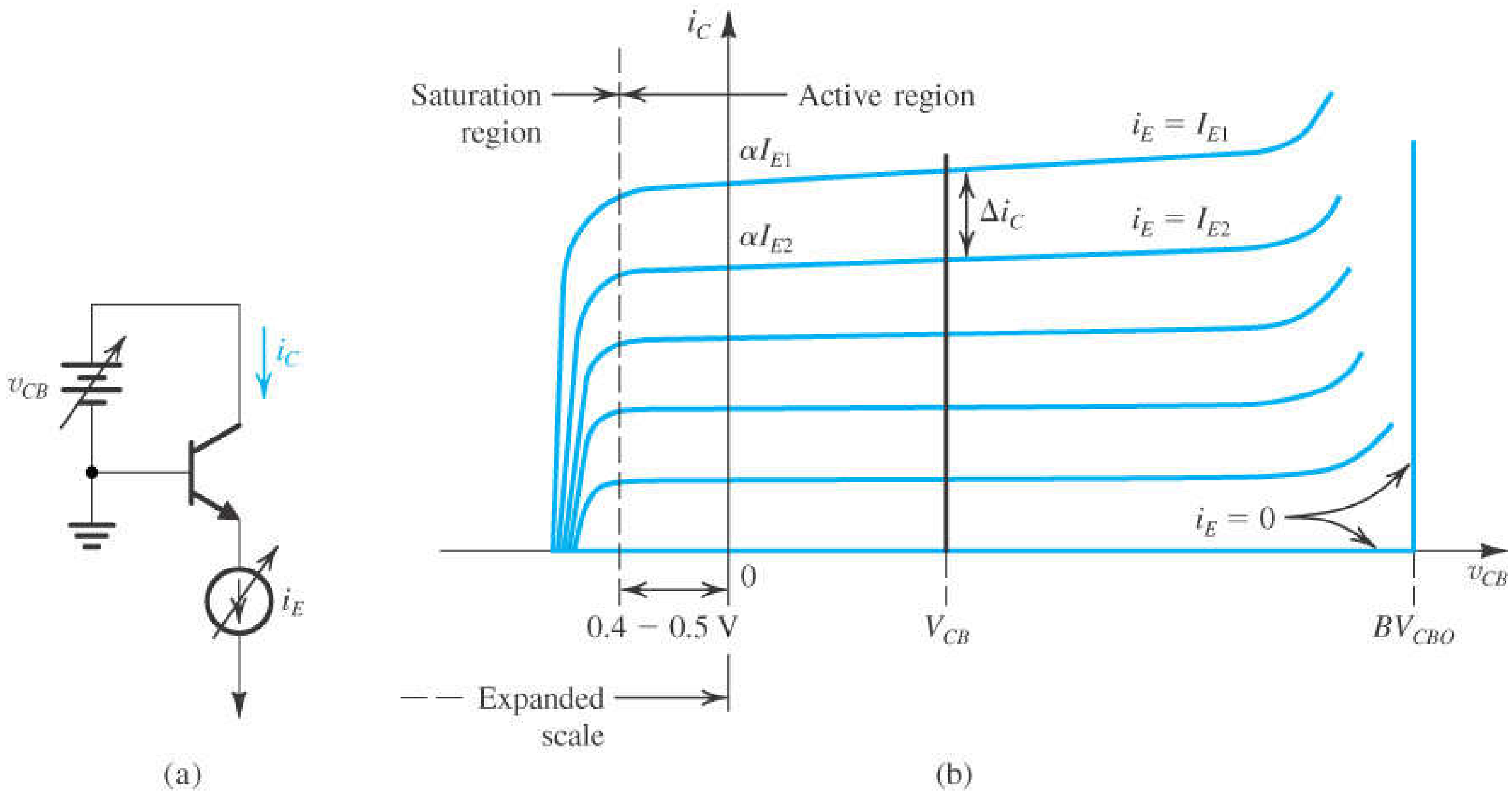

Figure 5.18 The i_C–v_{CB} characteristics of an *npn* transistor.

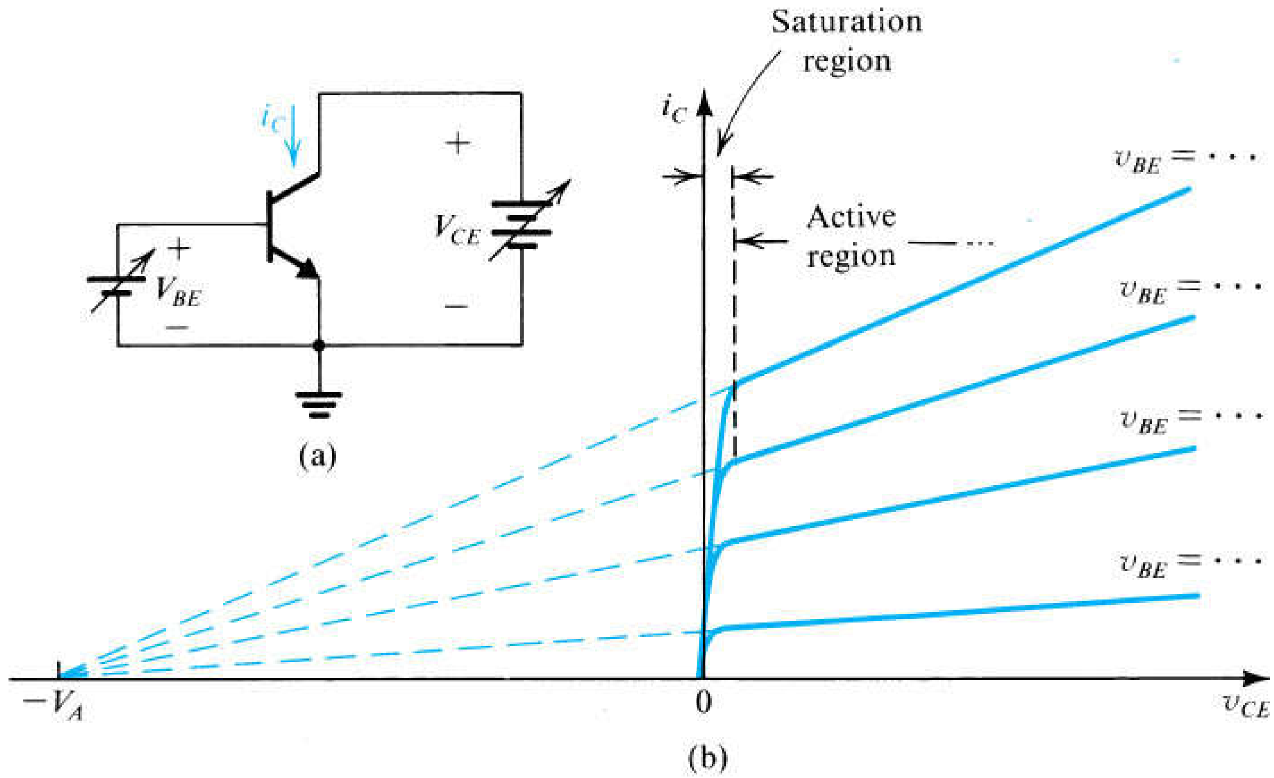

Figure 5.19 **(a)** Conceptual circuit for measuring the i_C–v_{CE} characteristics of the BJT. **(b)** The i_C–v_{CE} characteristics of a practical BJT.

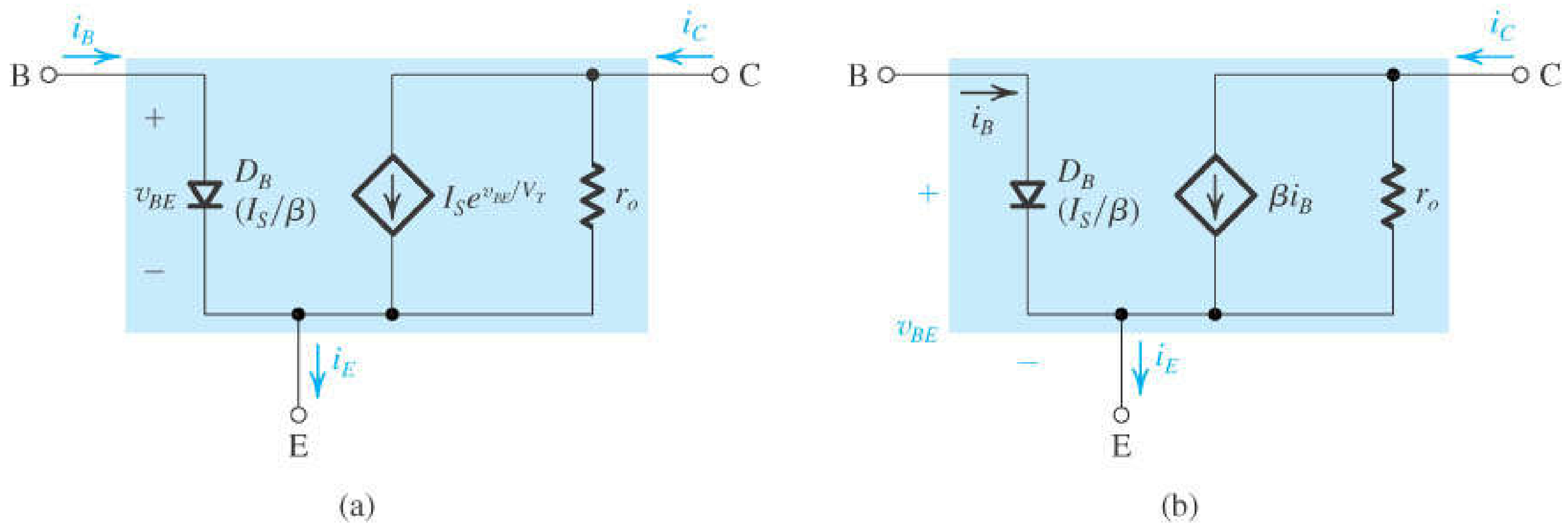

Figure 5.20 Large-signal equivalent-circuit models of an *npn* BJT operating in the active mode in the common-emitter configuration.

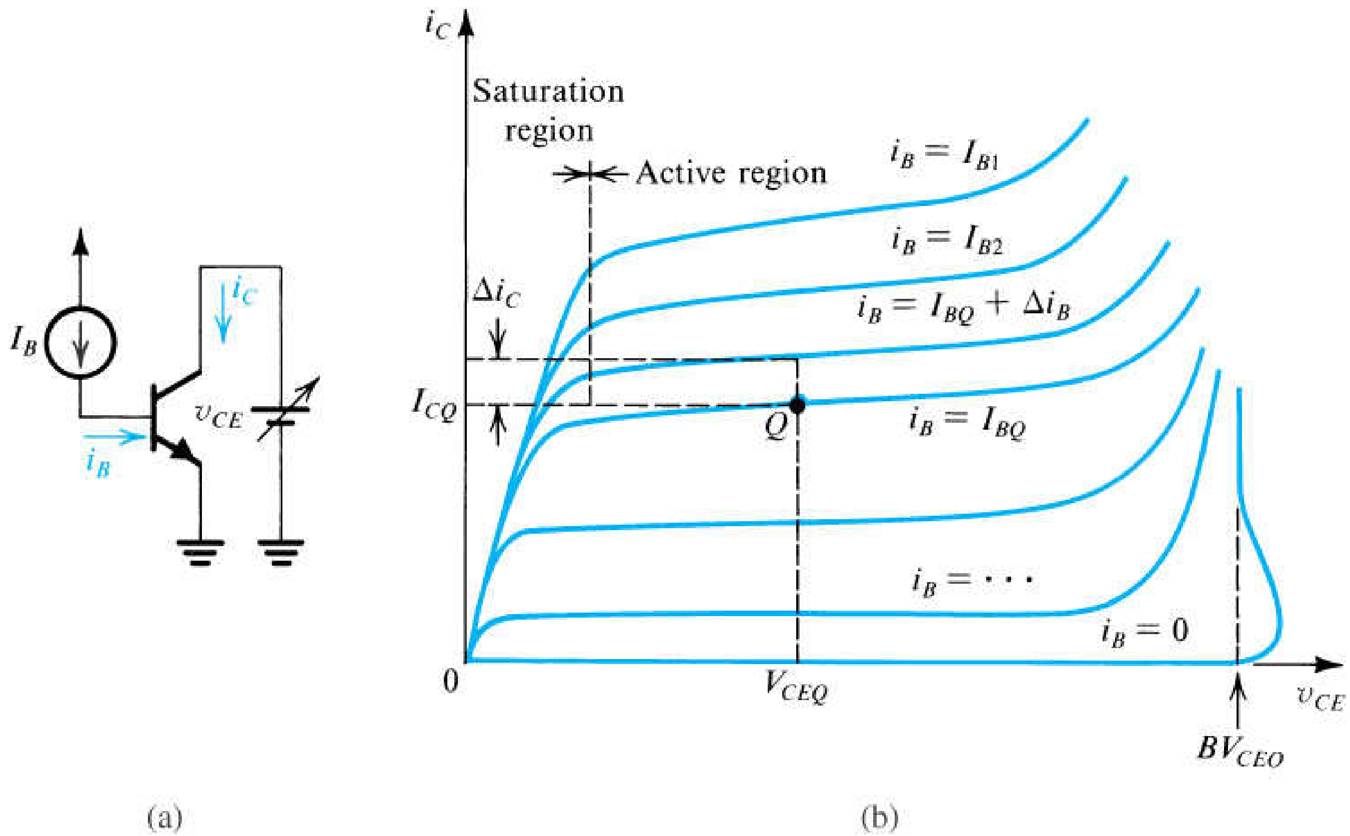

Figure 5.21 Common-emitter characteristics. Note that the horizontal scale is expanded around the origin to show the saturation region in some detail.

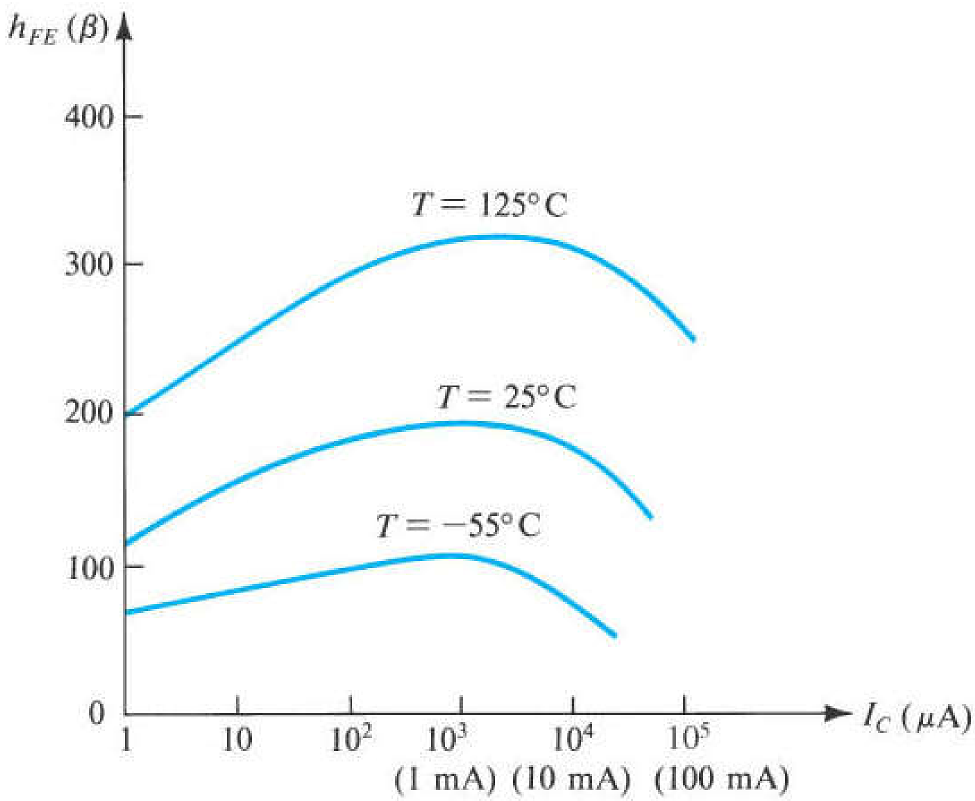

Figure 5.22 Typical dependence of β on I_C and on temperature in a modern integrated-circuit *npn* silicon transistor intended for operation around 1 mA.

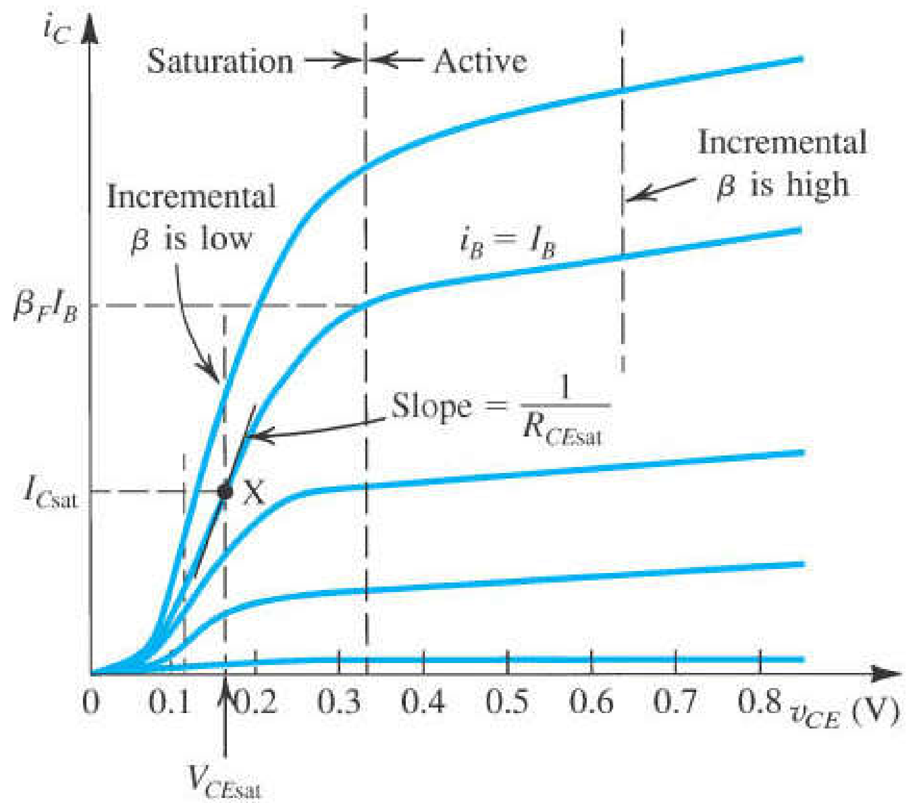

Figure 5.23 An expanded view of the common-emitter characteristics in the saturation region.

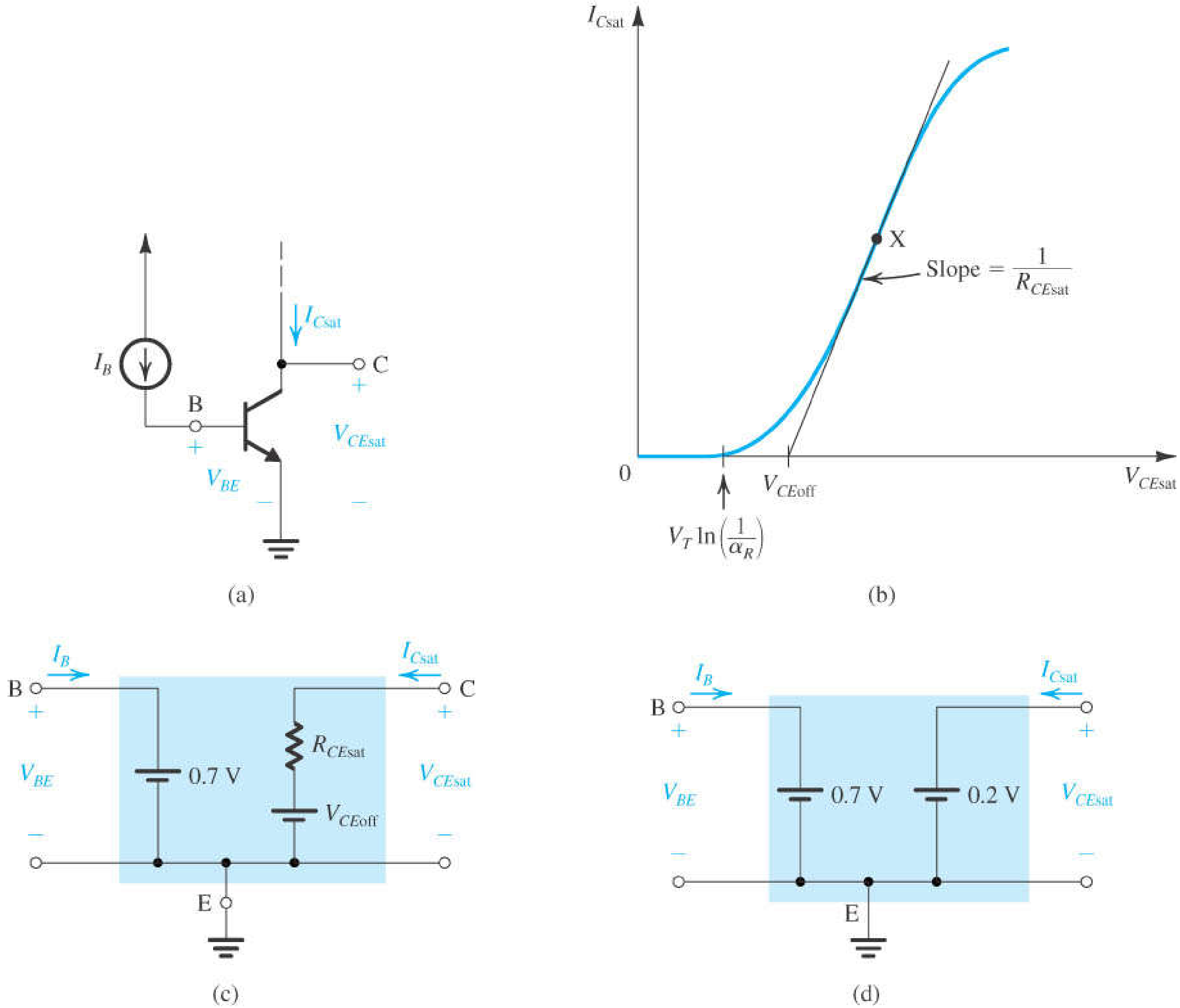

Figure 5.24 **(a)** An *npn* transistor operated in saturation mode with a constant base current I_B. **(b)** The i_C–v_{CE} characteristic curve corresponding to $i_B = I_B$. The curve can be approximated by a straight line of slope $1/R_{CEsat}$. **(c)** Equivalent-circuit representation of the saturated transistor. **(d)** A simplified equivalent-circuit model of the saturated transistor.

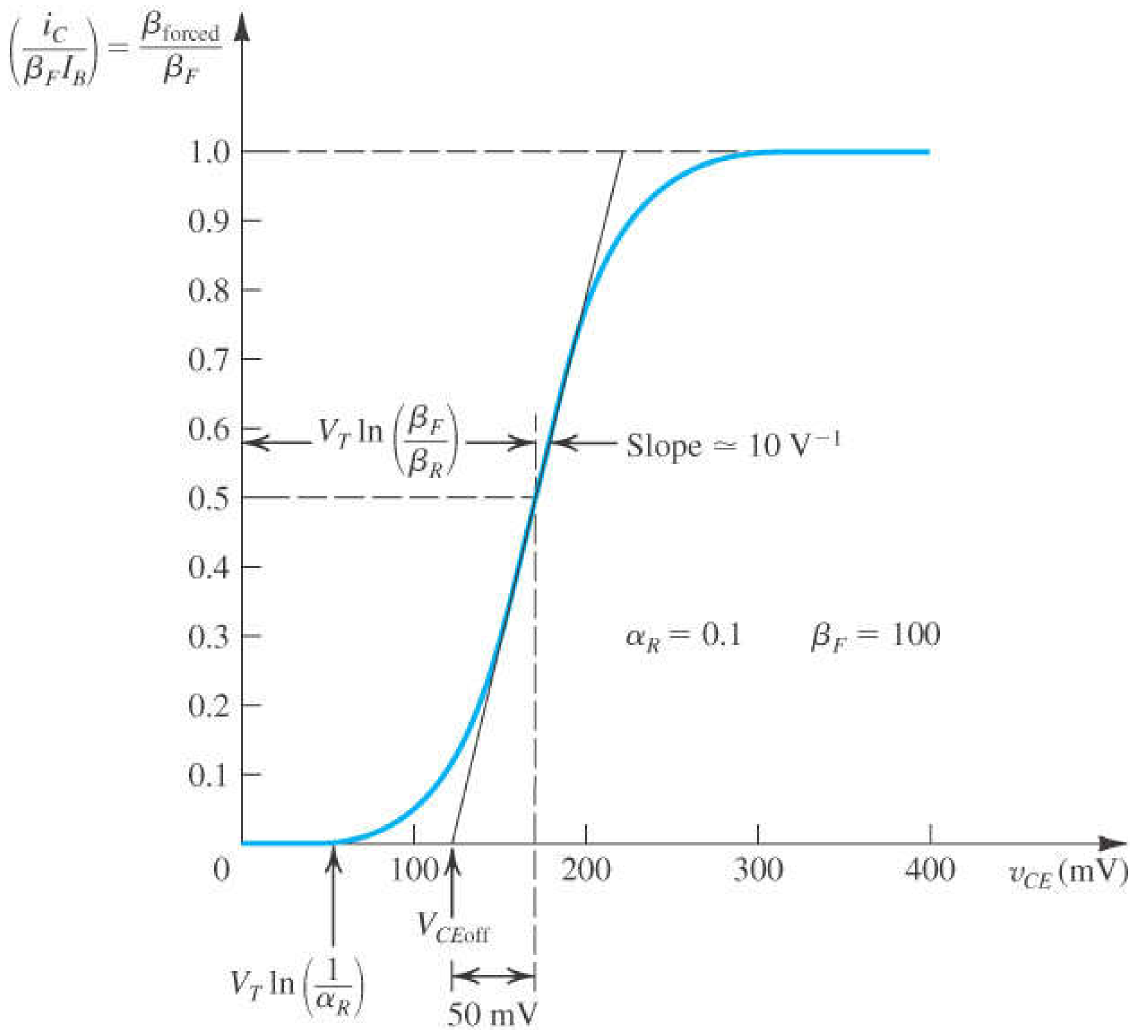

Figure 5.25 Plot of the normalized i_C versus v_{CE} for an *npn* transistor with $\beta_F = 100$ and $\alpha_R = 0.1$. This is a plot of Eq. (5.47), which is derived using the Ebers-Moll model.

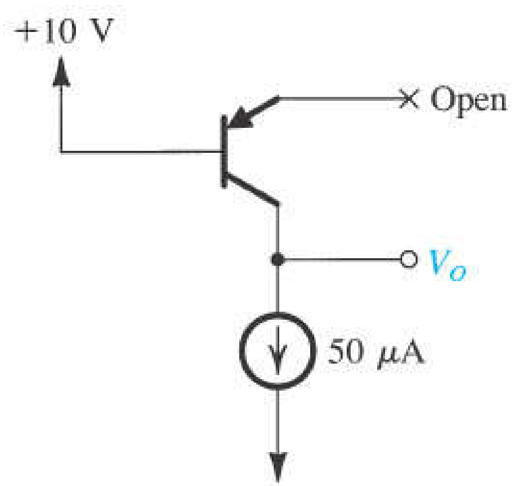

Figure E5.18

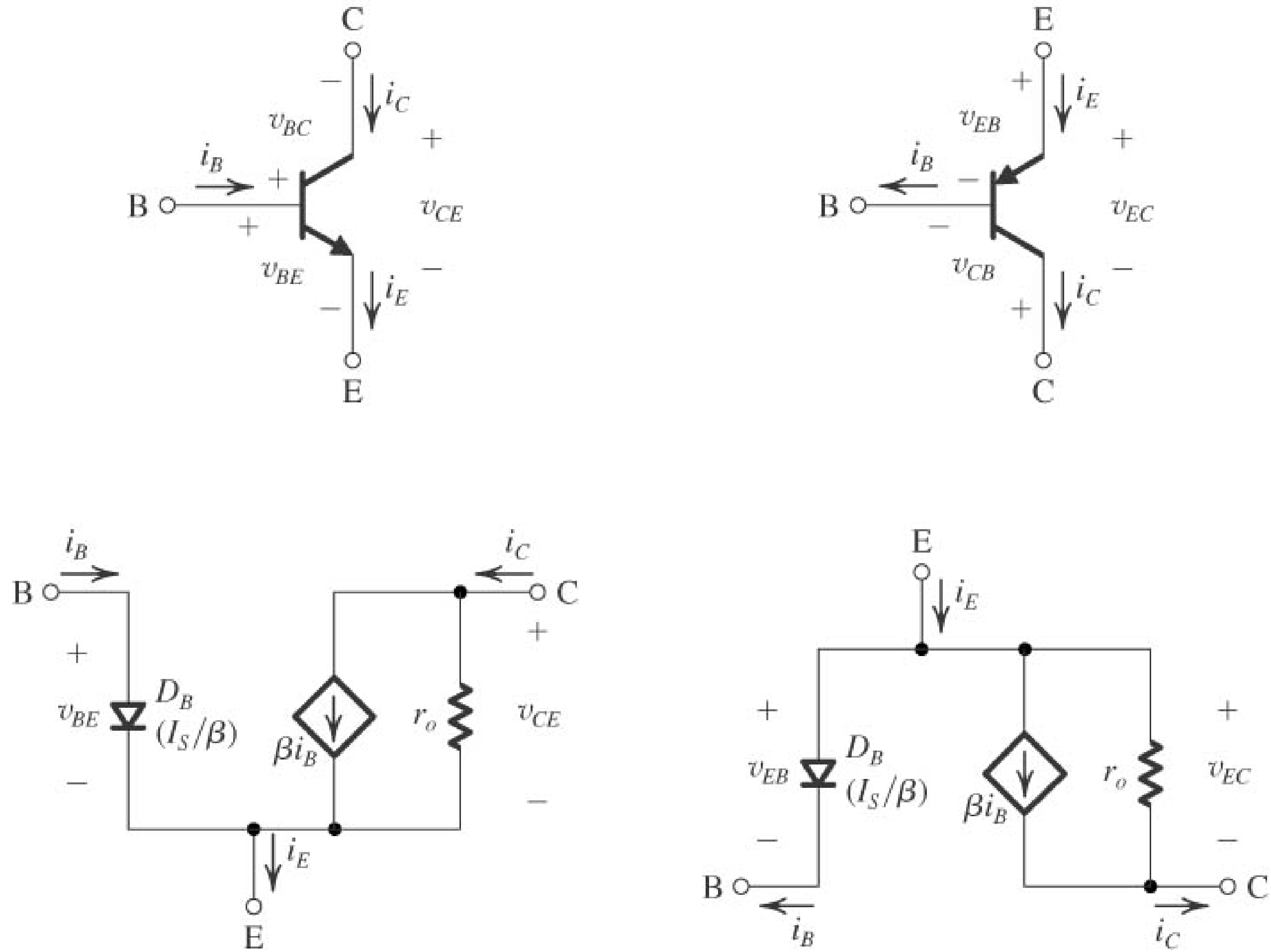
C
E
B
i_C
i_E
i_B
v_{BC}
v_{BE}
v_{CE}
E
C
B
i_E
i_C
i_B
v_{EB}
v_{CB}
v_{EC}
B
C
E
i_B
i_C
i_E
v_{BE}
D_B
(I_S/β)
βi_B
r_o
v_{CE}
E
B
C
i_E
i_B
i_C
v_{EB}
D_B
(I_S/β)
βi_B
r_o
v_{EC}

Table 5.3

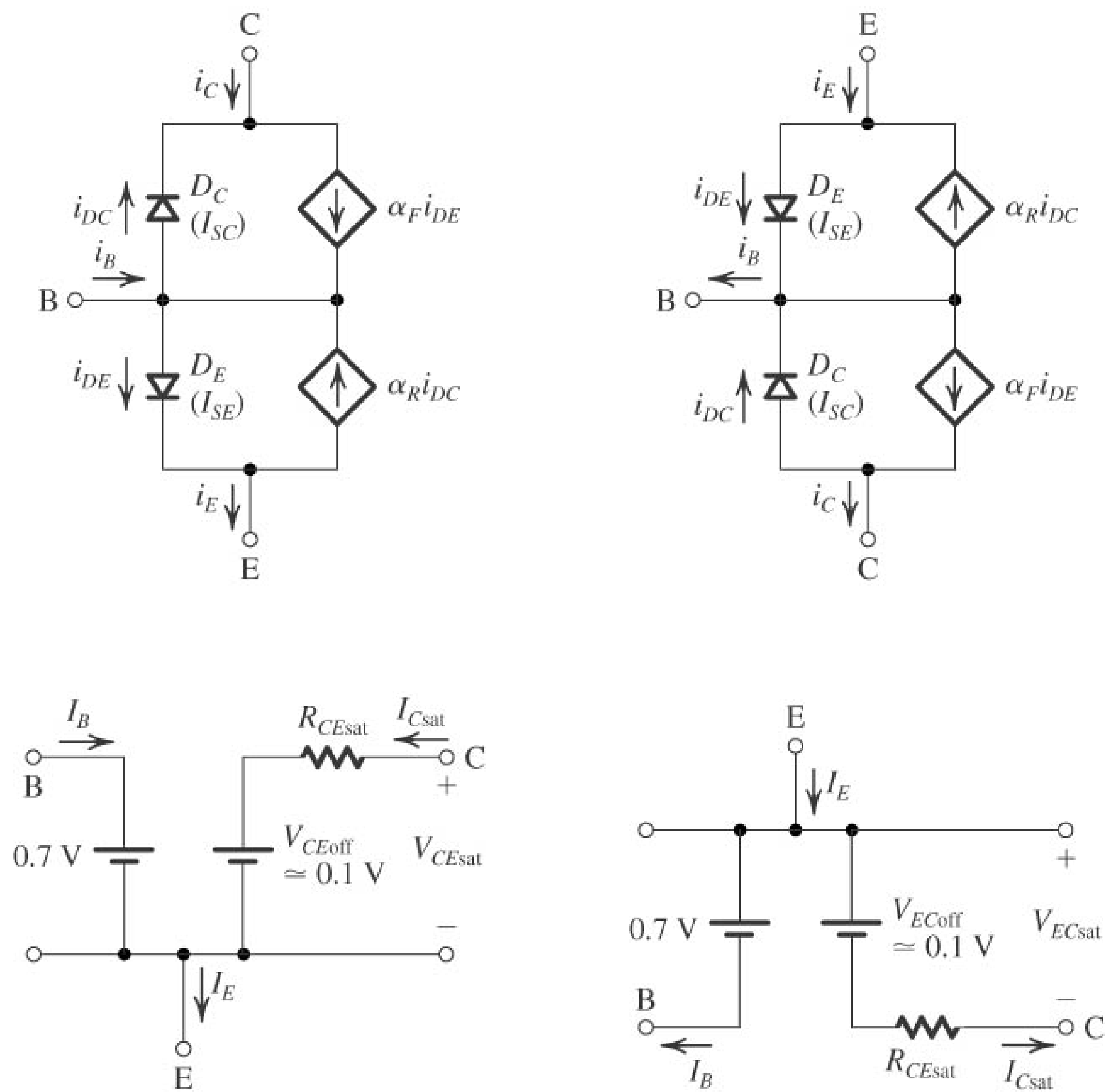

Table 5.3 *(Continued)*

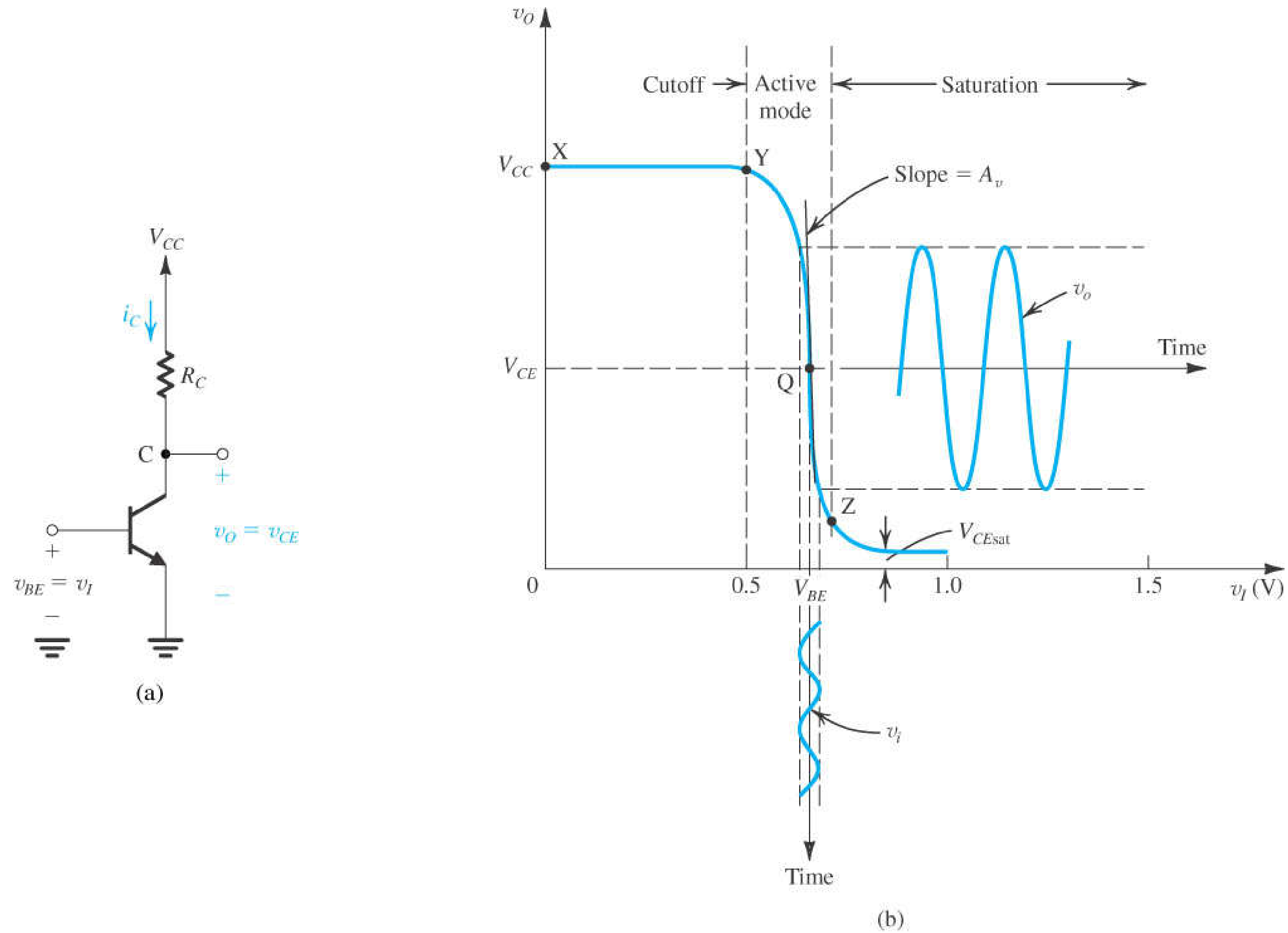

Figure 5.26 (a) Basic common-emitter amplifier circuit. **(b)** Transfer characteristic of the circuit in (a). The amplifier is biased at a point Q, and a small voltage signal v_i is superimposed on the dc bias voltage V_{BE}. The resulting output signal v_o appears superimposed on the dc collector voltage V_{CE}. The amplitude of v_o is larger than that of v_i by the voltage gain A_v.

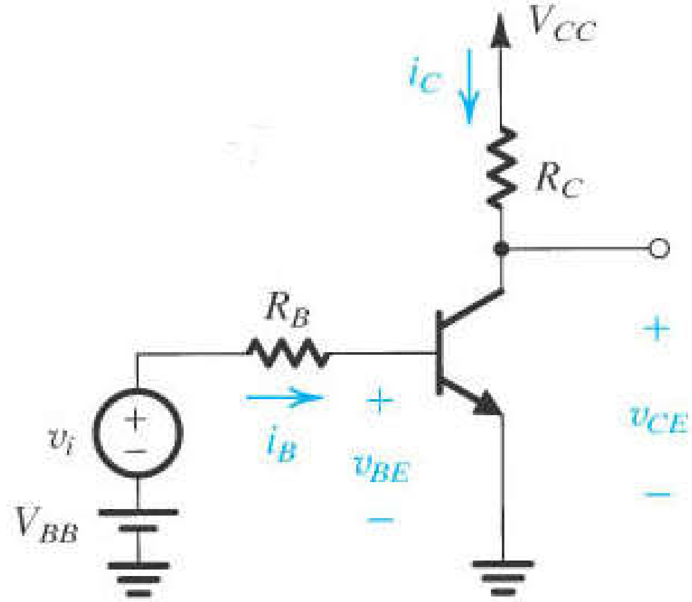

Figure 5.27 Circuit whose operation is to be analyzed graphically.

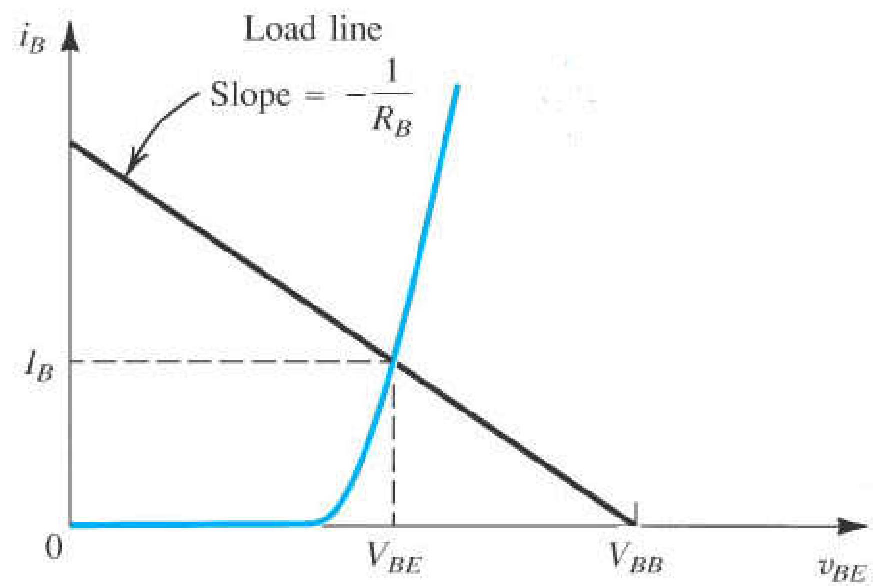

Figure 5.28 Graphical construction for the determination of the dc base current in the circuit of Fig. 5.27.

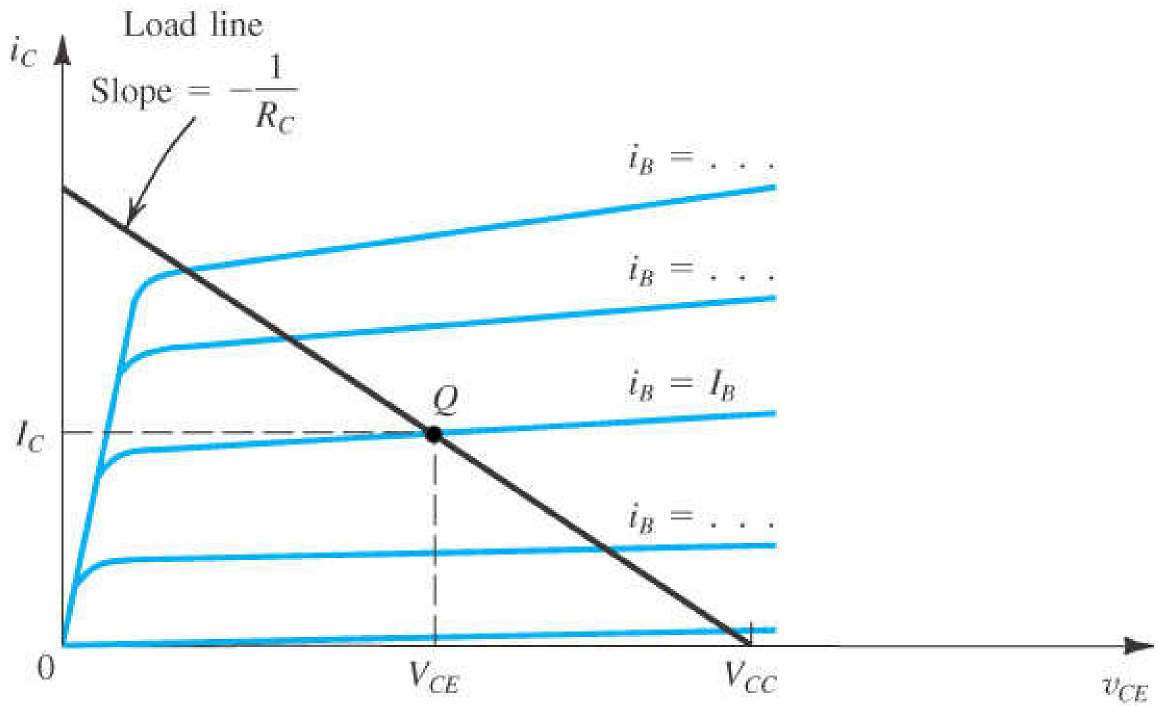

Figure 5.29 Graphical construction for determining the dc collector current I_C and the collector-to-emitter voltage V_{CE} in the circuit of Fig. 5.27.

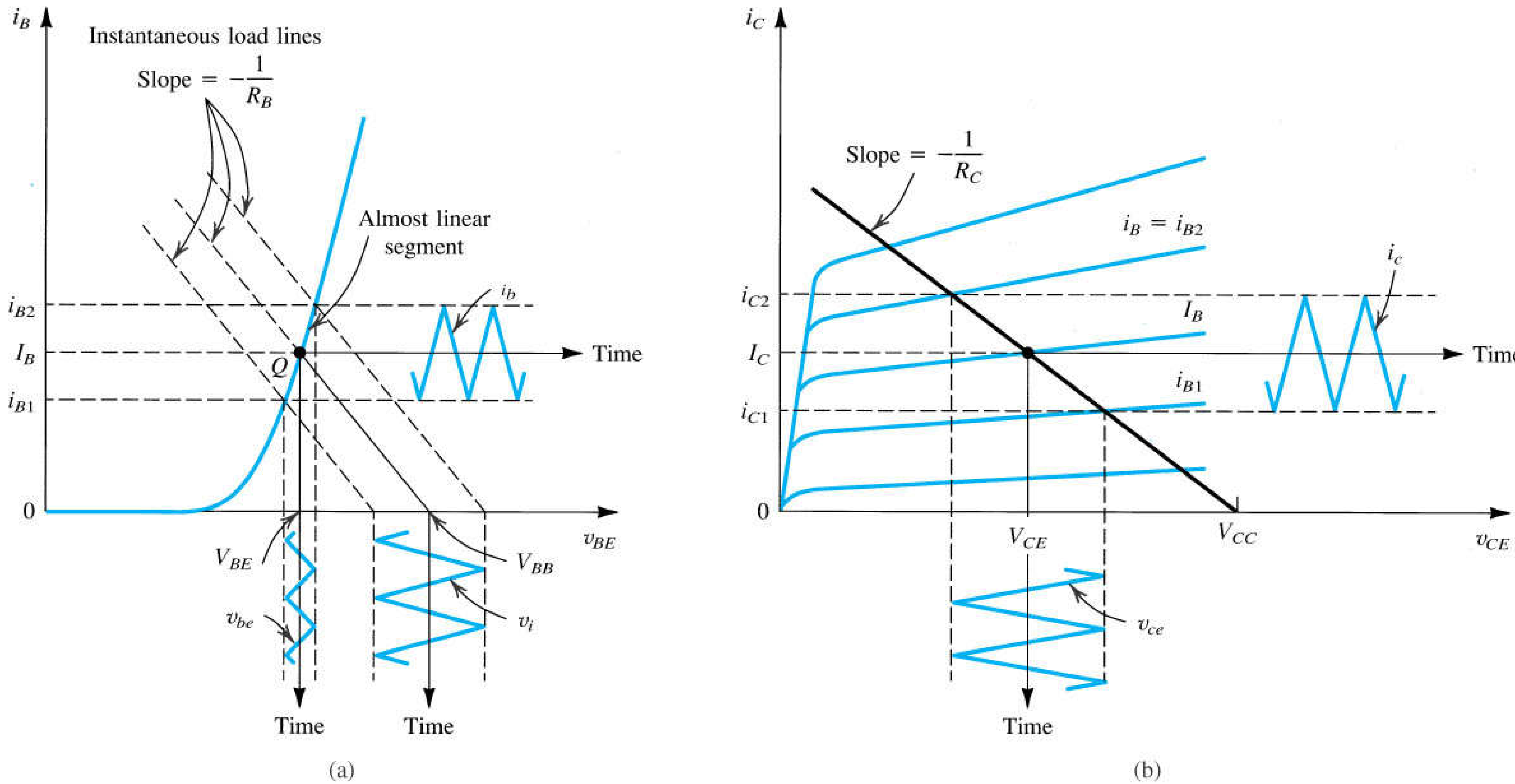

Figure 5.30 Graphical determination of the signal components v_{be}, i_b, i_c, and v_{ce} when a signal component v_i is superimposed on the dc voltage V_{BB} (see Fig. 5.27).

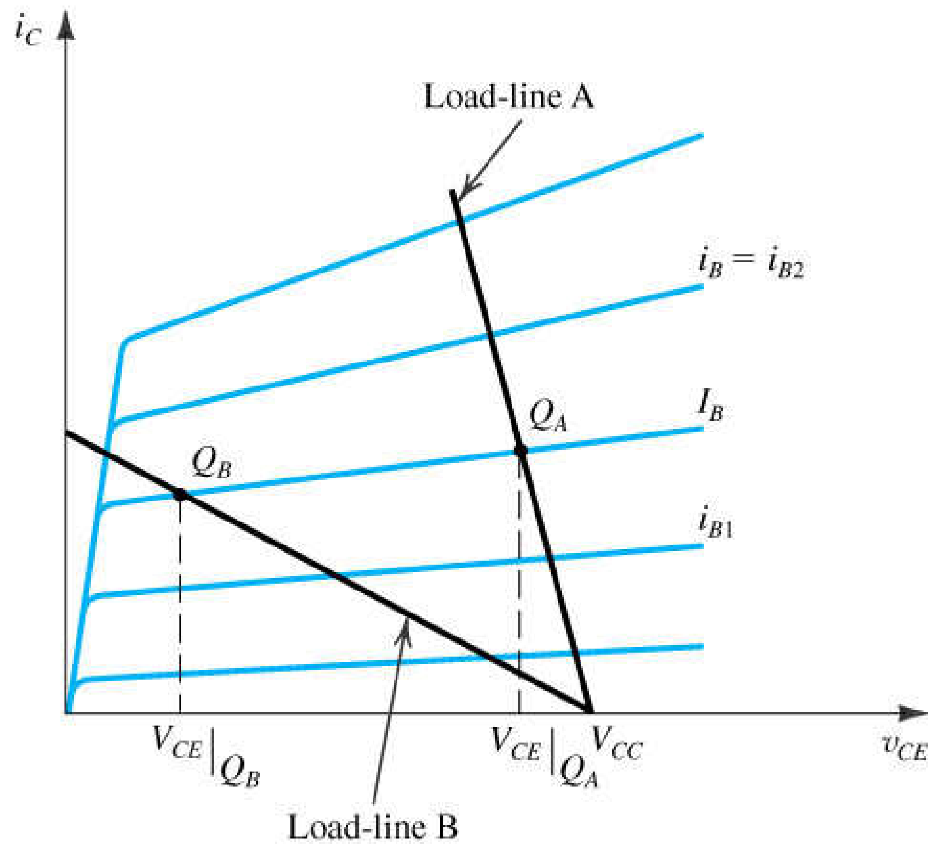

Figure 5.31 Effect of bias-point location on allowable signal swing: Load-line A results in bias point Q_A with a corresponding V_{CE} which is too close to V_{CC} and thus limits the positive swing of v_{CE}. At the other extreme, load-line B results in an operating point too close to the saturation region, thus limiting the negative swing of v_{CE}.

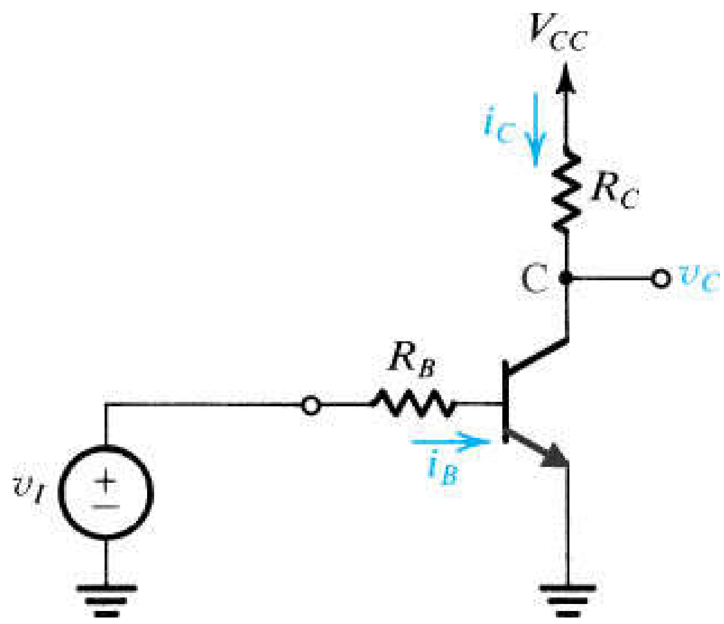

Figure 5.32 A simple circuit used to illustrate the different modes of operation of the BJT.

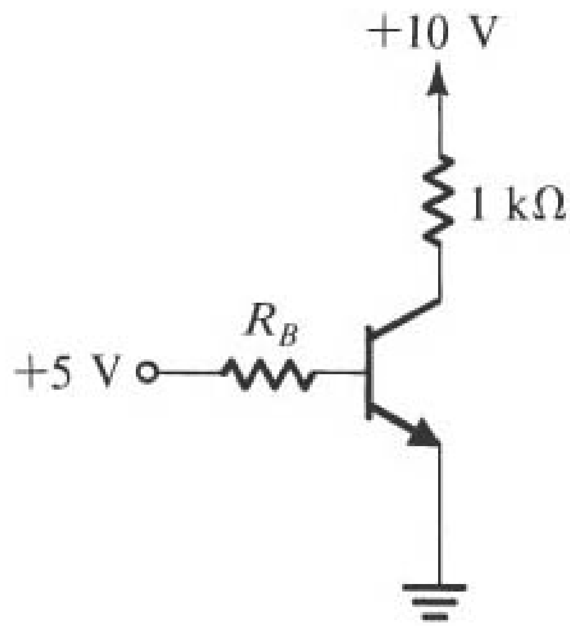

Figure 5.33 Circuit for Example 5.3.

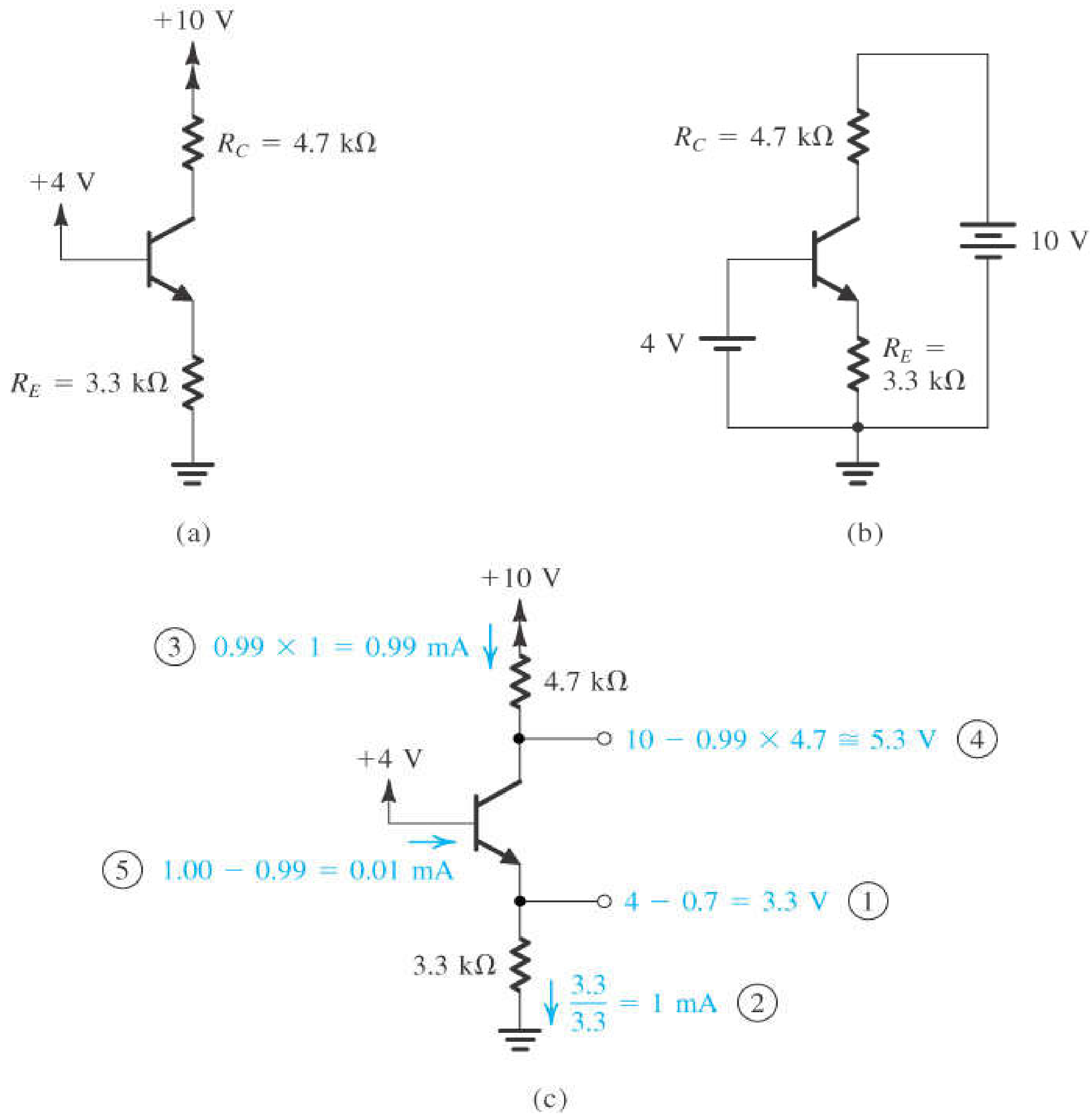

Figure 5.34 Analysis of the circuit for Example 5.4: **(a)** circuit; **(b)** circuit redrawn to remind the reader of the convention used in this book to show connections to the power supply; **(c)** analysis with the steps numbered.

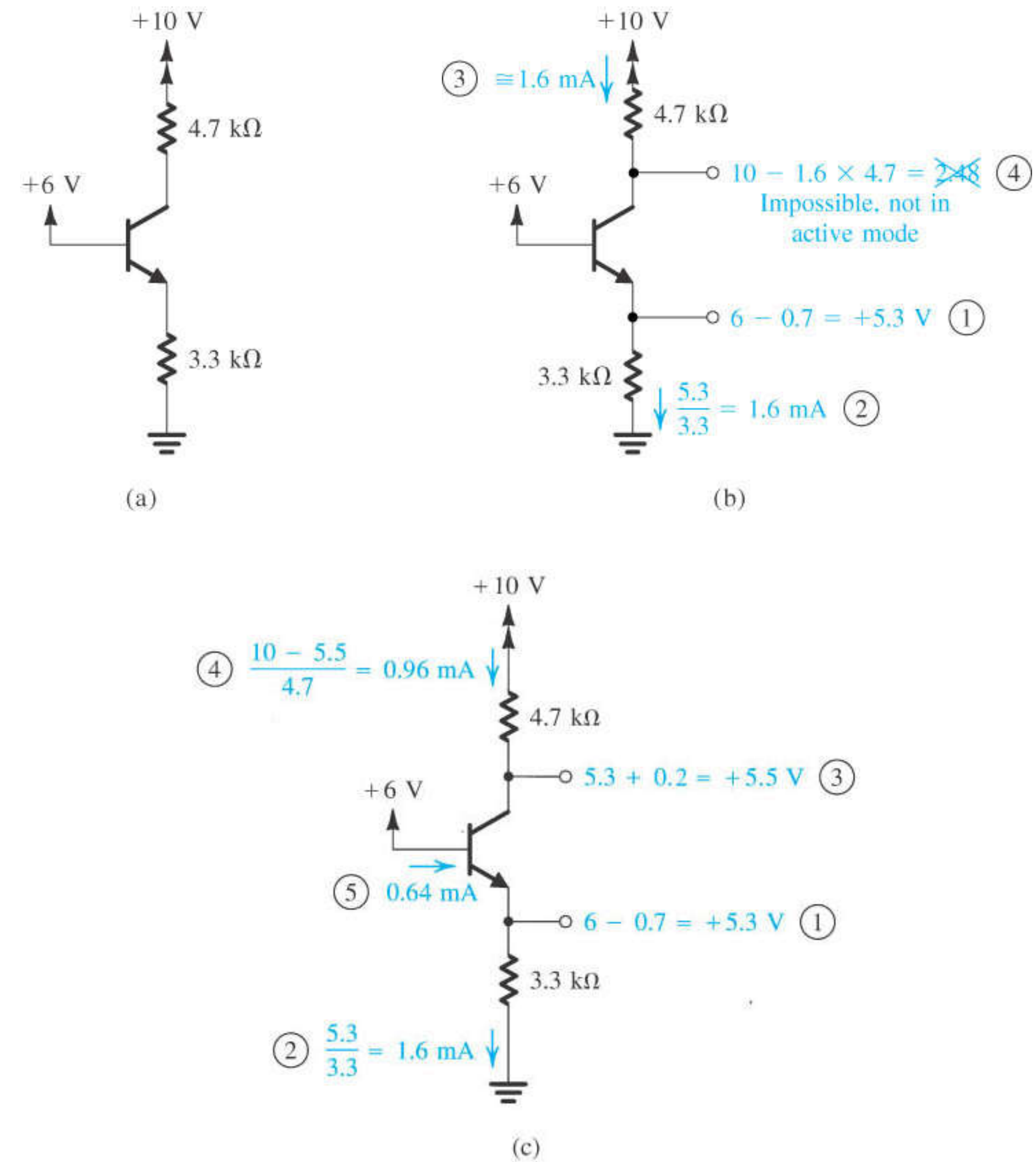

Figure 5.35 Analysis of the circuit for Example 5.5. Note that the circled numbers indicate the order of the analysis steps.

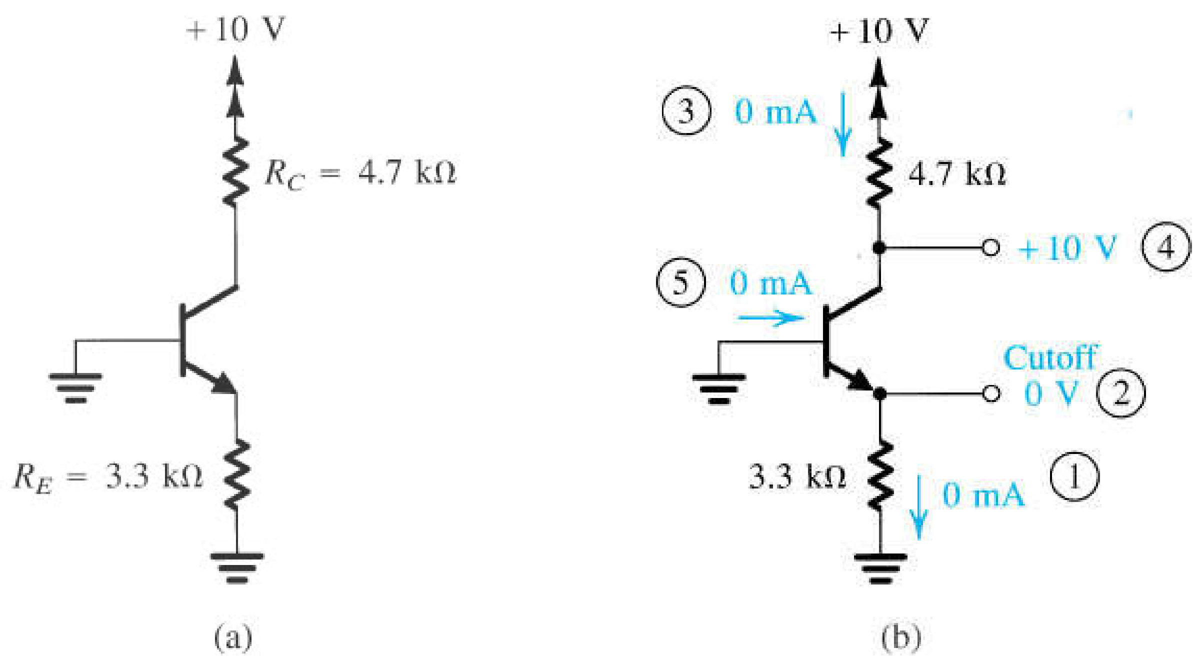

Figure 5.36 Example 5.6: **(a)** circuit; **(b)** analysis with the order of the analysis steps indicated by circled numbers.

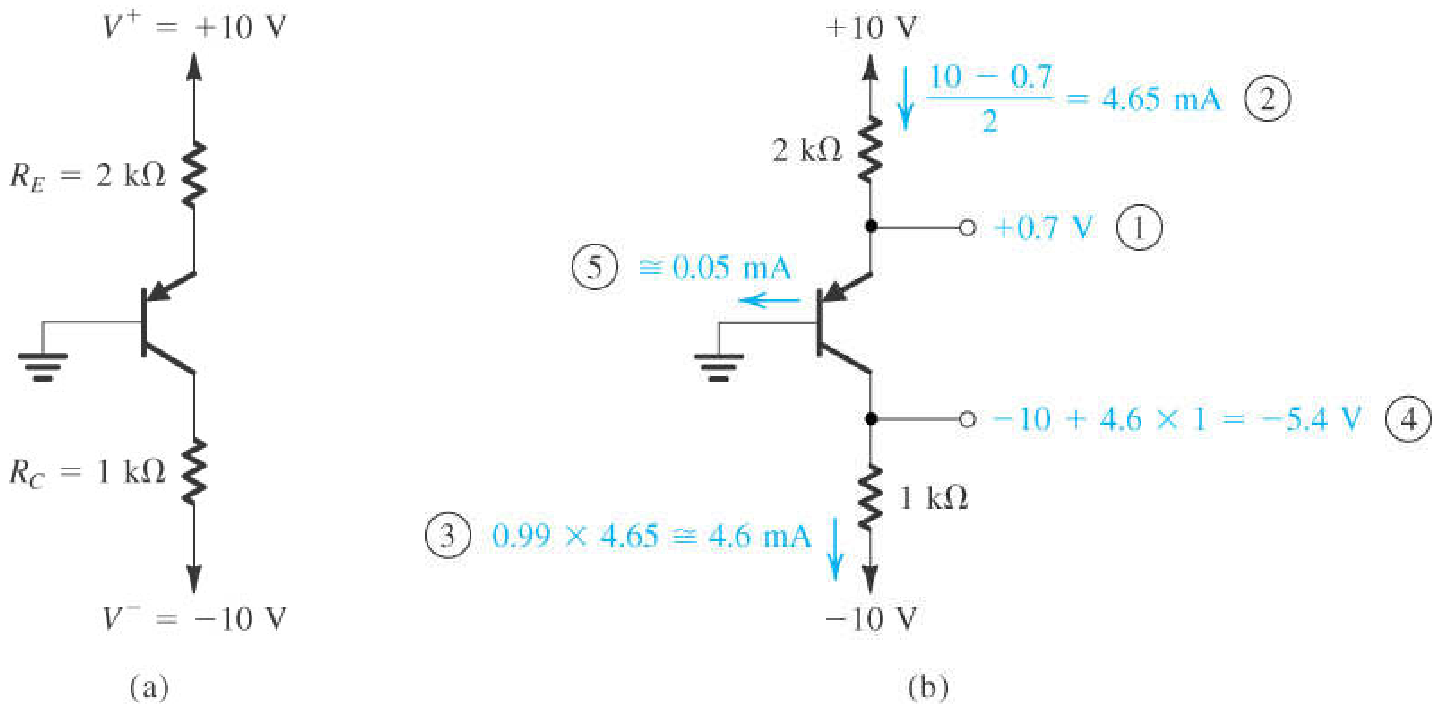

Figure 5.37 Example 5.7: **(a)** circuit; **(b)** analysis with the steps indicated by circled numbers.

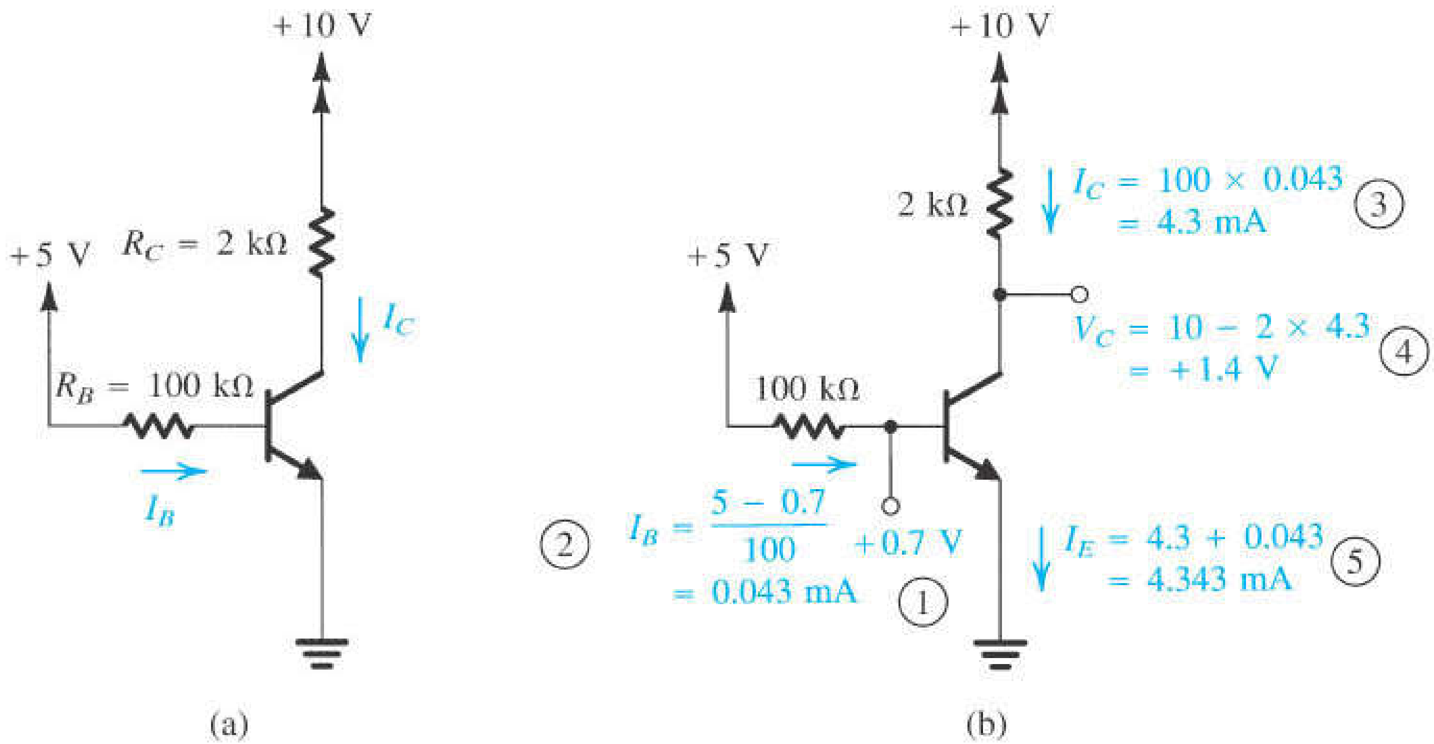

Figure 5.38 Example 5.8: **(a)** circuit; **(b)** analysis with the steps indicated by the circled numbers.

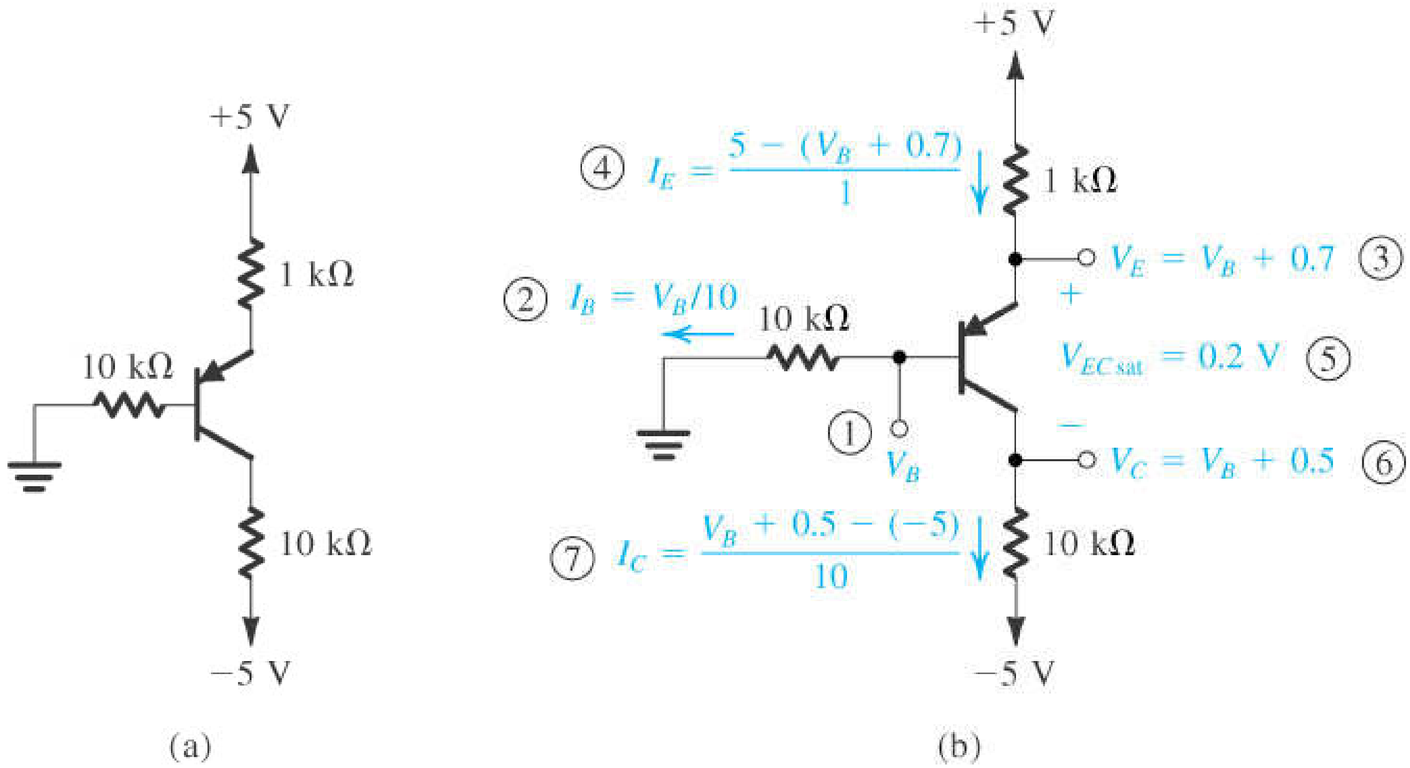

Figure 5.39 Example 5.9: **(a)** circuit; **(b)** analysis with steps numbered.

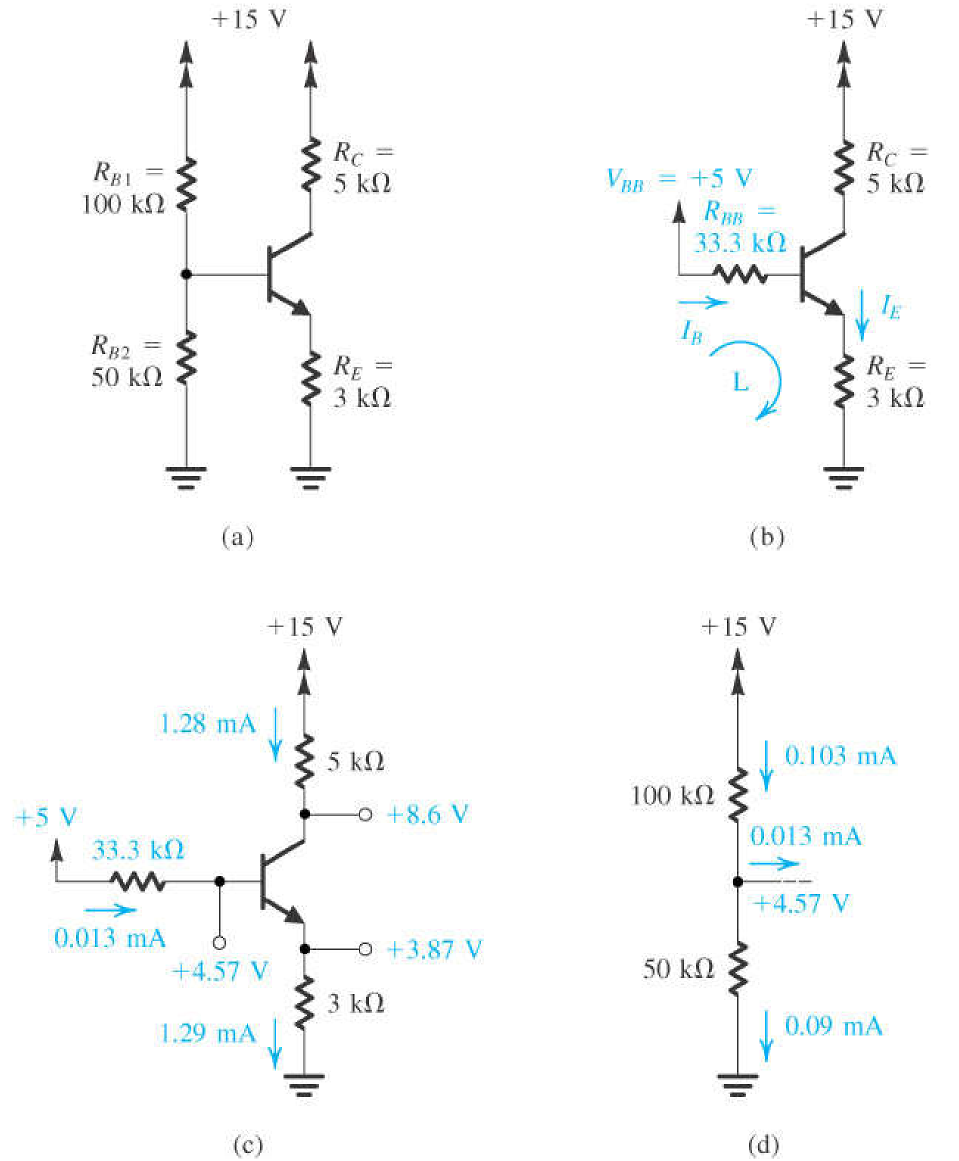

Figure 5.40 Circuits for Example 5.10.

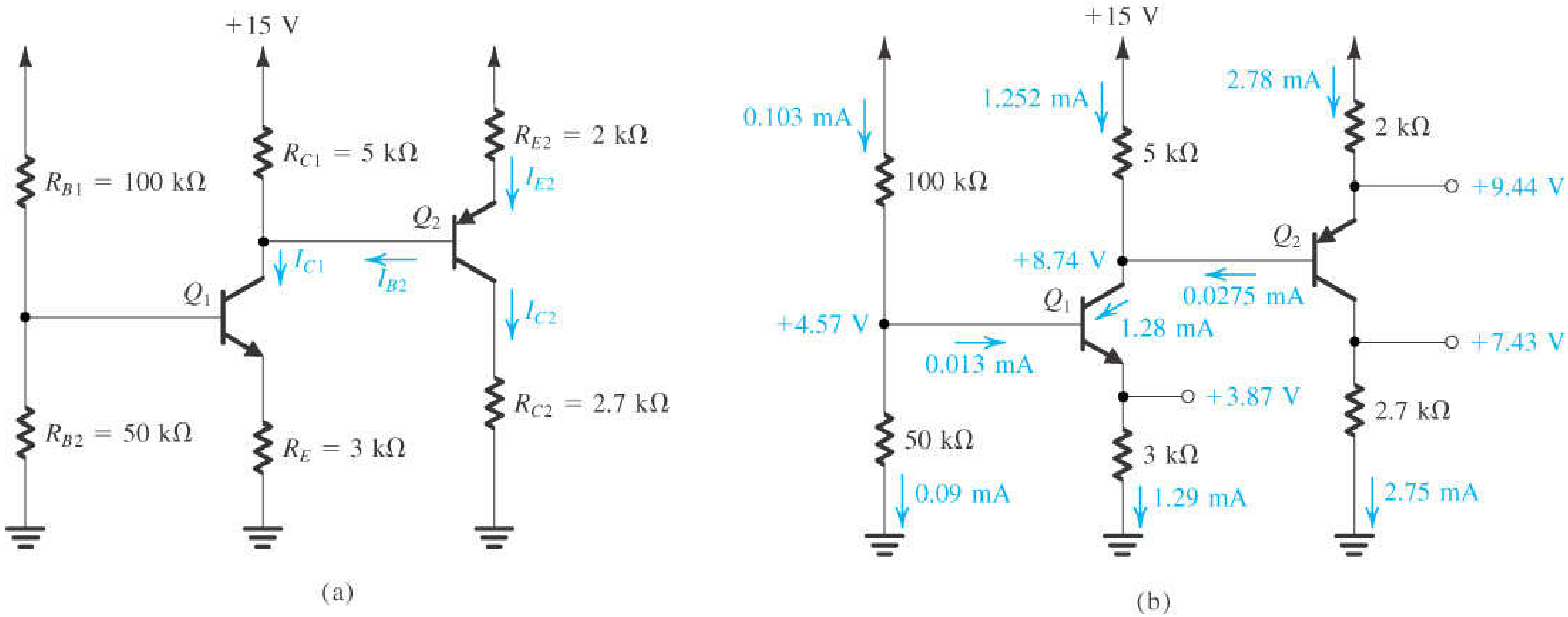

Figure 5.41 Circuits for Example 5.11.

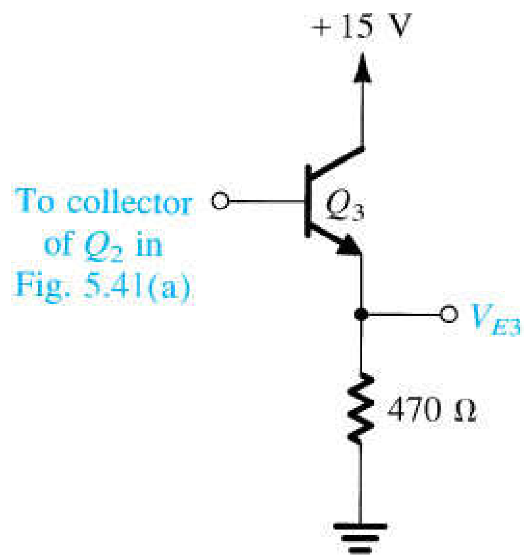

Figure E5.30

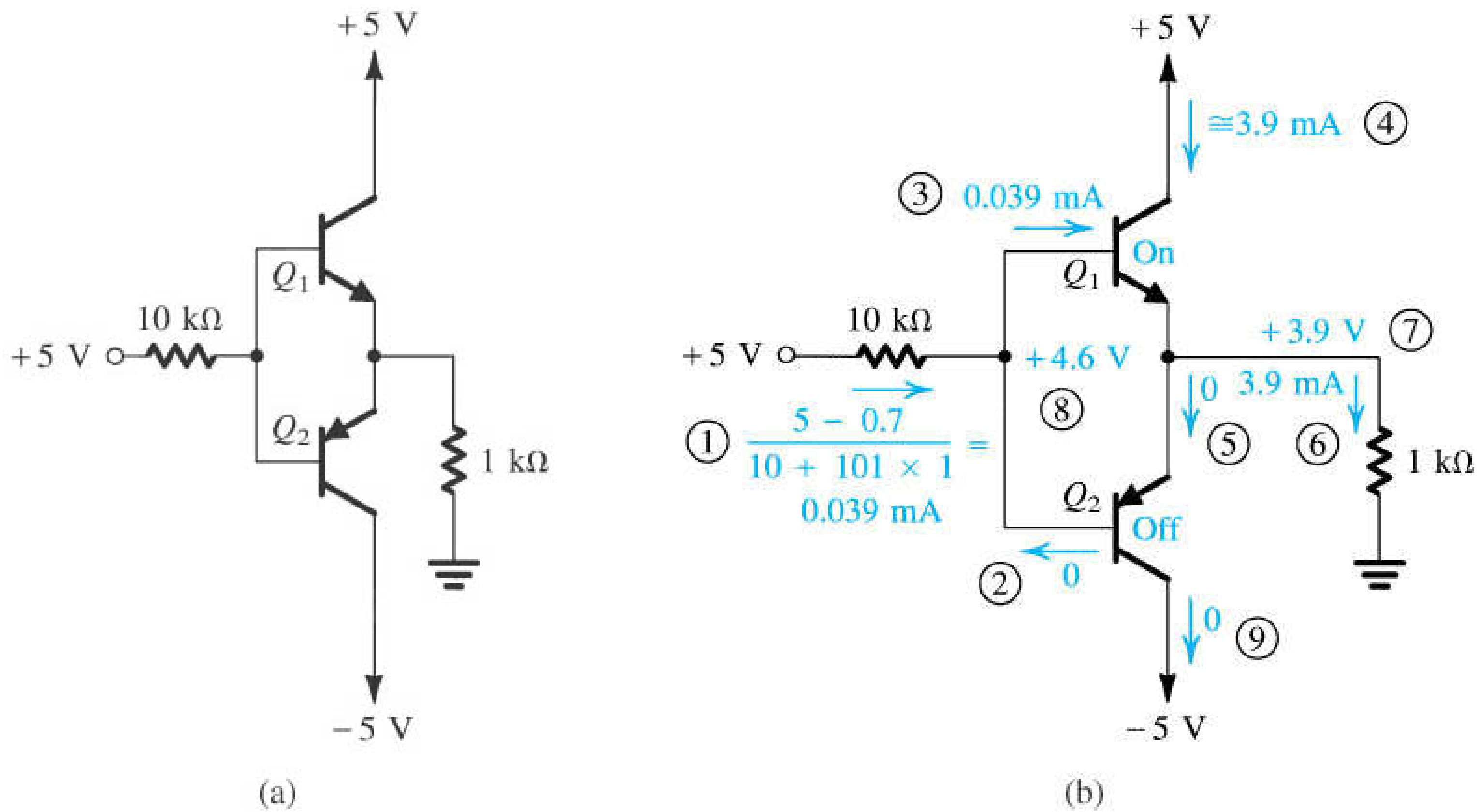

Figure 5.42 Example 5.12: **(a)** circuit; **(b)** analysis with the steps numbered.

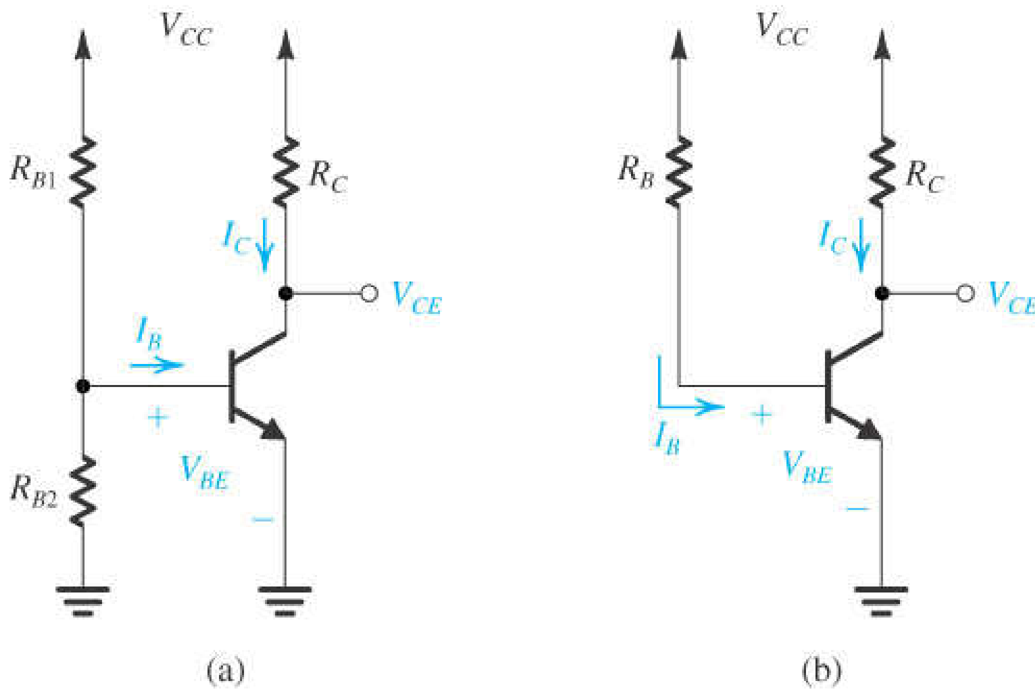

Figure 5.43 Two obvious schemes for biasing the BJT: **(a)** by fixing V_{BE}; **(b)** by fixing I_B. Both result in wide variations in I_C and hence in V_{CE} and therefore are considered to be "bad." Neither scheme is recommended.

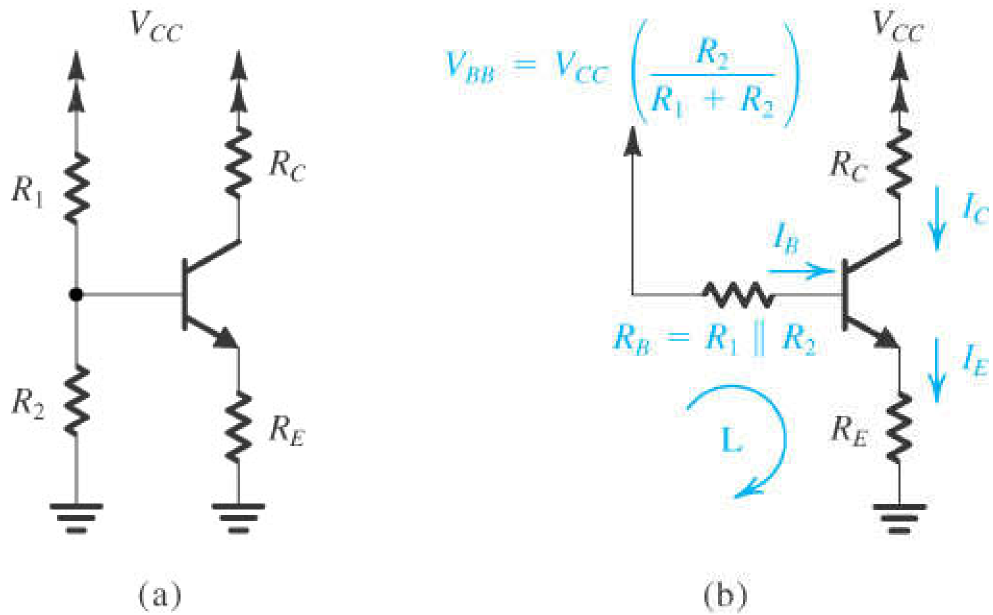

Figure 5.44 Classical biasing for BJTs using a single power supply: **(a)** circuit; **(b)** circuit with the voltage divider supplying the base replaced with its Thévenin equivalent.

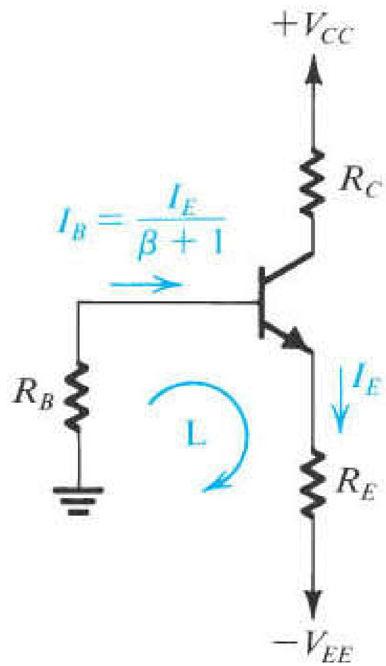

Figure 5.45 Biasing the BJT using two power supplies. Resistor R_B is needed only if the signal is to be capacitively coupled to the base. Otherwise, the base can be connected directly to ground, or to a grounded signal source, resulting in almost total β-independence of the bias current.

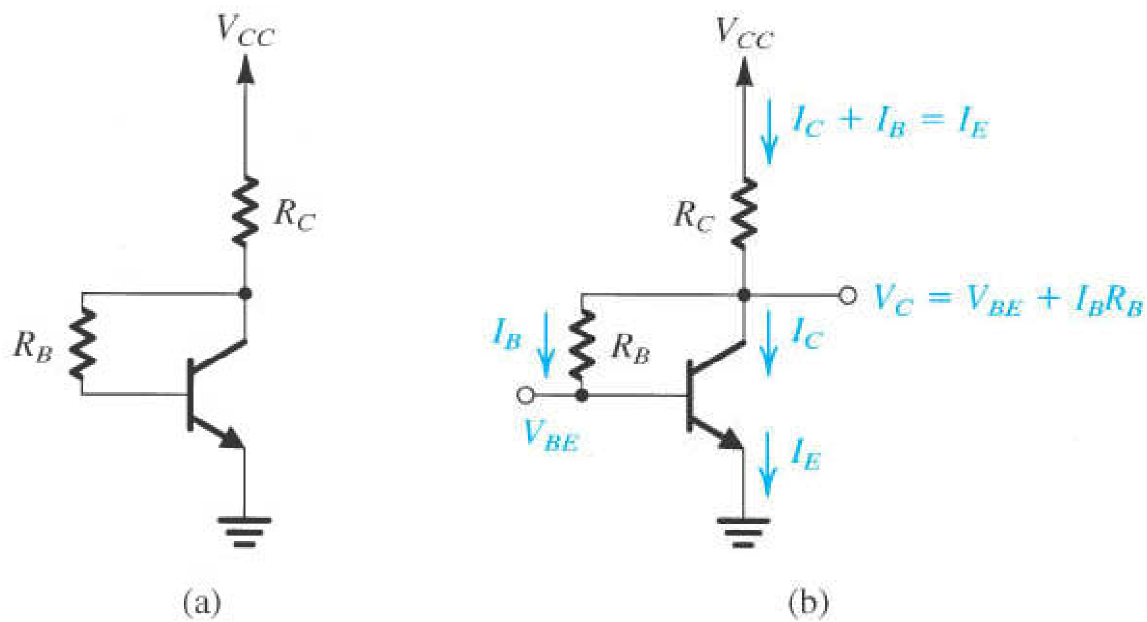

Figure 5.46 **(a)** A common-emitter transistor amplifier biased by a feedback resistor R_B. **(b)** Analysis of the circuit in (a).

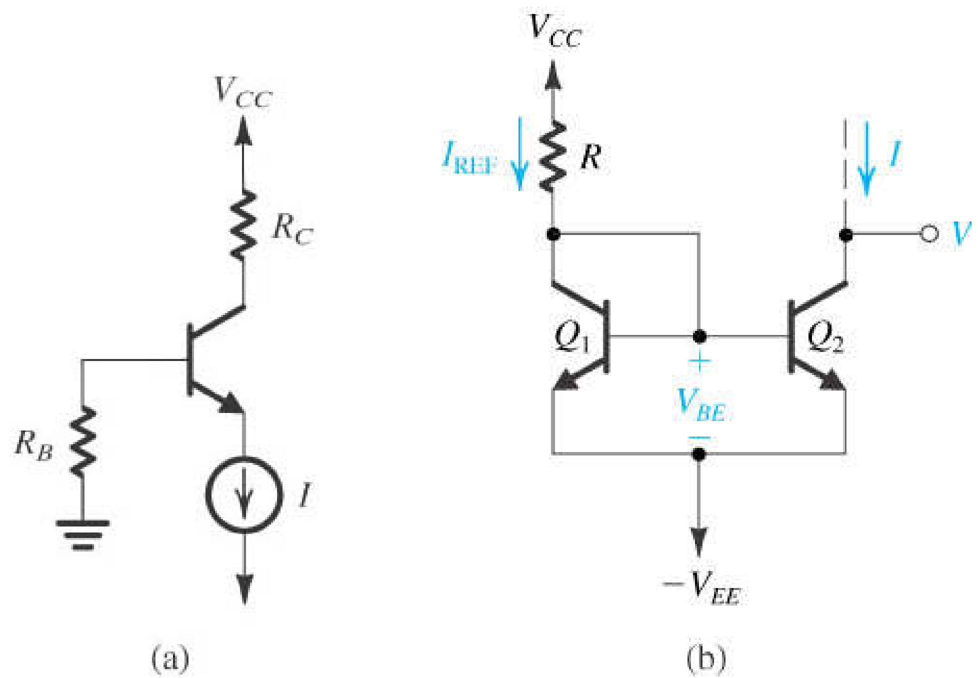

Figure 5.47 (a) A BJT biased using a constant-current source I. **(b)** Circuit for implementing the current source I.

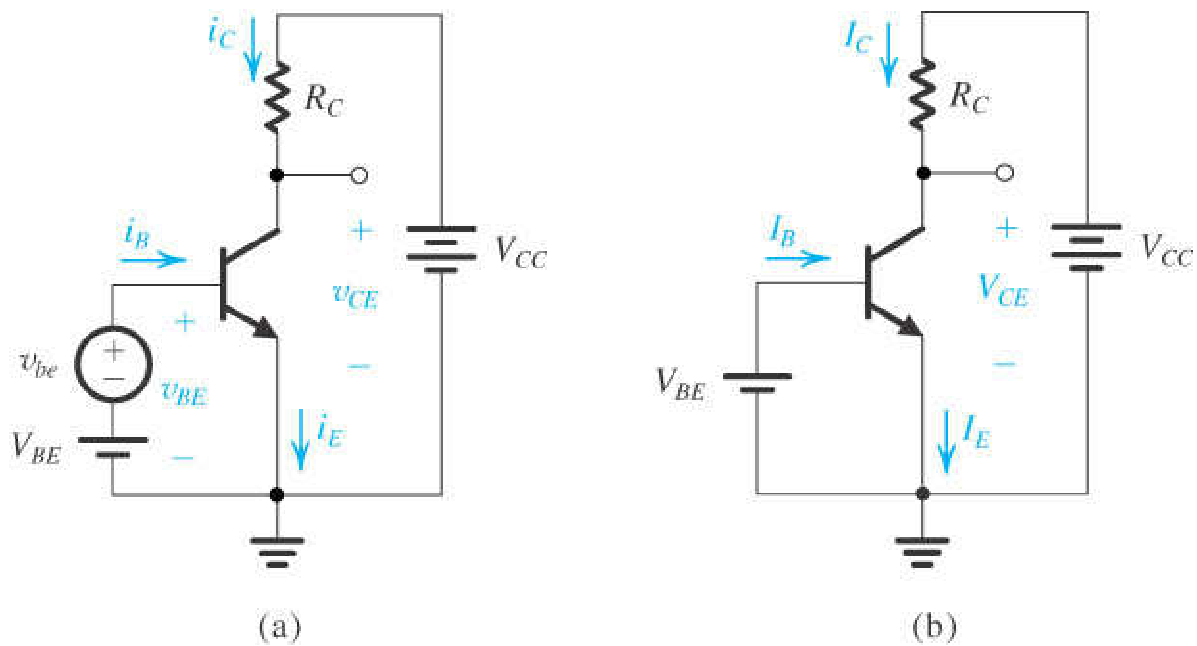

Figure 5.48 **(a)** Conceptual circuit to illustrate the operation of the transistor as an amplifier. **(b)** The circuit of (a) with the signal source v_{be} eliminated for dc (bias) analysis.

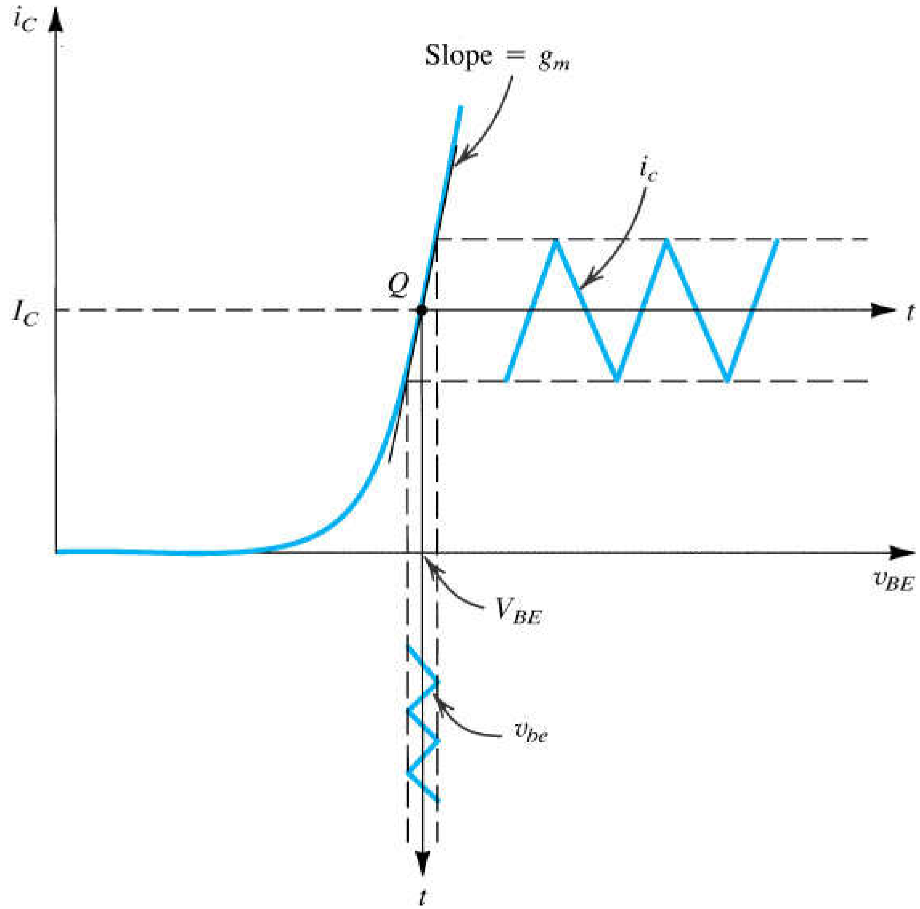

Figure 5.49 Linear operation of the transistor under the small-signal condition: A small signal v_{be} with a triangular waveform is superimposed on the dc voltage V_{BE}. It gives rise to a collector signal current i_c, also of triangular waveform, superimposed on the dc current I_C. Here, $i_c = g_m v_{be}$, where g_m is the slope of the i_C–v_{BE} curve at the bias point Q.

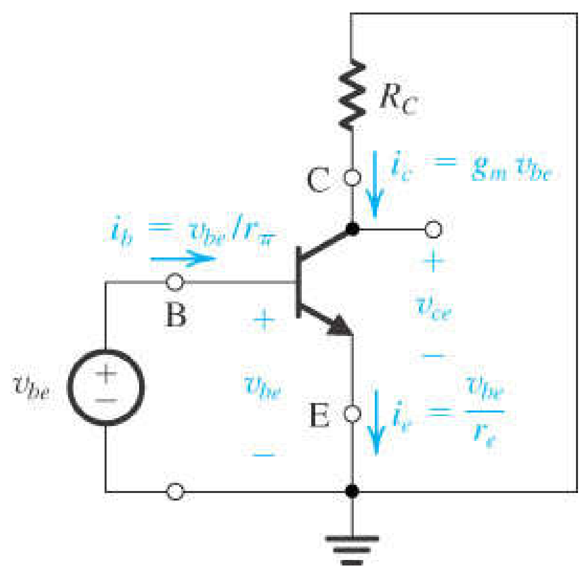

Figure 5.50 The amplifier circuit of Fig. 5.48(a) with the dc sources (V_{BE} and V_{CC}) eliminated (short circuited). Thus only the signal components are present. Note that this is a representation of the signal operation of the BJT and not an actual amplifier circuit.

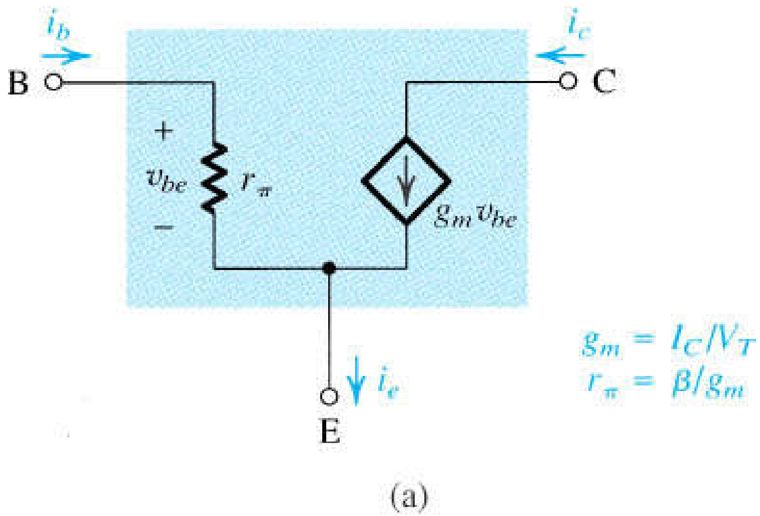

Figure 5.51 Two slightly different versions of the simplified hybrid-π model for the small-signal operation of the BJT. The equivalent circuit in **(a)** represents the BJT as a voltage-controlled current source (a transconductance amplifier), and that in **(b)** represents the BJT as a current-controlled current source (a current amplifier).

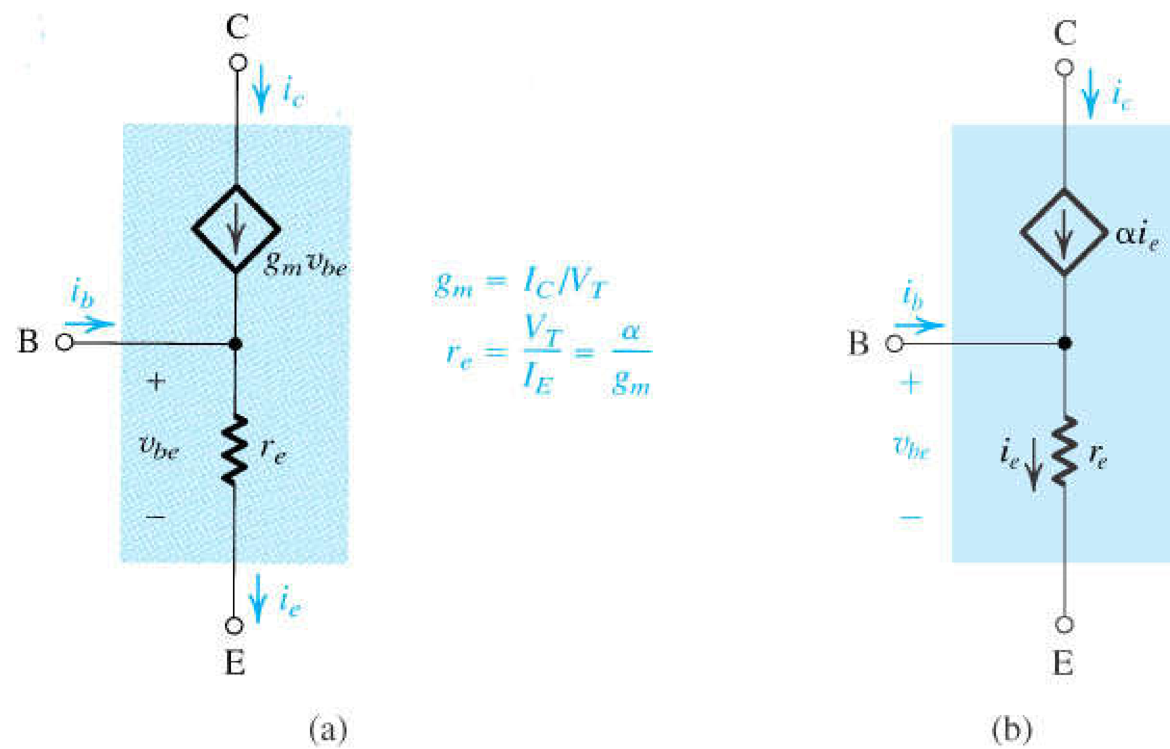

Figure 5.52 Two slightly different versions of what is known as the *T model* of the BJT. The circuit in **(a)** is a voltage-controlled current source representation and that in **(b)** is a current-controlled current source representation. These models explicitly show the emitter resistance r_e rather than the base resistance r_π featured in the hybrid-π model.

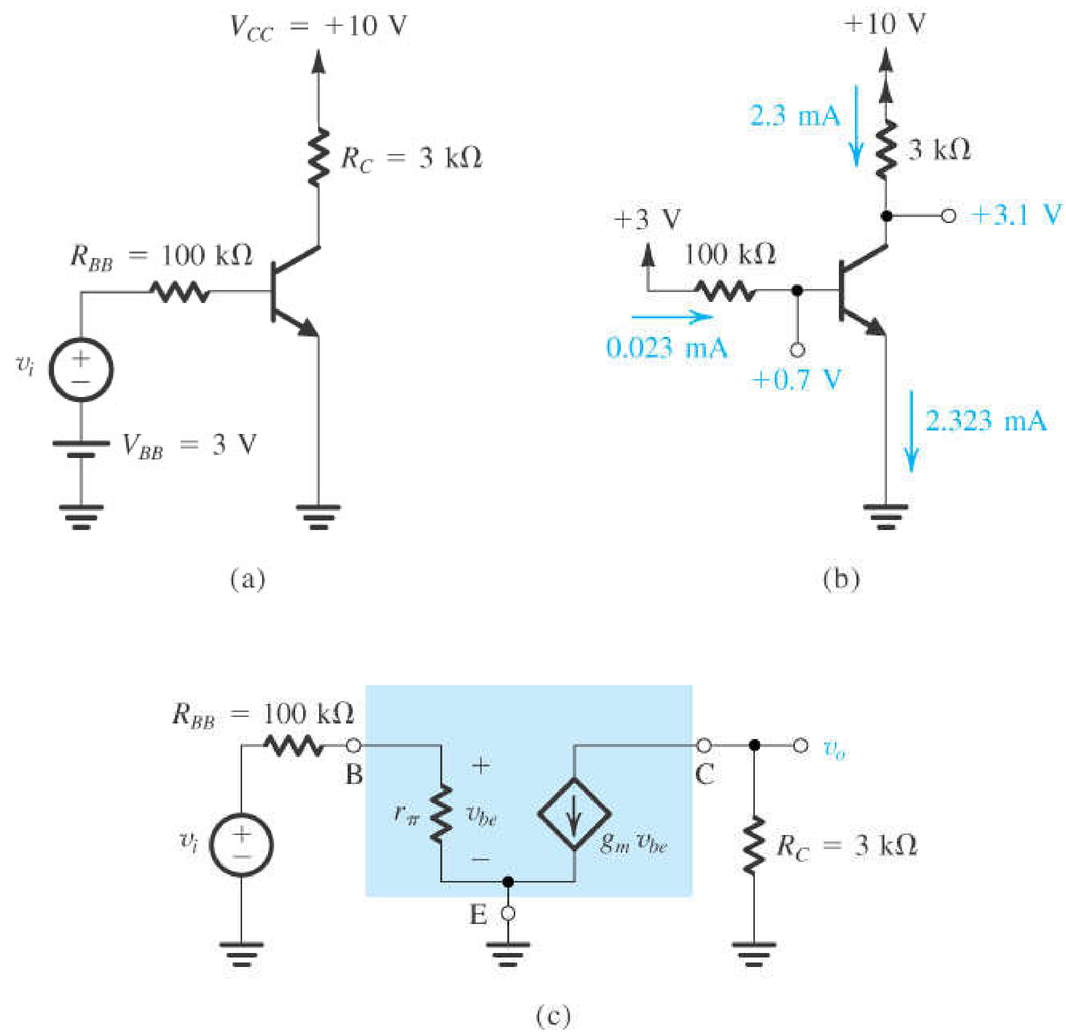

Figure 5.53 Example 5.14: **(a)** circuit; **(b)** dc analysis; **(c)** small-signal model.

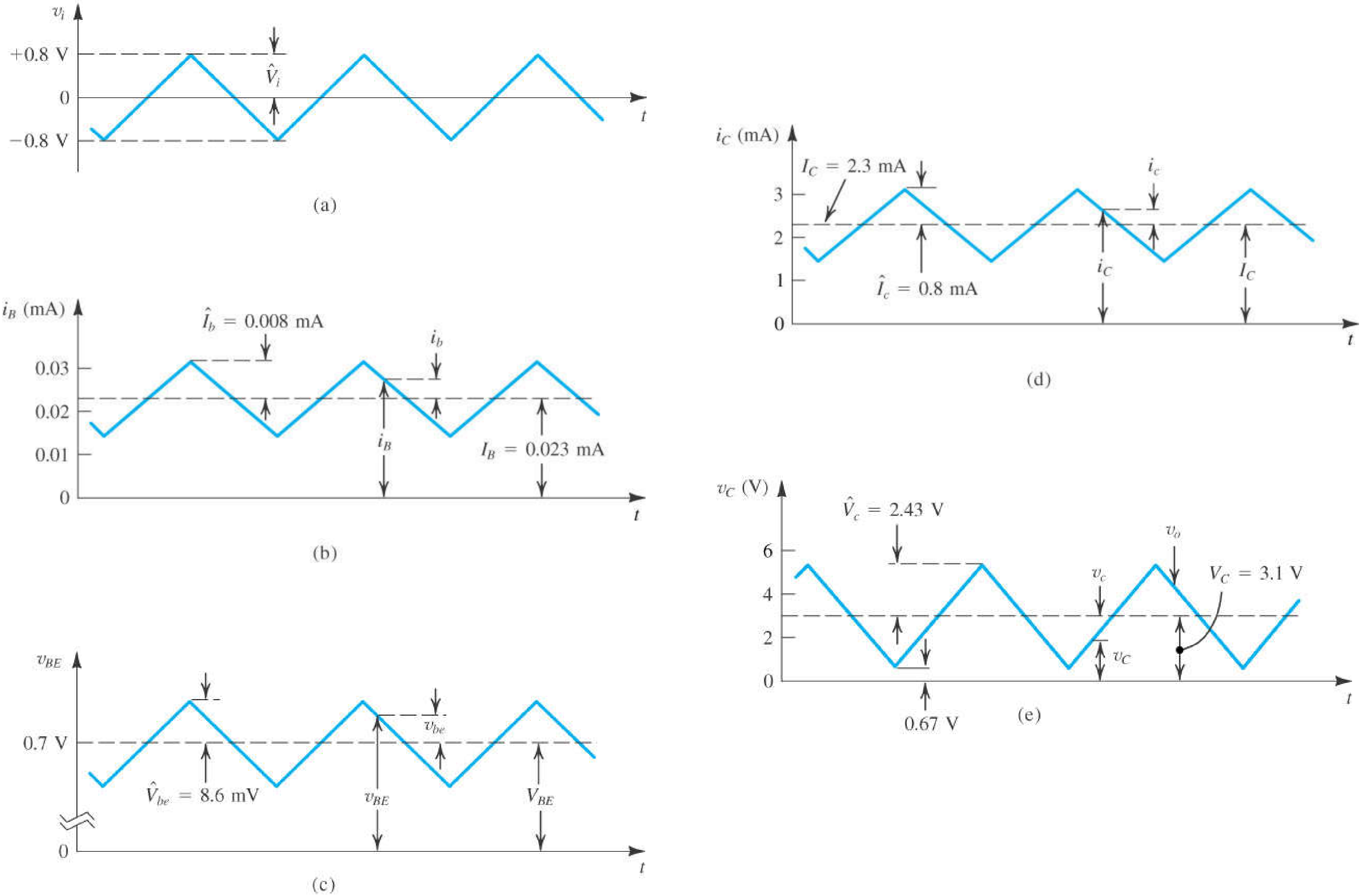

Figure 5.54 Signal waveforms in the circuit of Fig. 5.53.

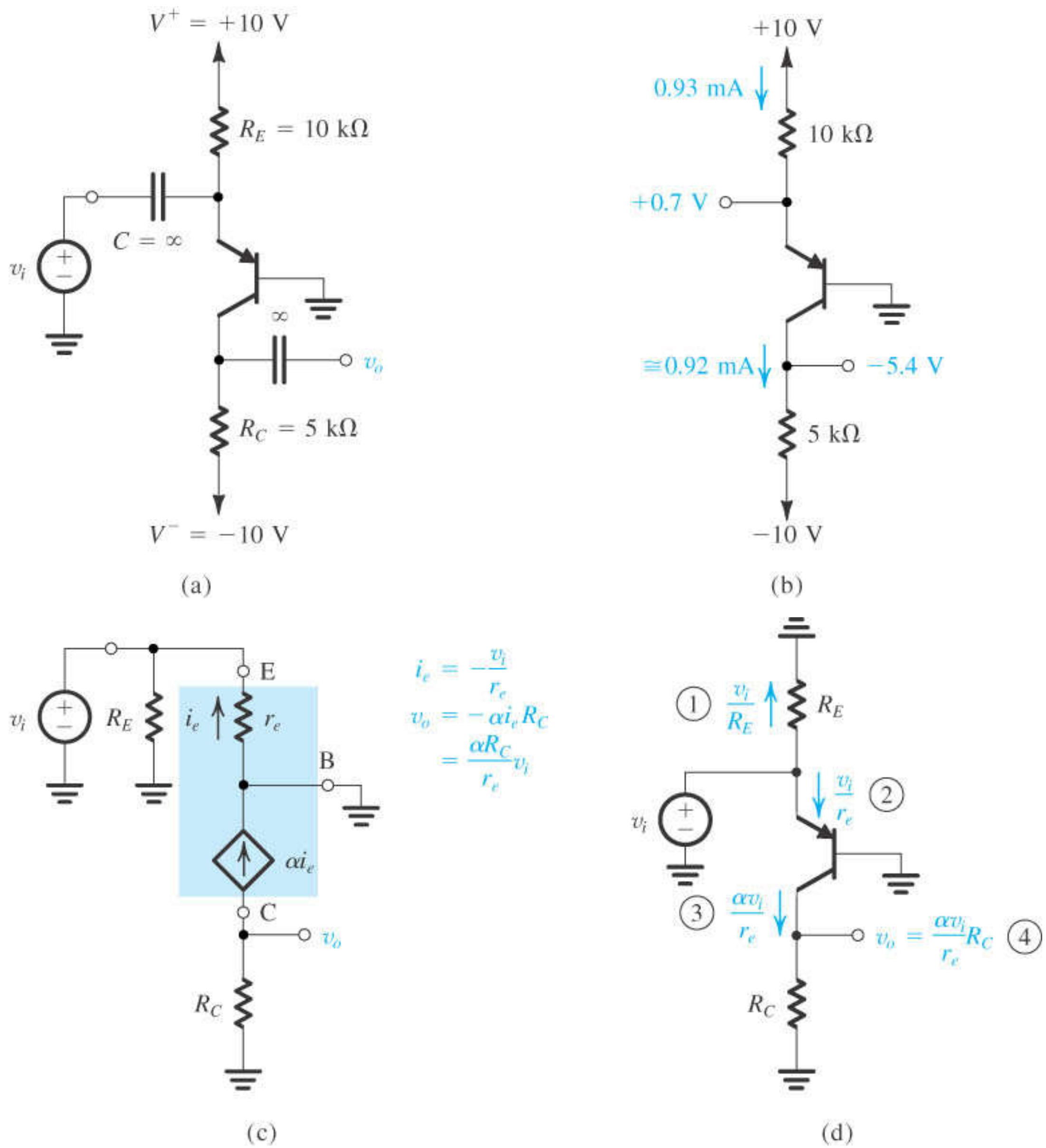

Figure 5.55 Example 5.16: **(a)** circuit; **(b)** dc analysis; **(c)** small-signal model; **(d)** small-signal analysis performed directly on the circuit.

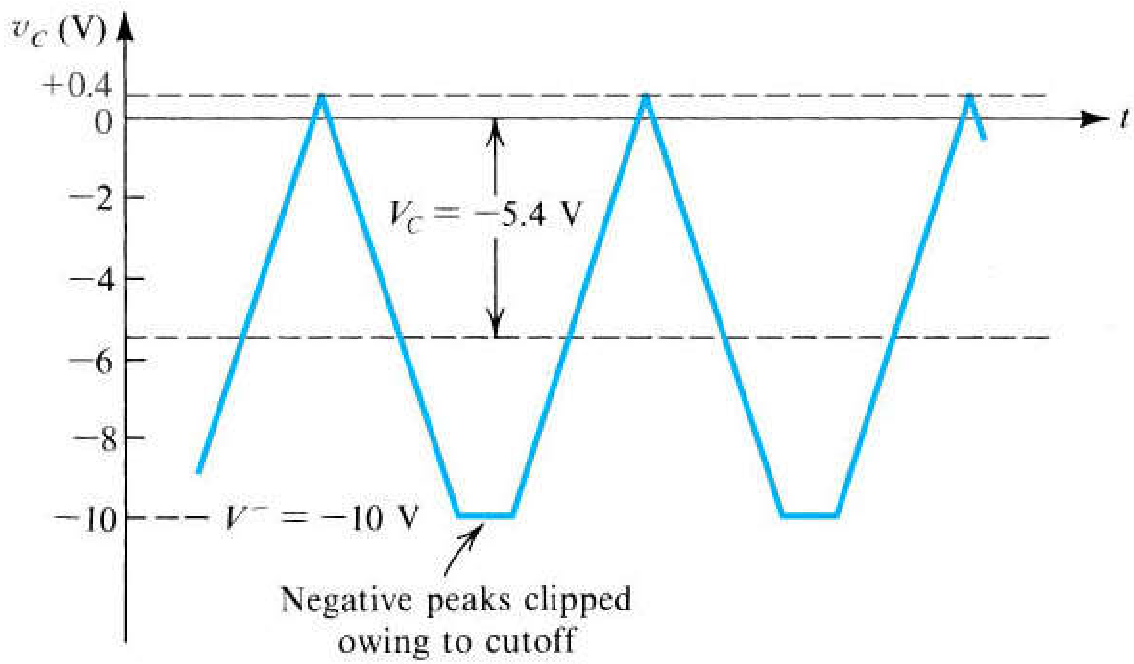

Figure 5.56 Distortion in output signal due to transistor cutoff. Note that it is assumed that no distortion due to the transistor nonlinear characteristics is occurring.

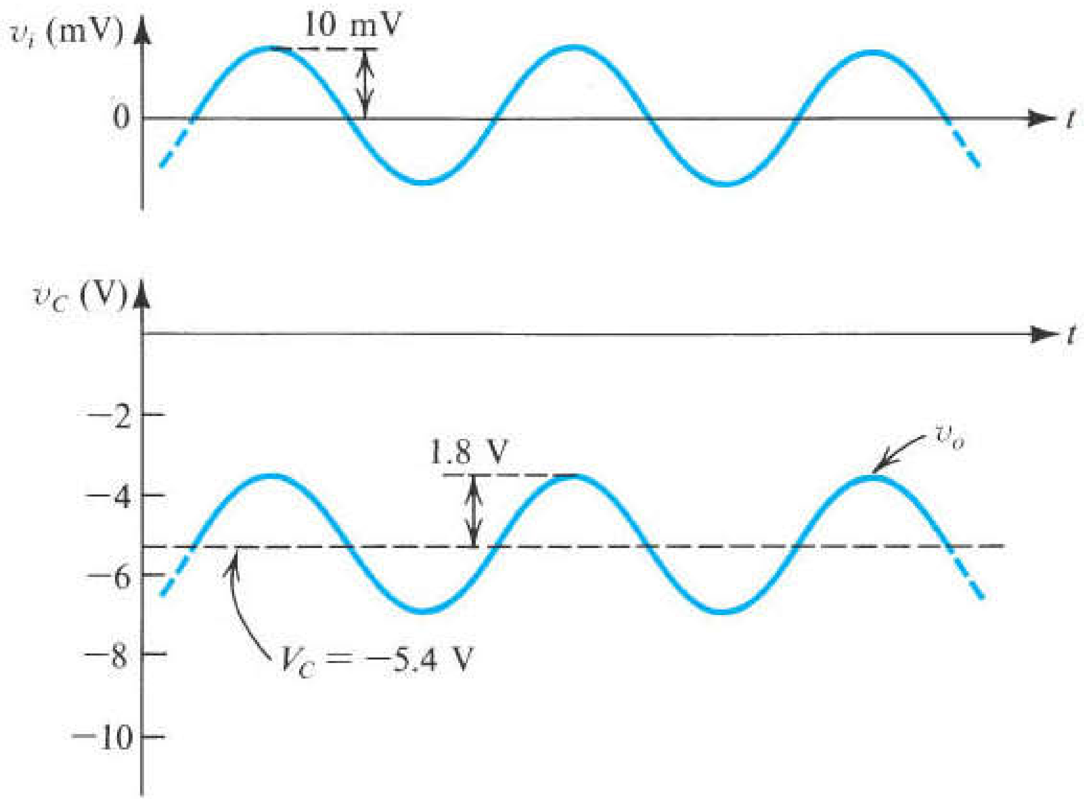

Figure 5.57 Input and output waveforms for the circuit of Fig. 5.55. Observe that this amplifier is noninverting, a property of the common-base configuration.

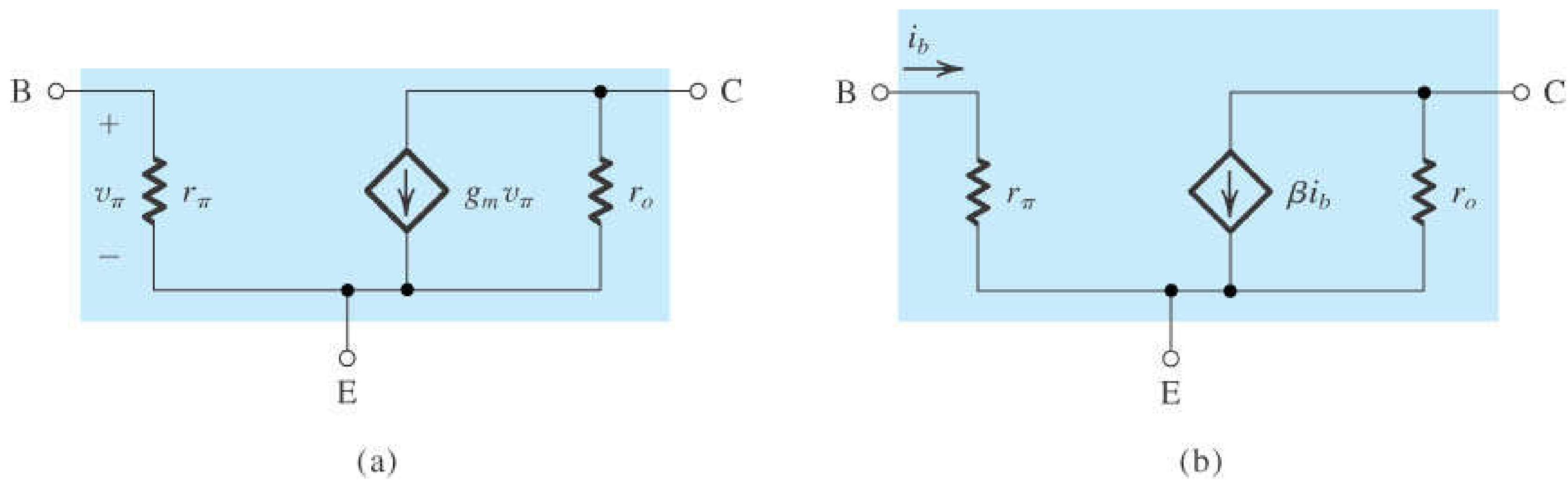

Figure 5.58 The hybrid-π small-signal model, in its two versions, with the resistance r_o included.

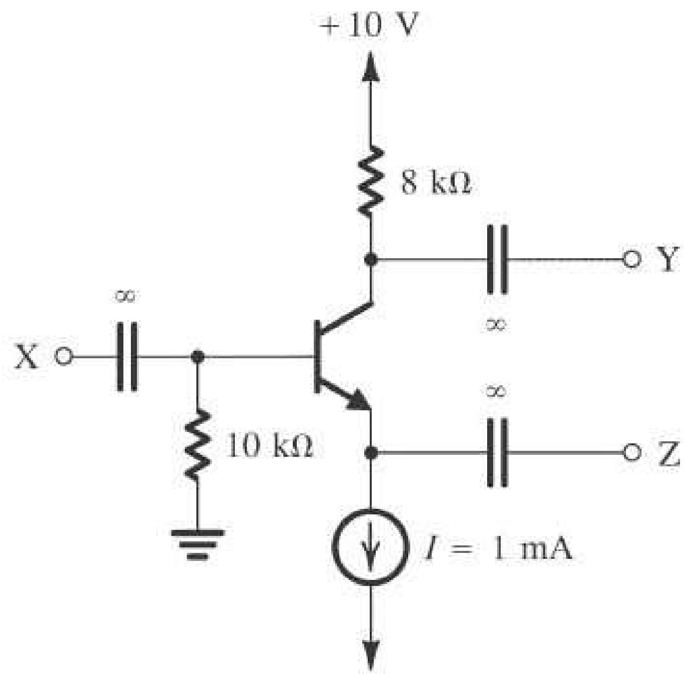

Figure E5.40

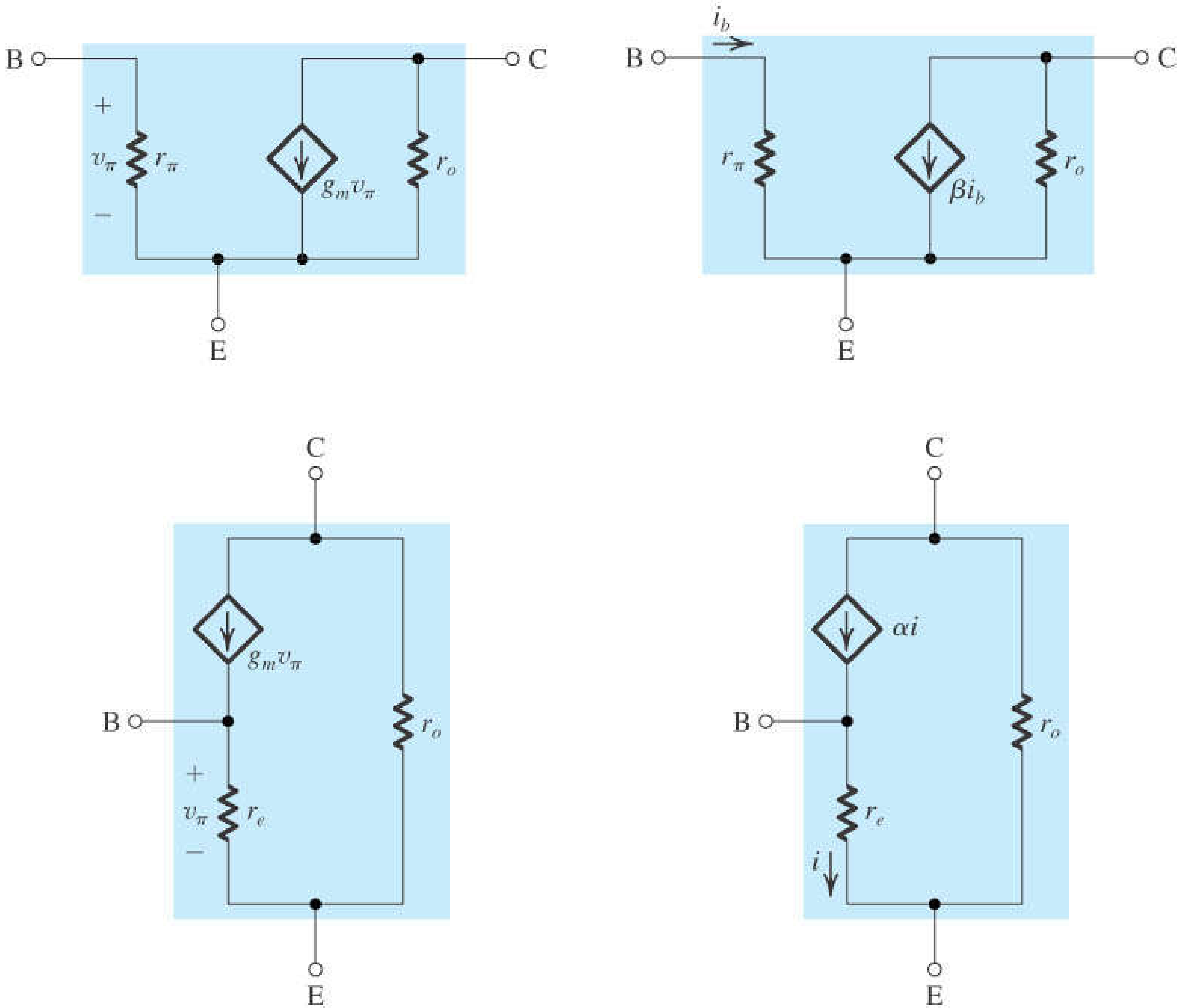

Table 5.4

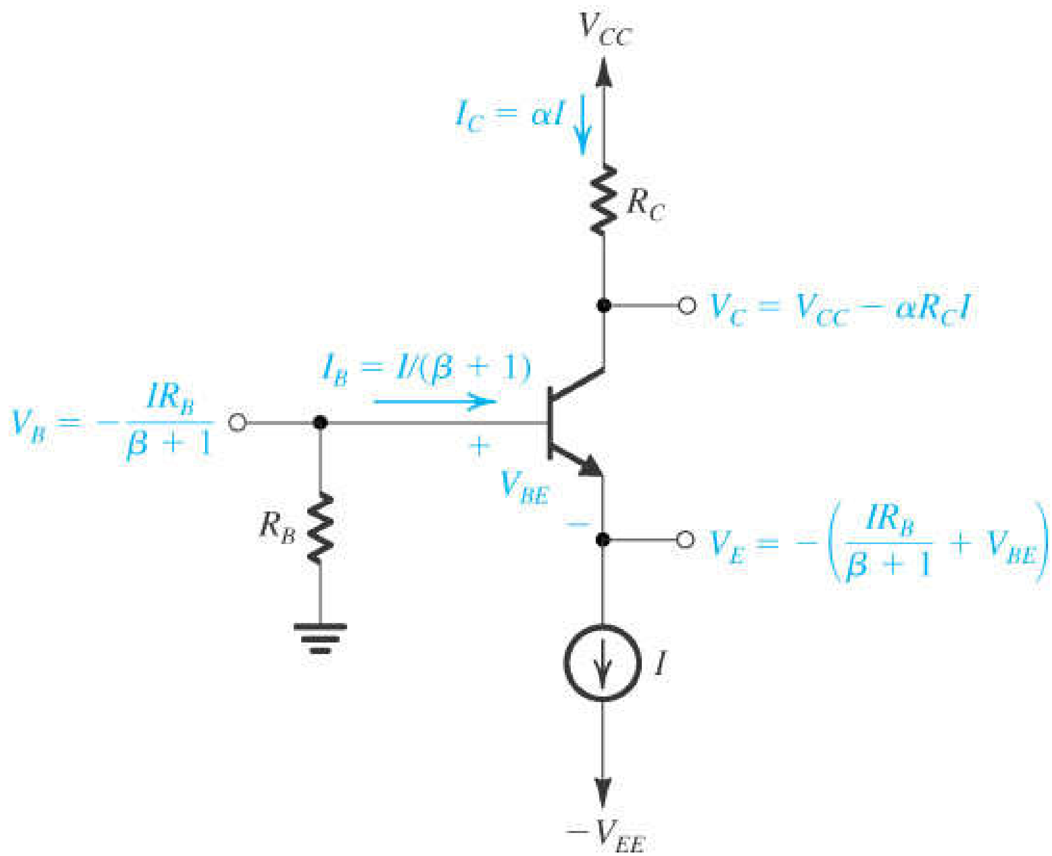

Figure 5.59 Basic structure of the circuit used to realize single-stage, discrete-circuit BJT amplifier configurations.

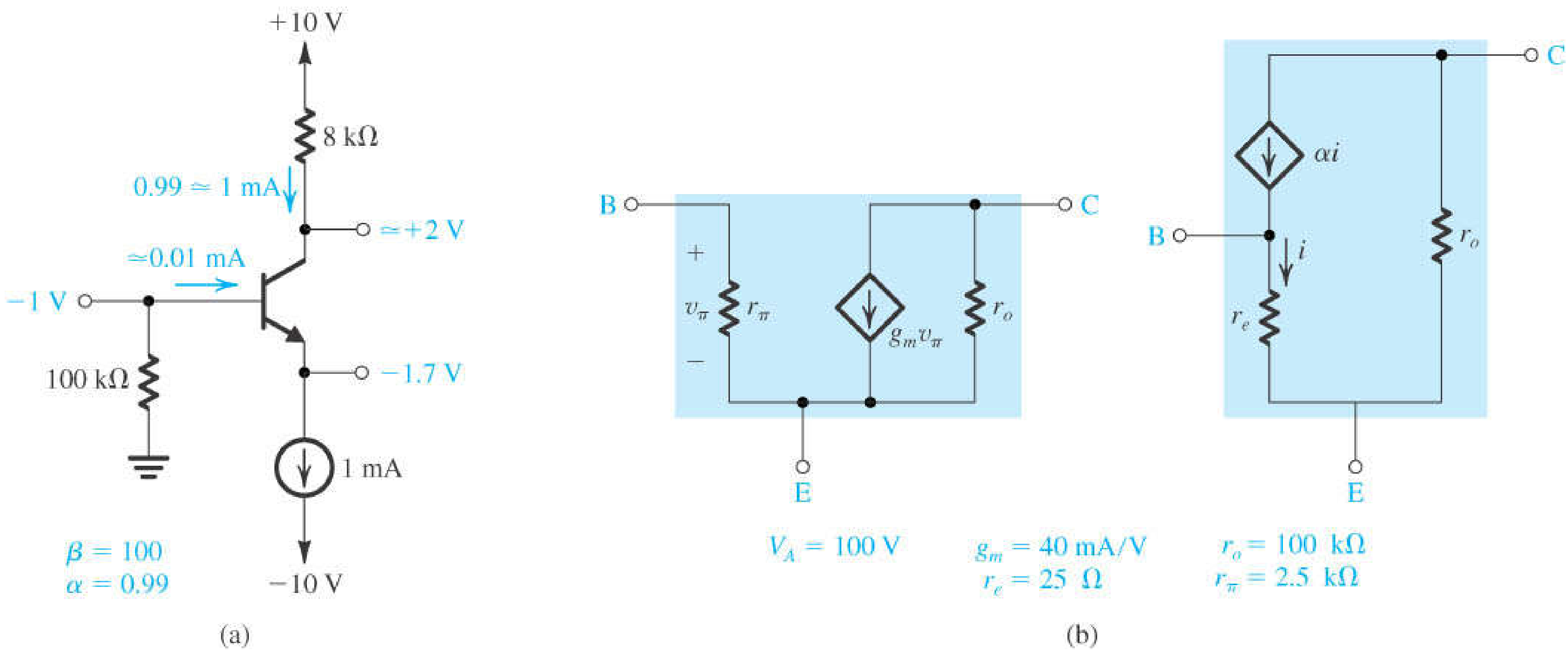
+10 V
8 kΩ
0.99 ≃ 1 mA
≃+2 V
≃0.01 mA
−1 V
100 kΩ
−1.7 V
1 mA
β = 100
α = 0.99
−10 V
(a)
B
C
+
v_π
r_π
$g_m v_\pi$
r_o
−
E
αi
i
r_e
r_o
B
C
E
V_A = 100 V
g_m = 40 mA/V
r_e = 25 Ω
r_o = 100 kΩ
r_π = 2.5 kΩ
(b)

Figure E5.41

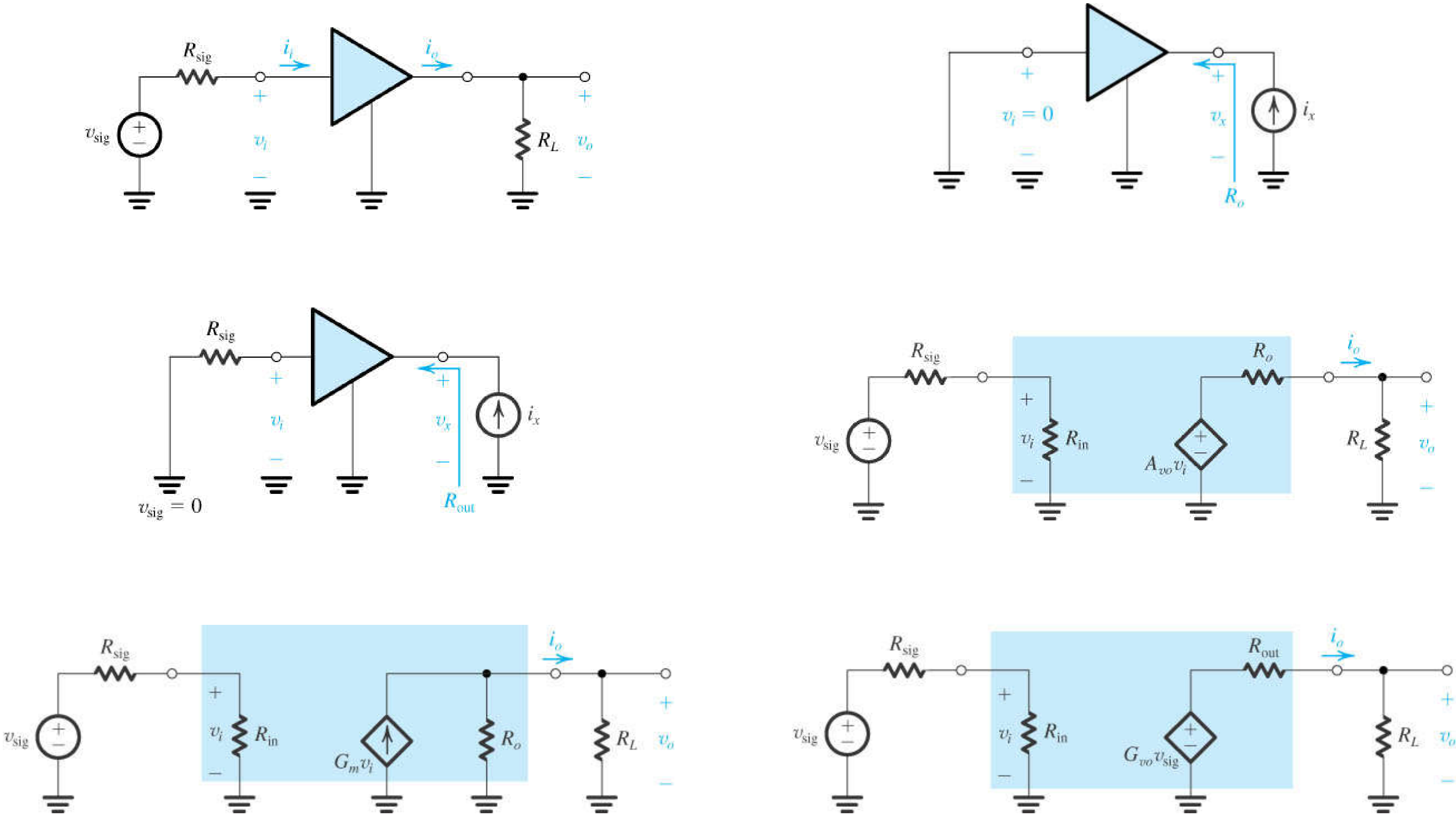
R_{sig}
i_i
i_o
v_{sig}
v_i
R_L
v_o
$v_i = 0$
v_x
i_x
R_o
$v_{sig} = 0$
R_{out}
R_{in}
$A_{vo}v_i$
$G_m v_i$
$G_{vo}v_{sig}$

Table 5.5

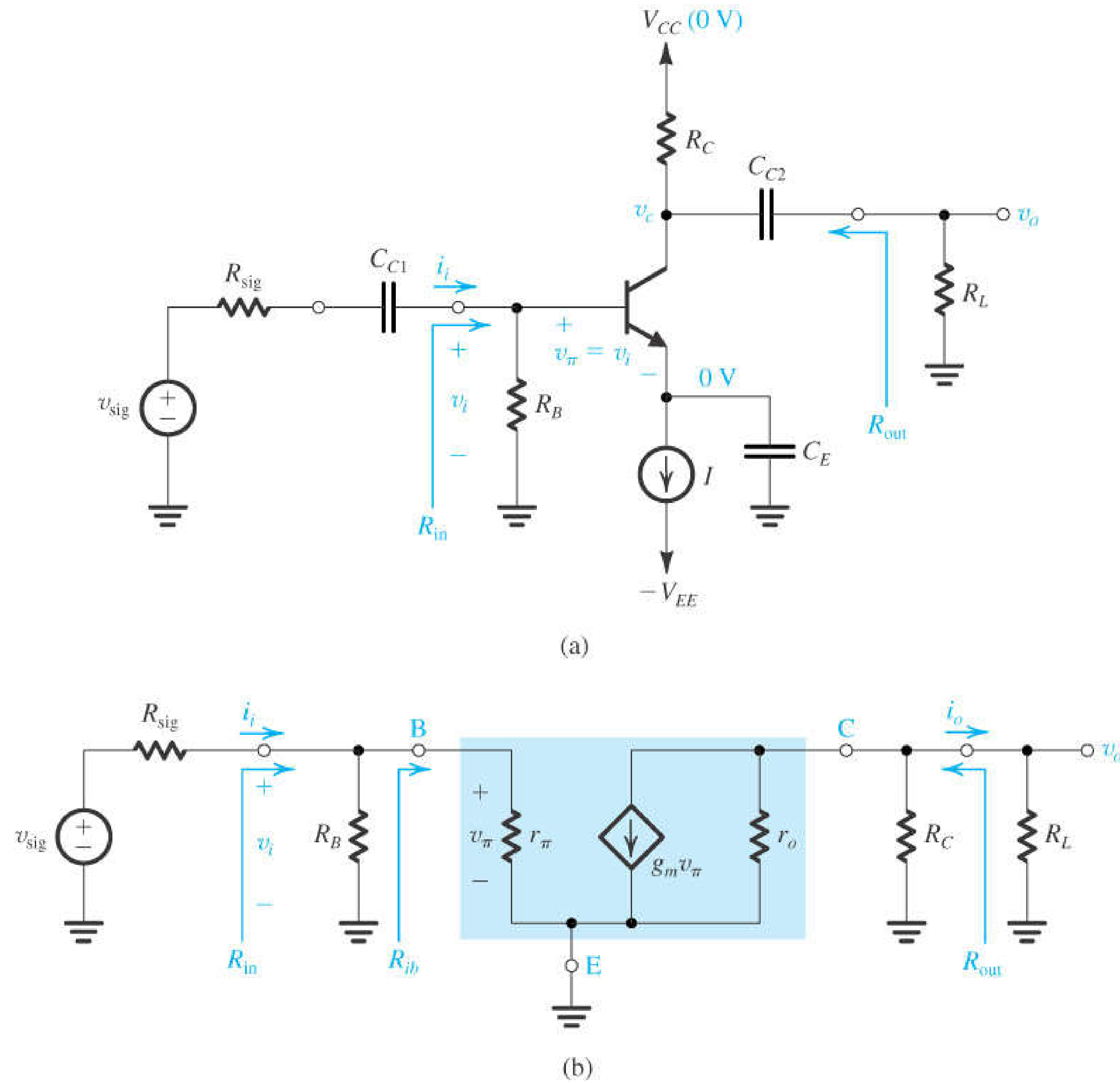

Figure 5.60 **(a)** A common-emitter amplifier using the structure of Fig. 5.59. **(b)** Equivalent circuit obtained by replacing the transistor with its hybrid-π model.

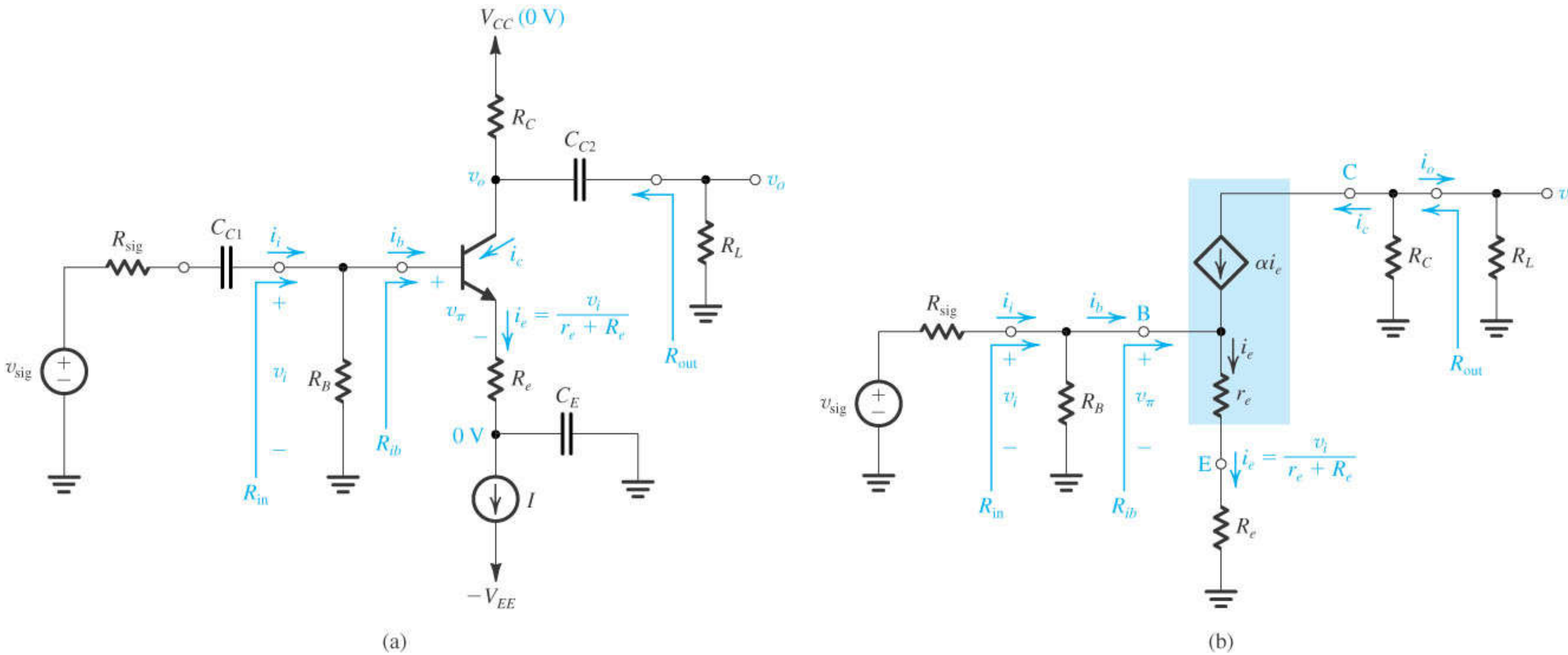

Figure 5.61 **(a)** A common-emitter amplifier with an emitter resistance R_e. **(b)** Equivalent circuit obtained by replacing the transistor with its T model.

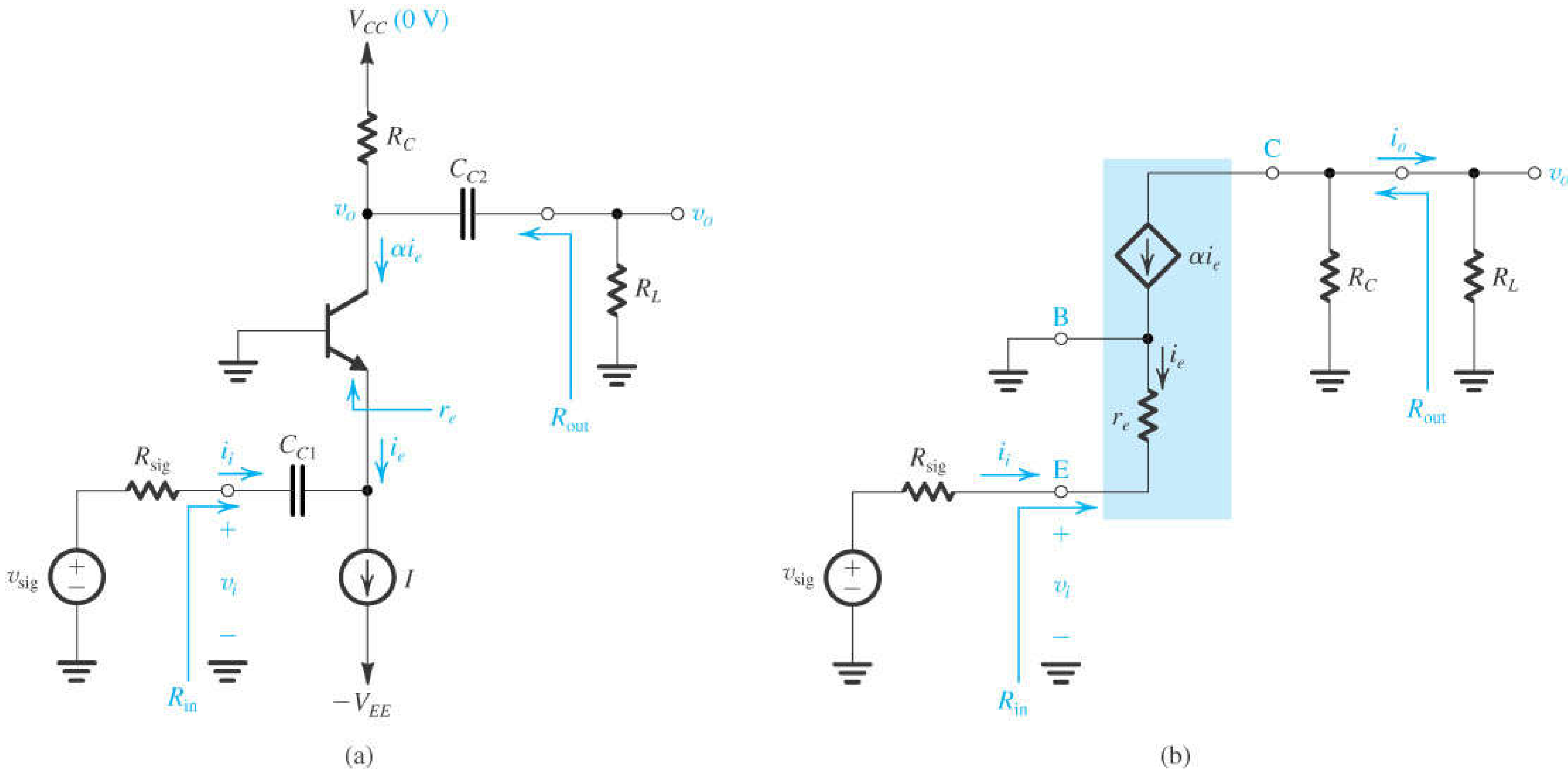

Figure 5.62 **(a)** A common-base amplifier using the structure of Fig. 5.59. **(b)** Equivalent circuit obtained by replacing the transistor with its T model.

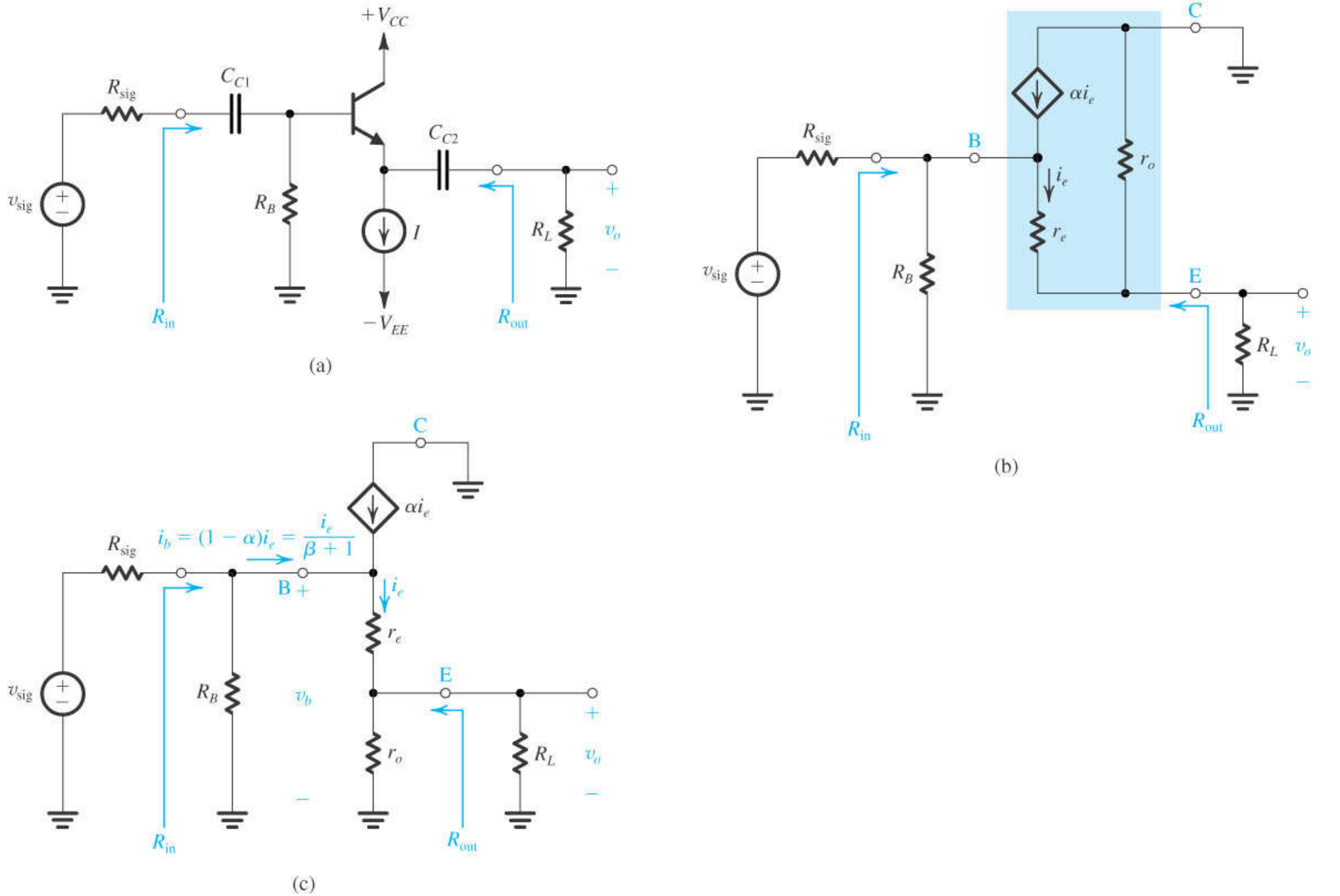

Figure 5.63 **(a)** An emitter-follower circuit based on the structure of Fig. 5.59. **(b)** Small-signal equivalent circuit of the emitter follower with the transistor replaced by its T model augmented with r_o. **(c)** The circuit in (b) redrawn to emphasize that r_o is in parallel with R_L. This simplifies the analysis considerably.

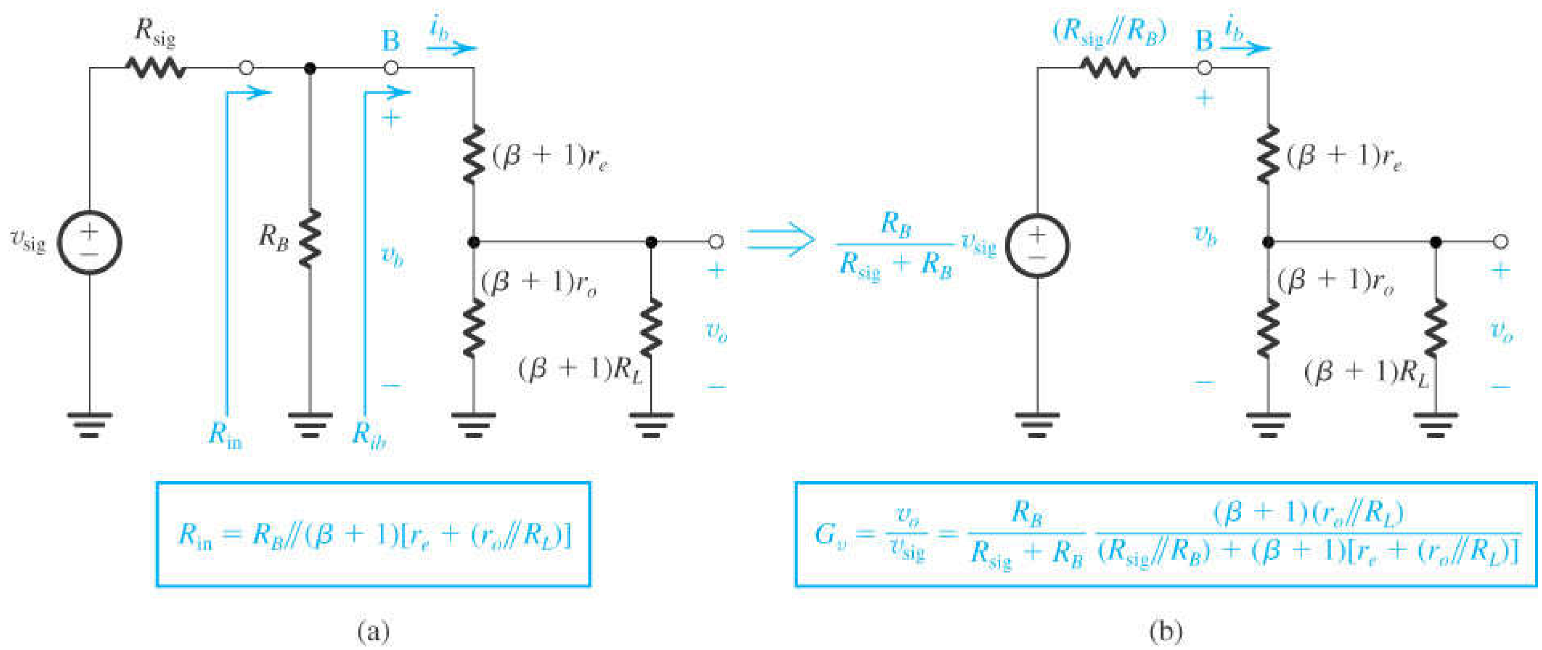

Figure 5.64 **(a)** An equivalent circuit of the emitter follower obtained from the circuit in Fig. 5.63(c) by reflecting all resistances in the emitter to the base side. **(b)** The circuit in (a) after application of Thévenin theorem to the input circuit composed of v_{sig}, R_{sig}, and R_B.

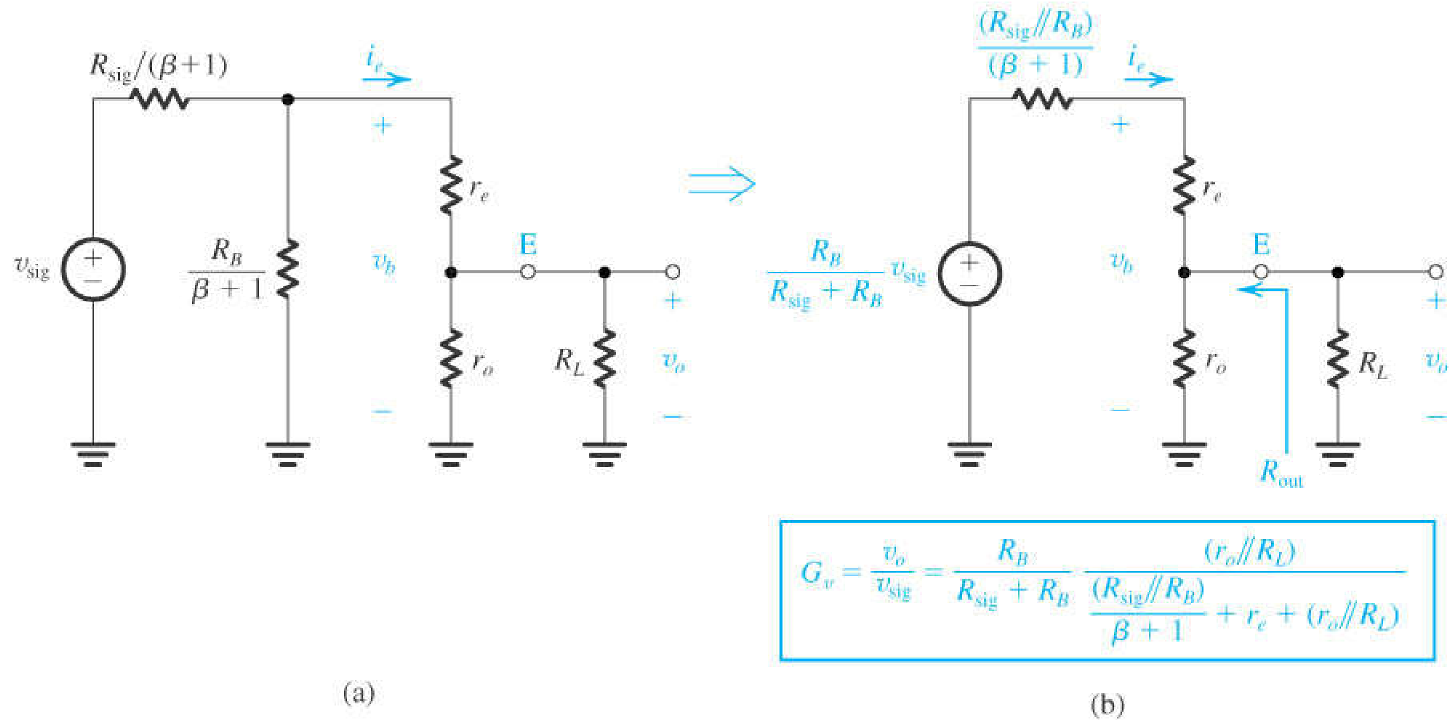

Figure 5.65 **(a)** An alternate equivalent circuit of the emitter follower obtained by reflecting all base-circuit resistances to the emitter side. **(b)** The circuit in (a) after application of Thévenin theorem to the input circuit composed of v_{sig}, R_{sig} / (β + 1), and R_B / (β + 1).

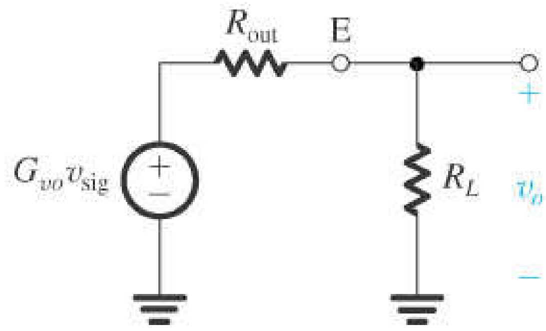

$$G_{vo} = \frac{R_B}{R_{sig} + R_B} \frac{r_o}{\frac{(R_{sig} /\!/ R_B)}{(\beta + 1)} + r_e + r_o}$$

$$R_{out} = r_o /\!/ \left(r_e + \frac{R_{sig} /\!/ R_B}{\beta + 1} \right)$$

Figure 5.66 Thévenin equivalent circuit of the output of the emitter follower of Fig. 5.63(a). This circuit can be used to find v_o and hence the overall voltage gain v_o/v_{sig} for any desired R_L.

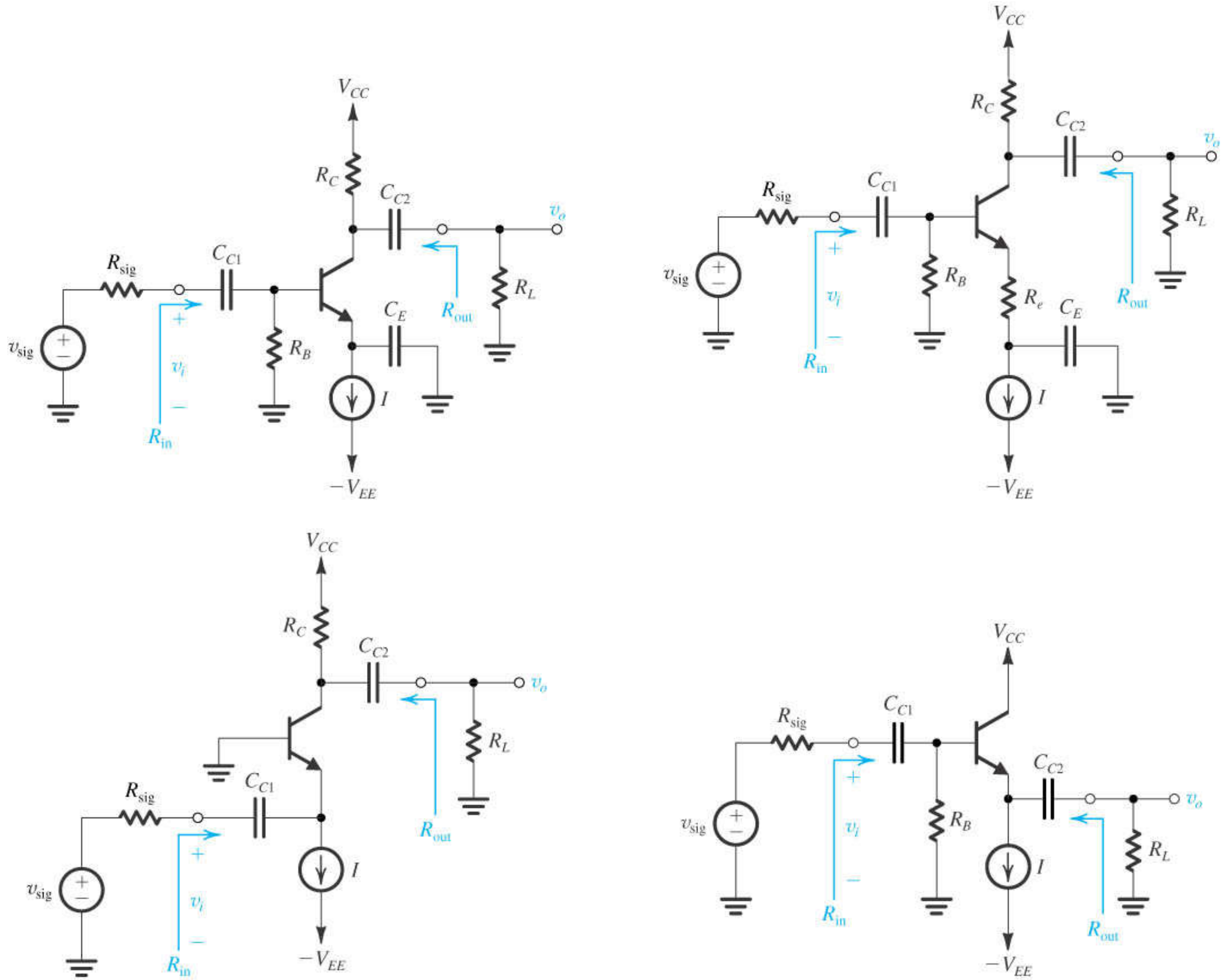
V_{CC}
R_C
C_{C2}
v_o
R_{sig}
C_{C1}
v_{sig}
v_i
R_B
C_E
R_L
R_{out}
R_{in}
I
$-V_{EE}$
V_{CC}
R_C
C_{C2}
v_o
R_{sig}
C_{C1}
v_{sig}
v_i
R_B
R_e
C_E
R_L
R_{out}
R_{in}
I
$-V_{EE}$
V_{CC}
R_C
C_{C2}
v_o
R_L
R_{sig}
C_{C1}
v_{sig}
v_i
R_{in}
R_{out}
I
$-V_{EE}$
V_{CC}
R_{sig}
C_{C1}
C_{C2}
v_o
v_{sig}
v_i
R_B
R_L
R_{in}
R_{out}
I
$-V_{EE}$

Table 5.6

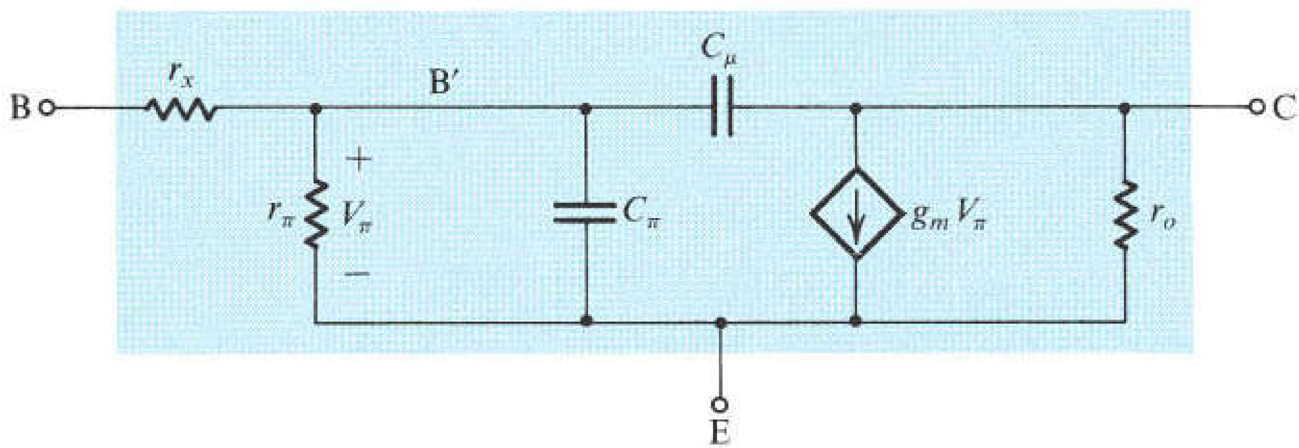

Figure 5.67 The high-frequency hybrid-π model.

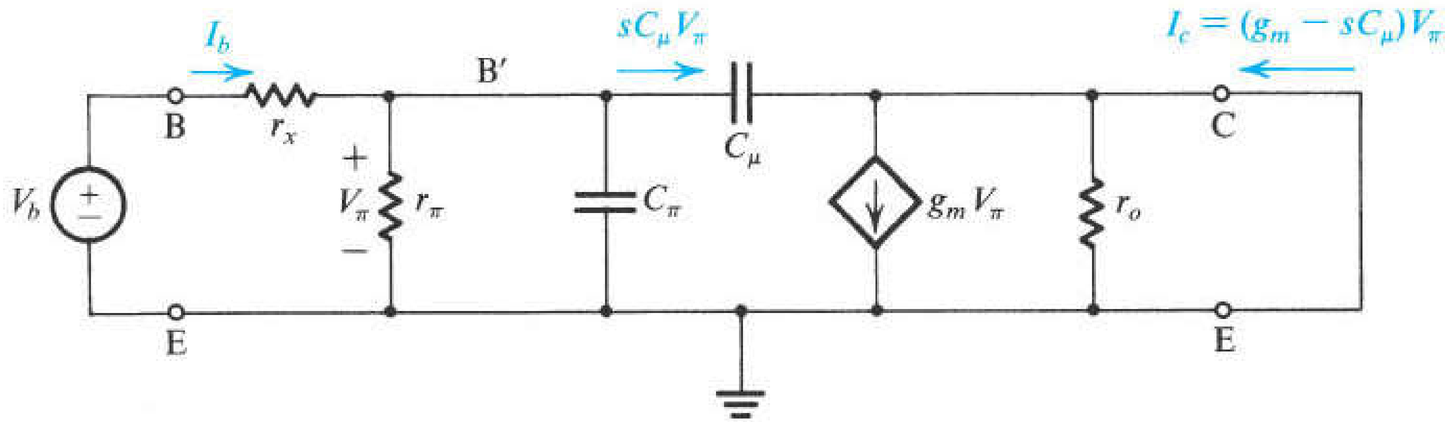

Figure 5.68 Circuit for deriving an expression for $h_{fe}(s) ; I_c/I_b$.

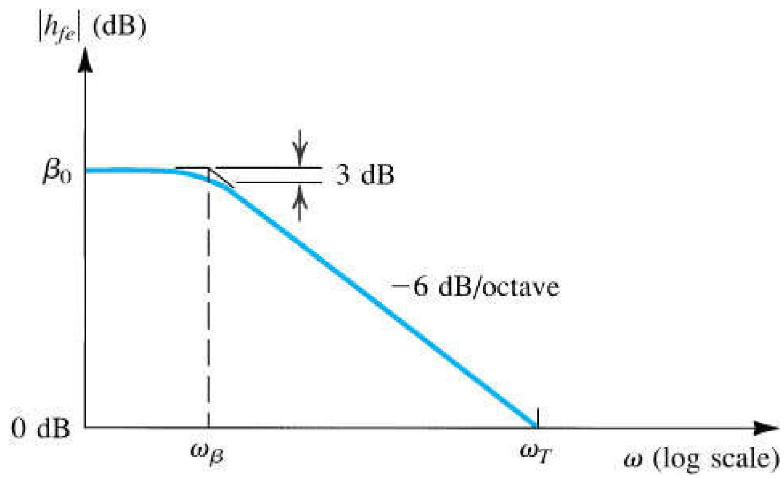

Figure 5.69 Bode plot for uh_{fe}u.

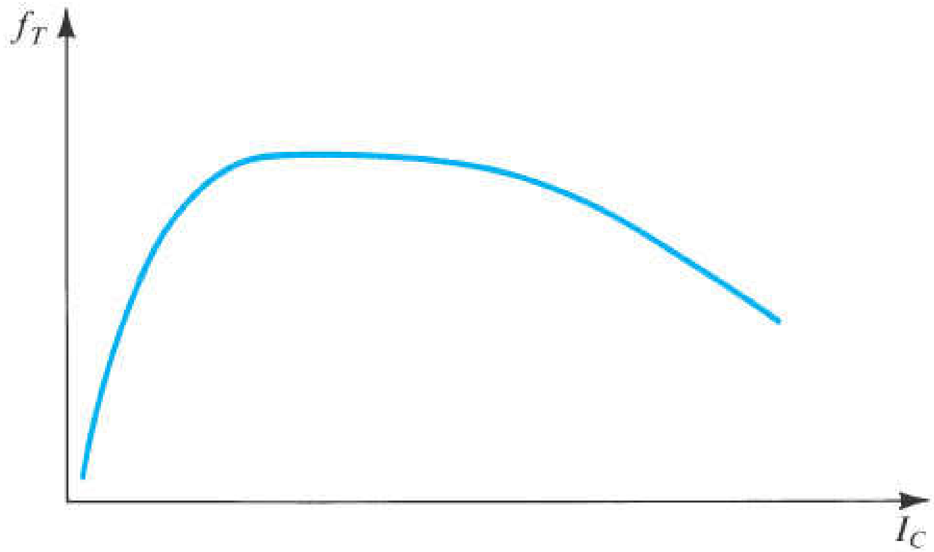

Figure 5.70 Variation of f_T with I_C.

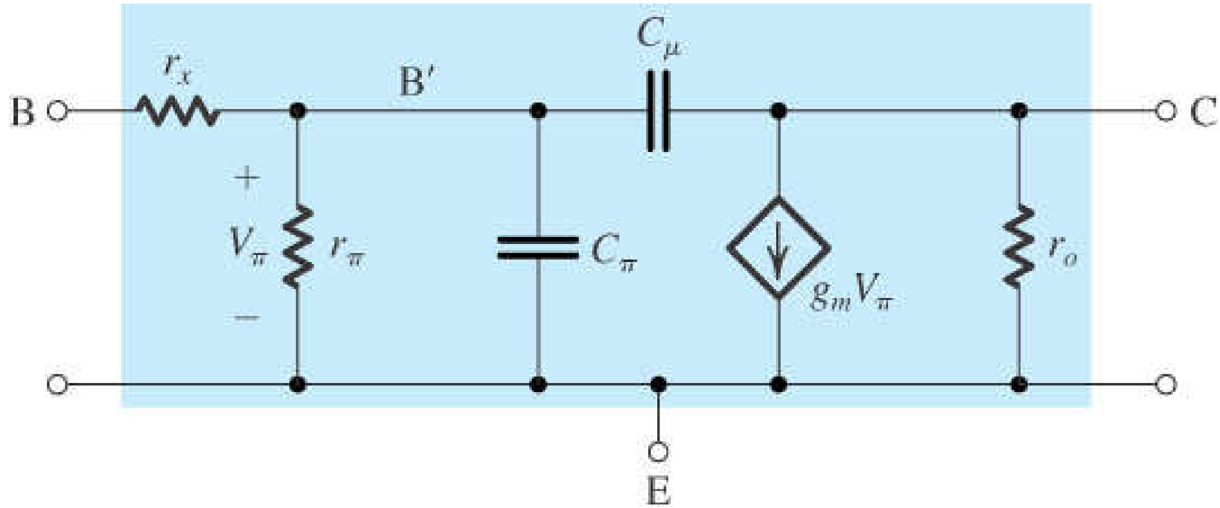

Table 5.7

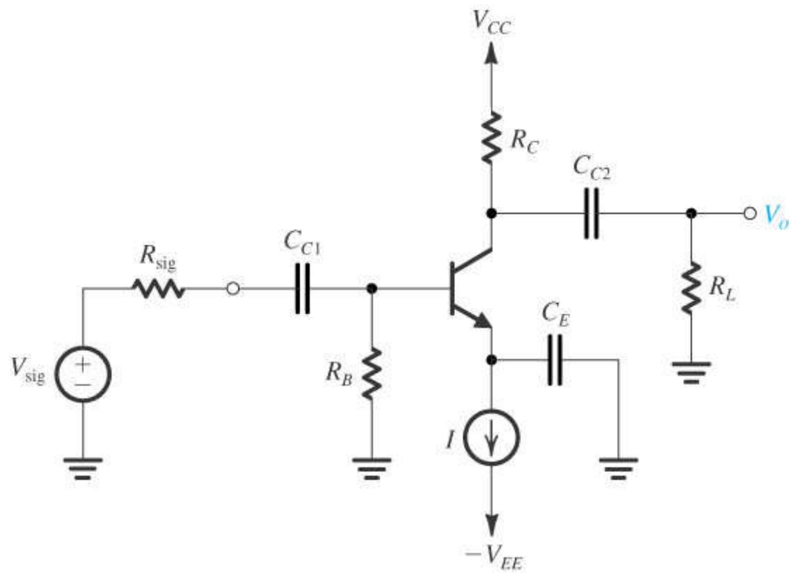

(a)

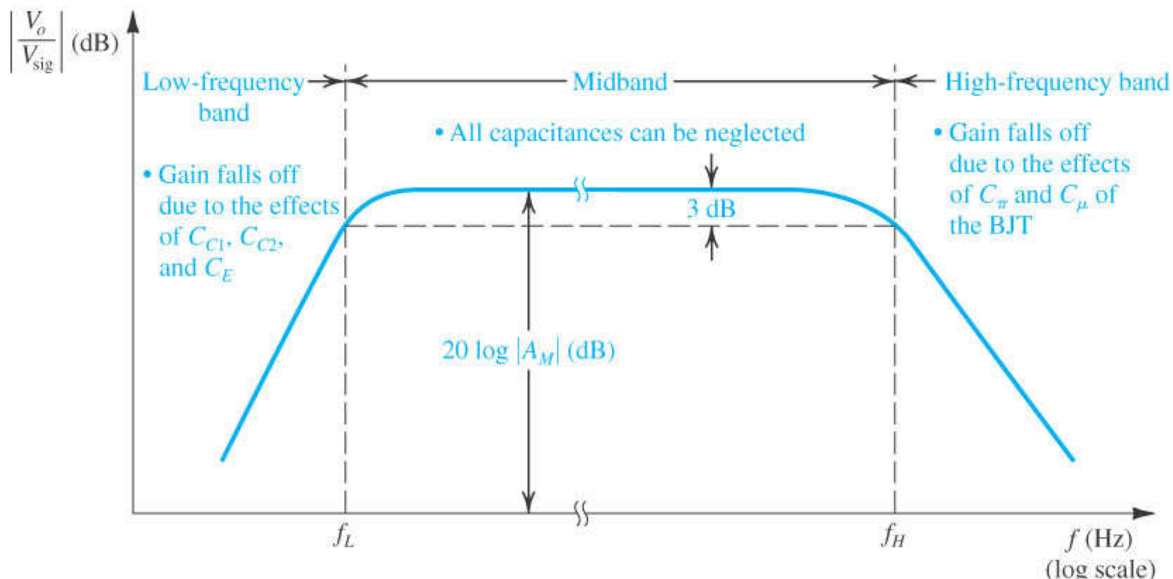

(b)

Figure 5.71 **(a)** Capacitively coupled common-emitter amplifier. **(b)** Sketch of the magnitude of the gain of the CE amplifier versus frequency. The graph delineates the three frequency bands relevant to frequency-response determination.

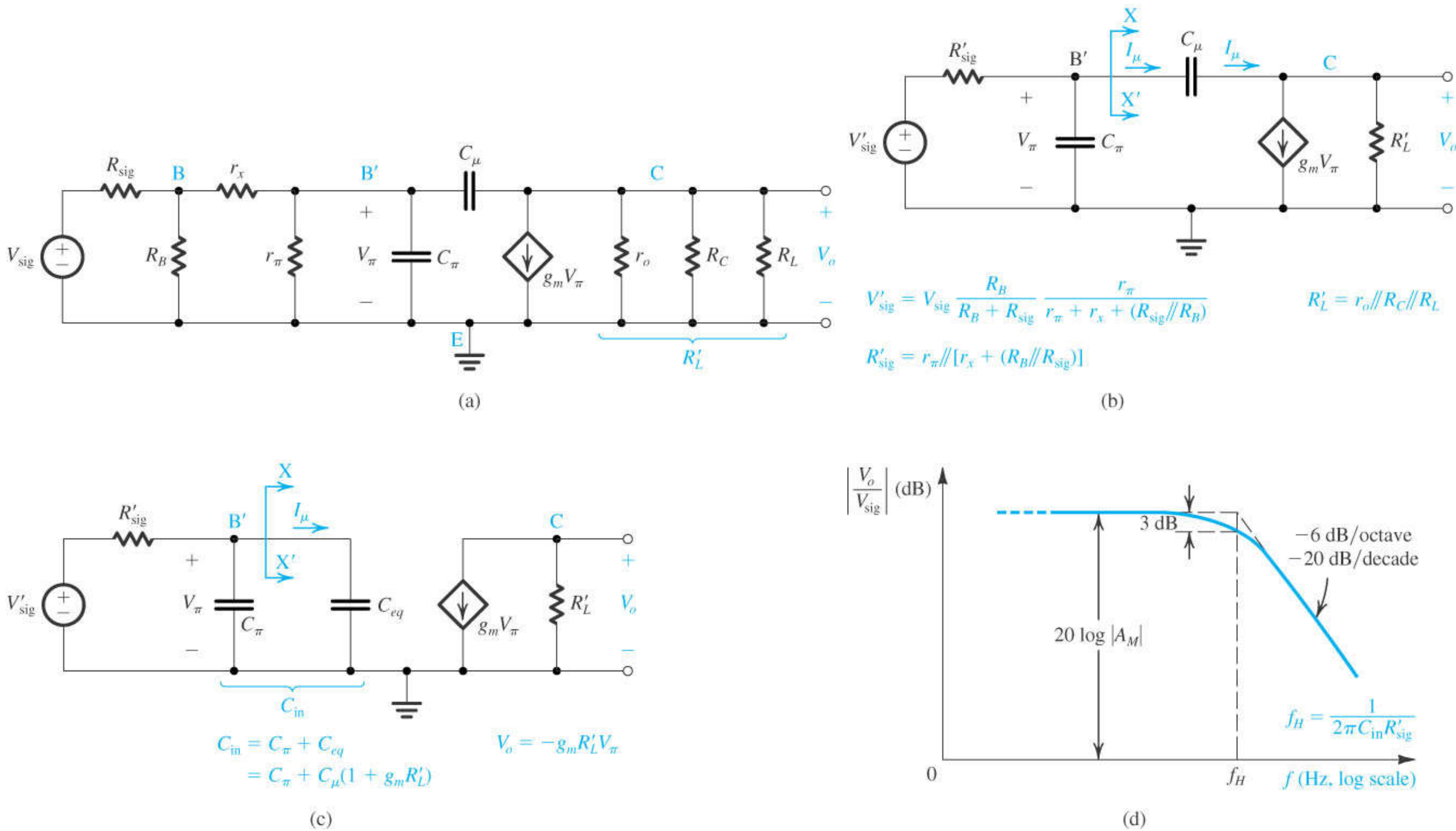

Figure 5.72 Determining the high-frequency response of the CE amplifier: **(a)** equivalent circuit; **(b)** the circuit of (a) simplified at both the input side and the output side; **(c)** equivalent circuit with C_μ replaced at the input side with the equivalent capacitance C_{eq}; **(d)** sketch of the frequency-response plot, which is that of a low-pass STC circuit.

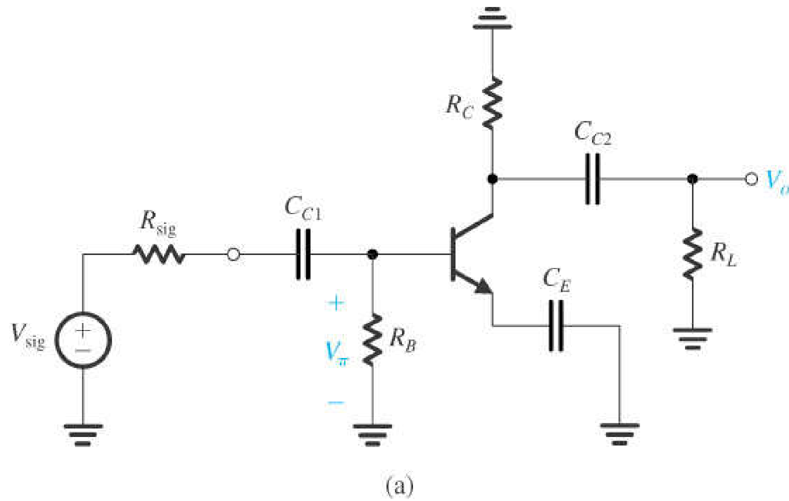

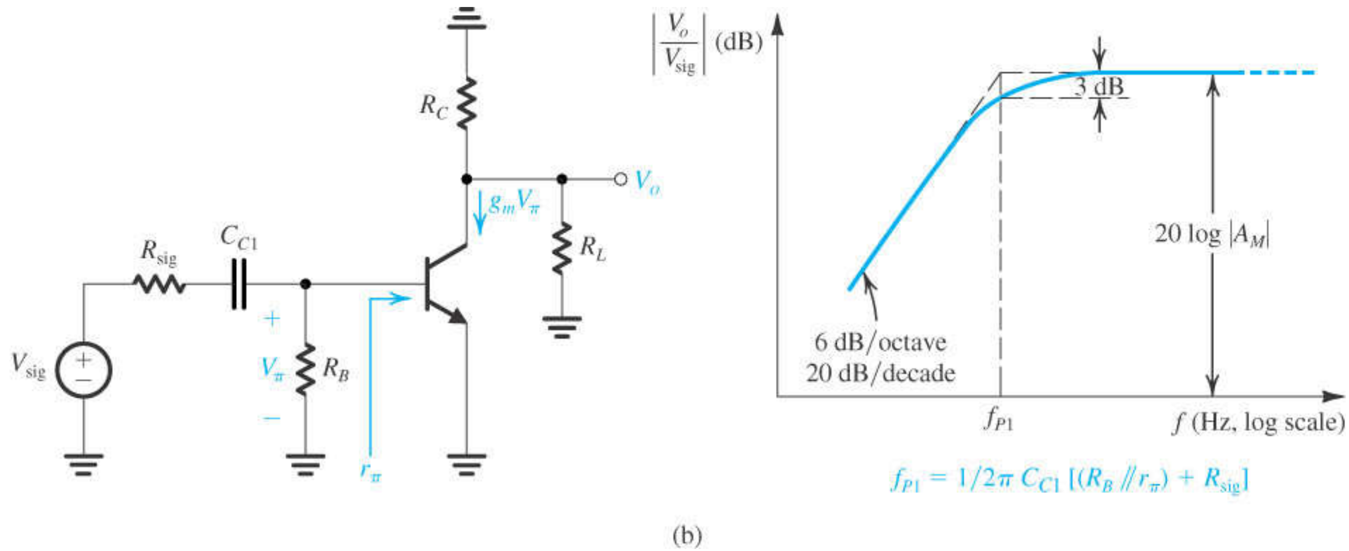

Figure 5.73 Analysis of the low-frequency response of the CE amplifier: **(a)** amplifier circuit with dc sources removed; **(b)** the effect of C_{C1} is determined with C_E and C_{C2} assumed to be acting as perfect short circuits;

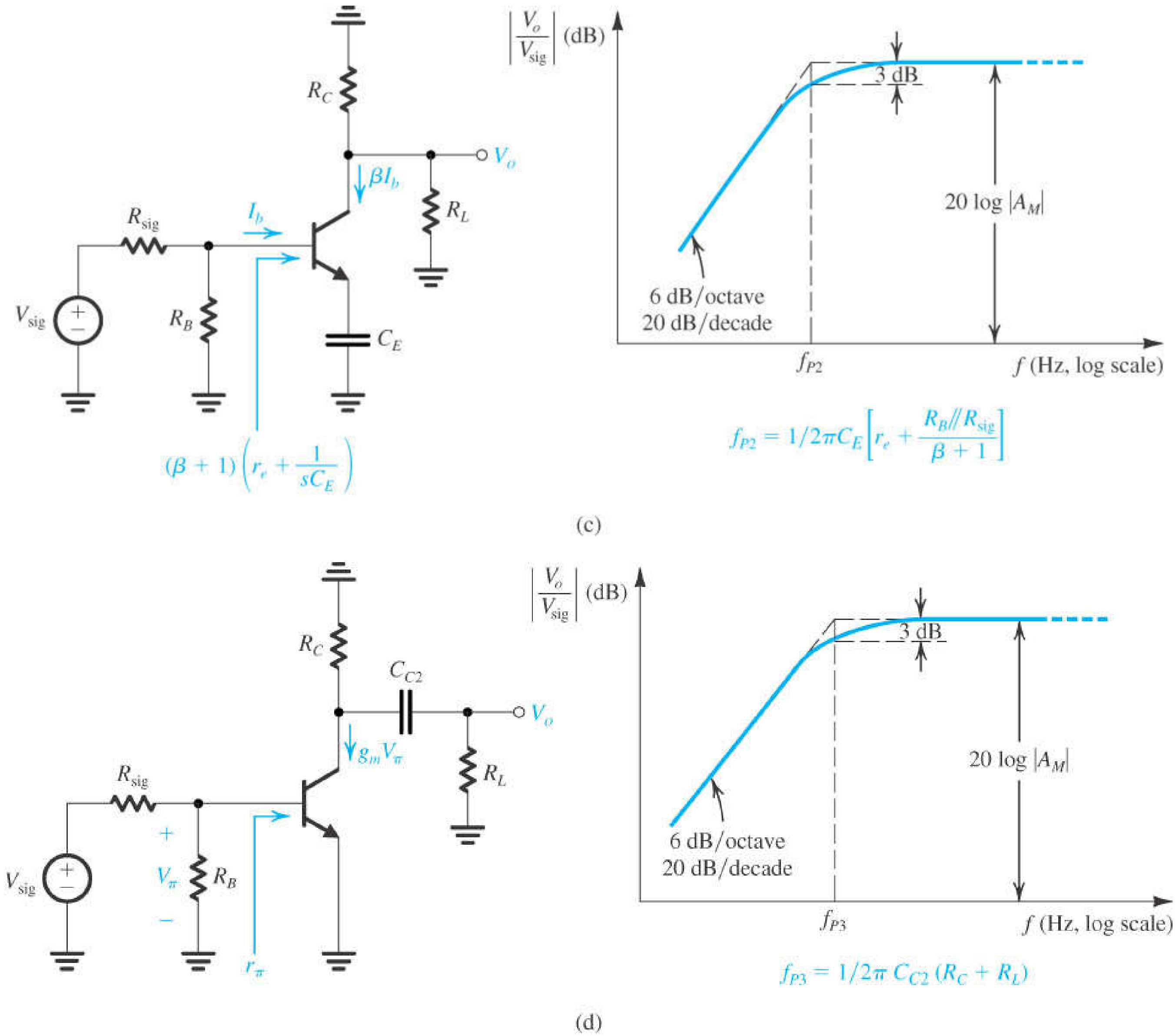

Figure 5.73 *(Continued)* **(c)** the effect of C_E is determined with C_{C1} and C_{C2} assumed to be acting as perfect short circuits; **(d)** the effect of C_{C2} is determined with C_{C1} and C_E assumed to be acting as perfect short circuits;

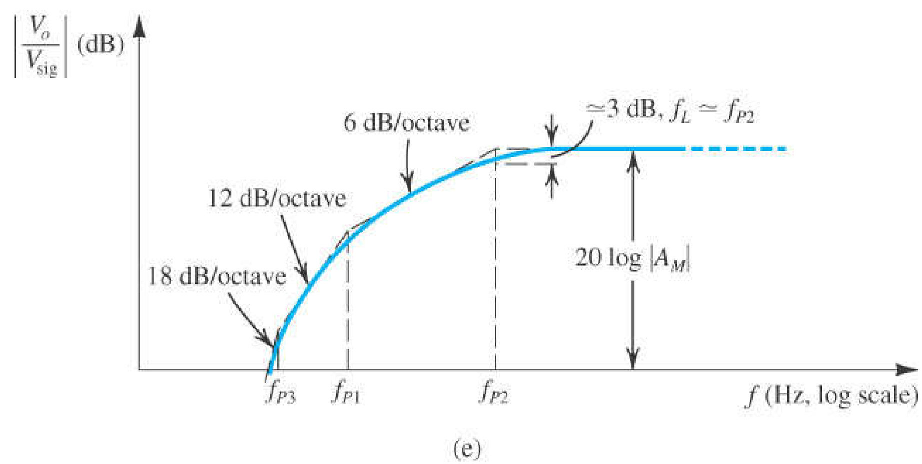

Figure 5.73 *(Continued)* **(e)** sketch of the low-frequency gain under the assumptions that C_{C1}, C_E, and C_{C2} do not interact and that their break (or pole) frequencies are widely separated.

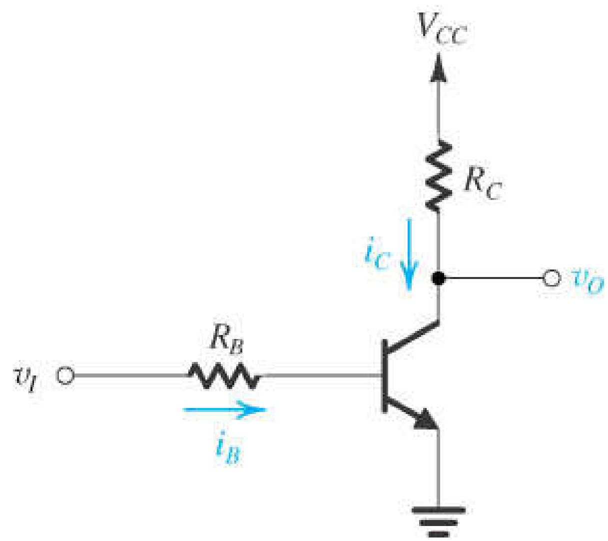

Figure 5.74 Basic BJT digital logic inverter.

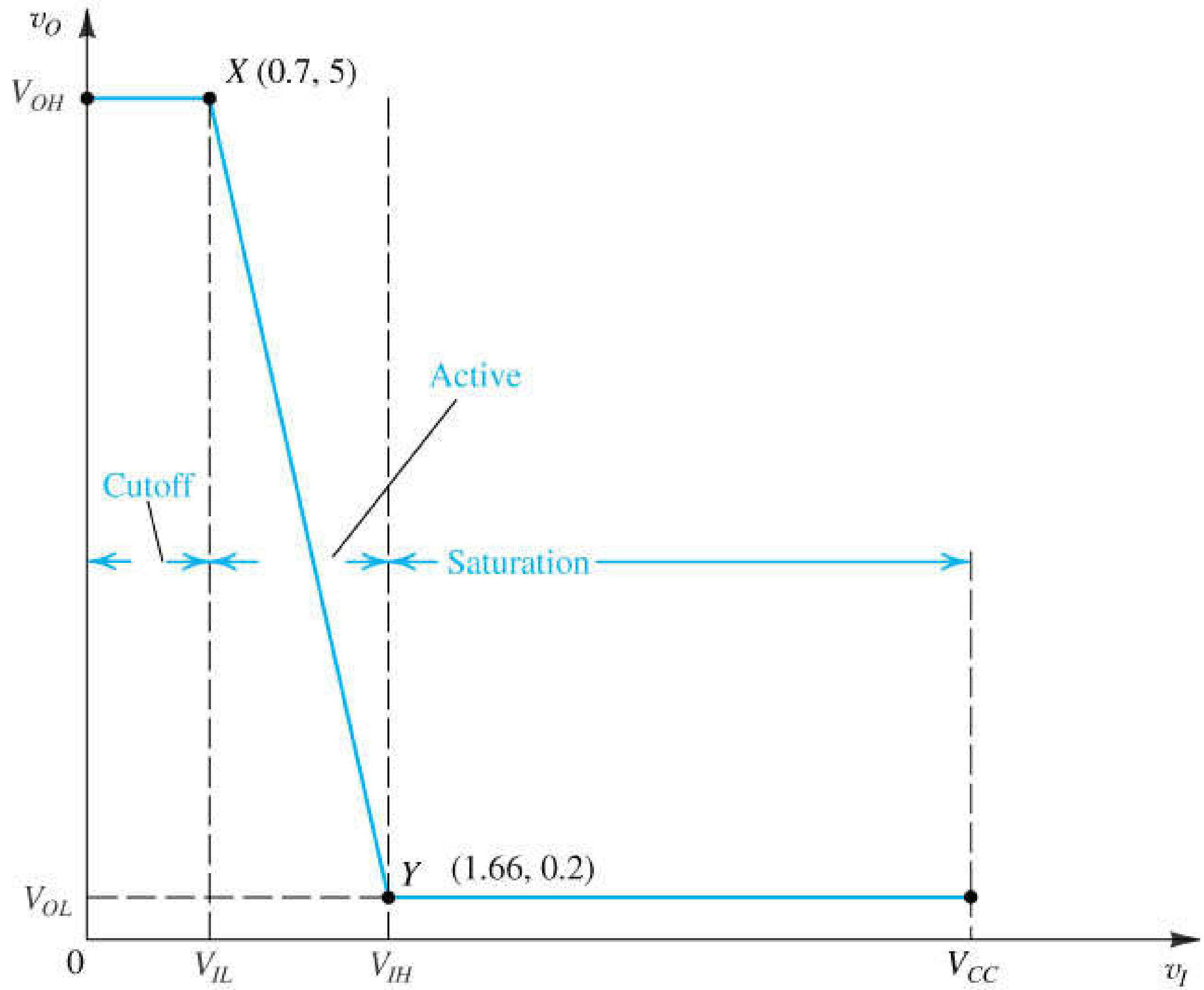

Figure 5.75 Sketch of the voltage transfer characteristic of the inverter circuit of Fig. 5.74 for the case R_B 5 10 kΩ, R_C 5 1 kΩ, β 5 50, and V_{CC} 5 5 V. For the calculation of the coordinates of X and Y, refer to the text.

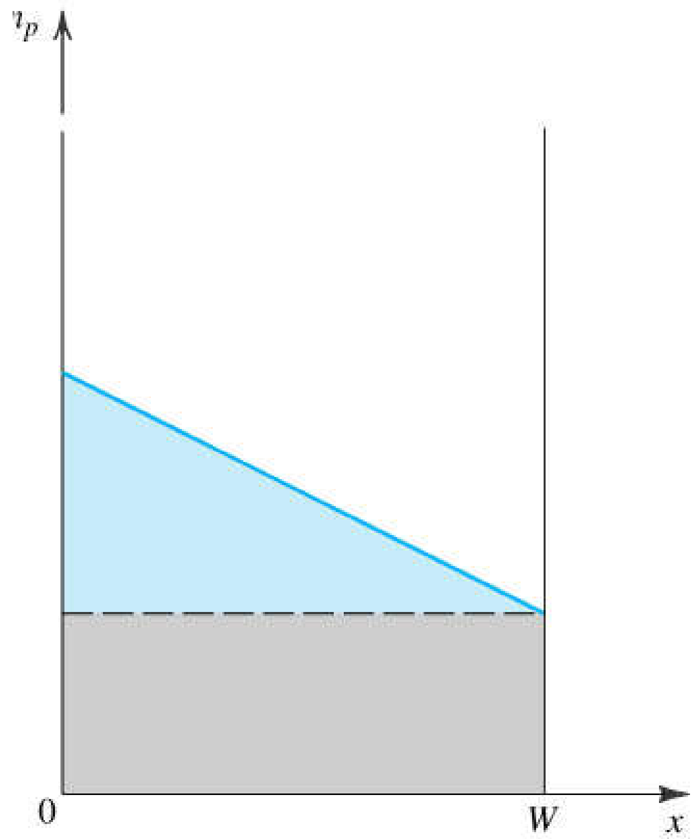

Figure 5.76 The minority-carrier charge stored in the base of a saturated transistor can be divided into two components: That in blue produces the gradient that gives rise to the diffusion current across the base, and that in gray results from driving the transistor deeper into saturation.

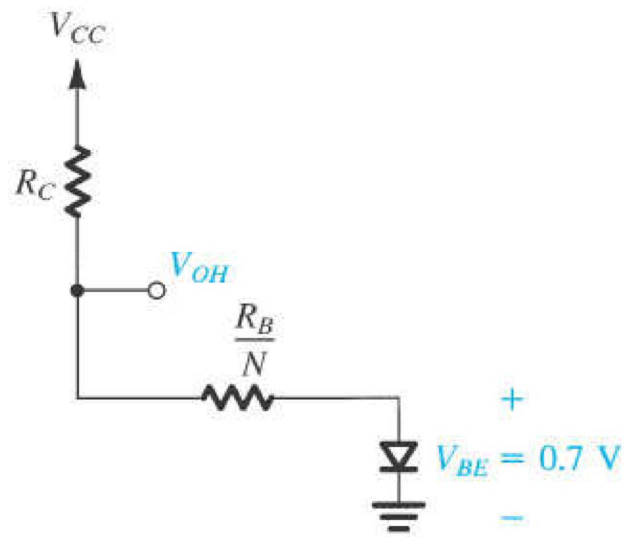

Figure E5.53

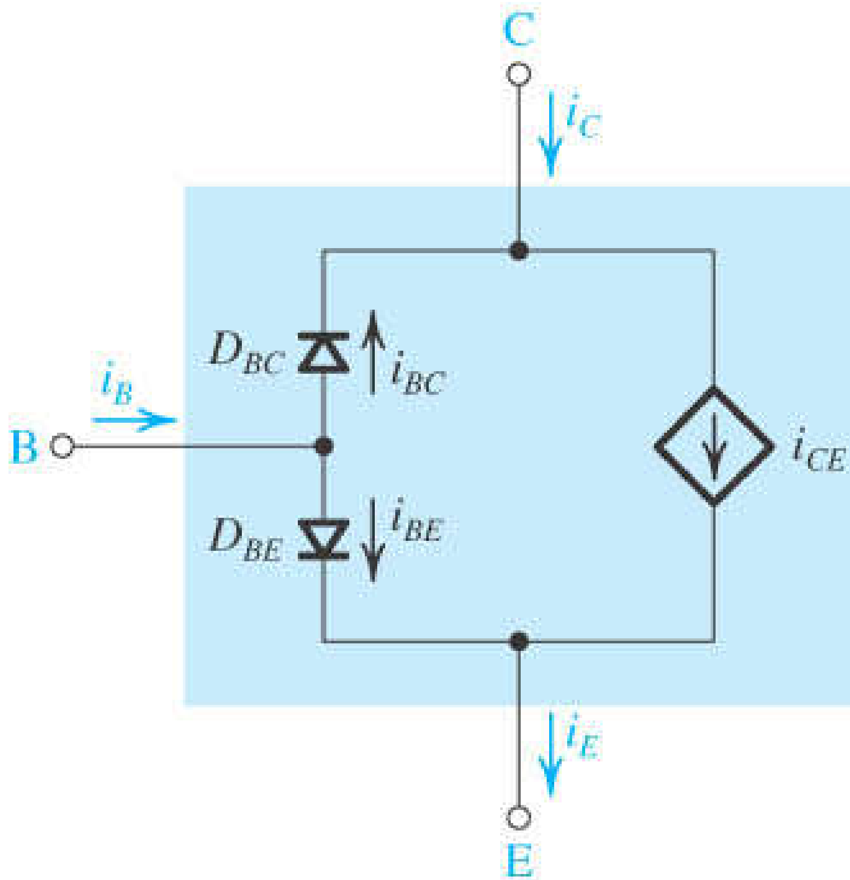

Figure 5.77 The transport form of the Ebers-Moll model for an *npn* BJT.

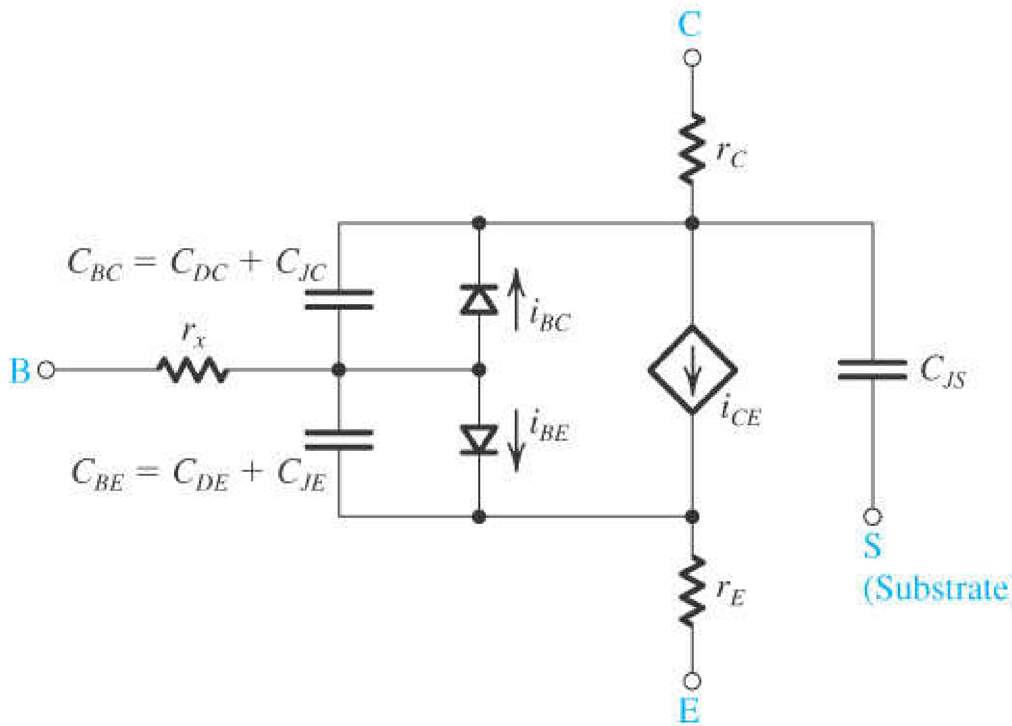

Figure 5.78 The SPICE large-signal Ebers-Moll model for an *npn* BJT.

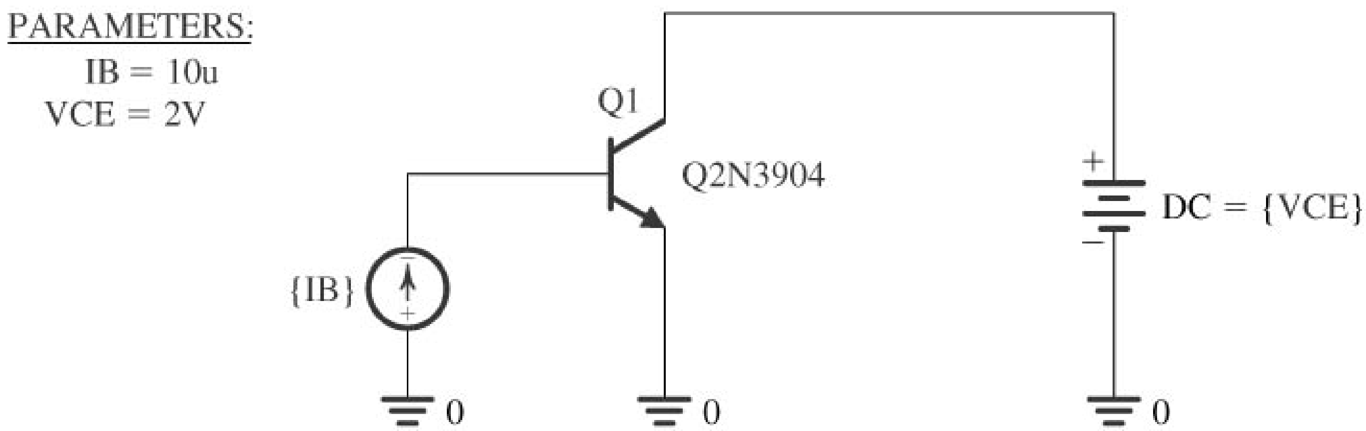

Figure 5.79 The PSpice testbench used to demonstrate the dependence of β_{dc} on the collector bias current I_C for the Q2N3904 discrete BJT (Example 5.20).

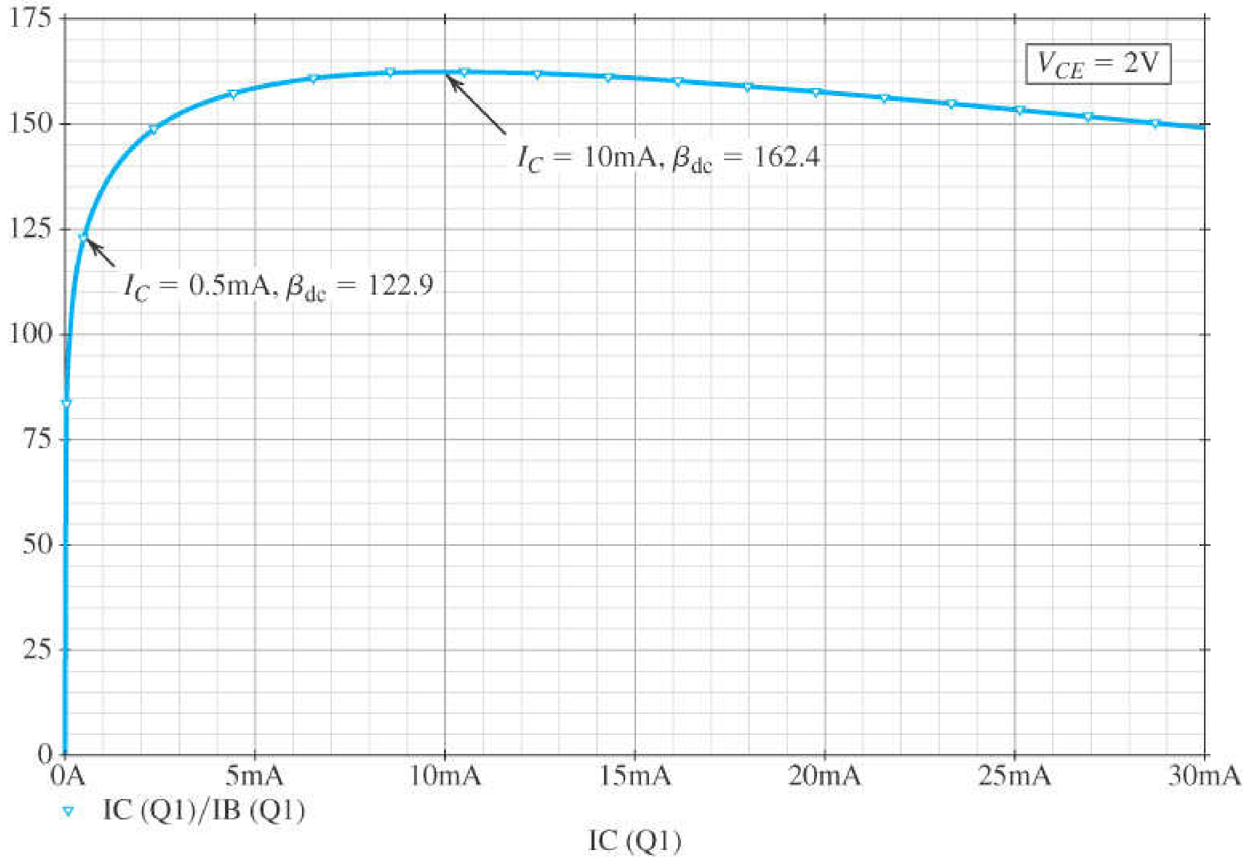

Figure 5.80 Dependence of β_{dc} on I_C (at $V_{CE\ 5}$ 2 V) in the Q2N3904 discrete BJT (Example 5.20).

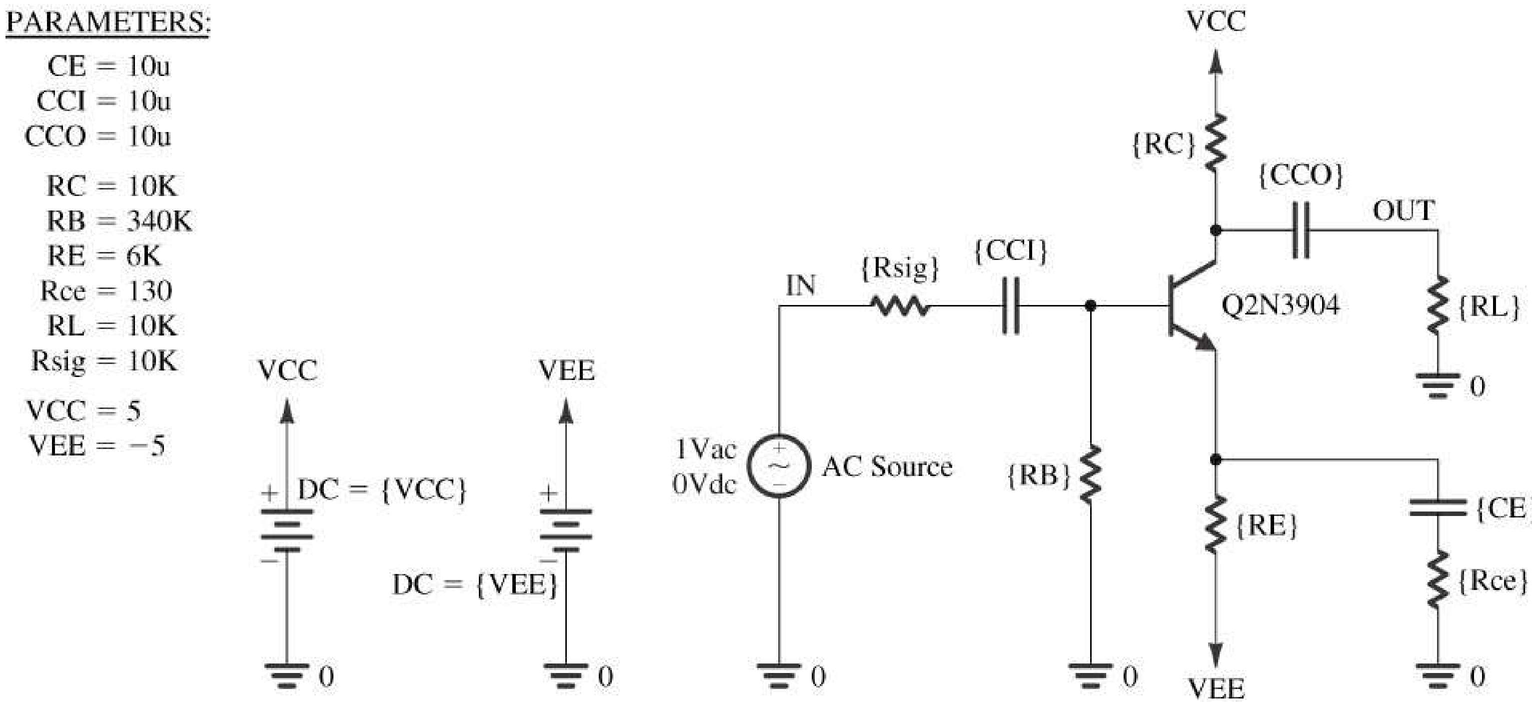

Figure 5.81 Capture schematic of the CE amplifier in Example 5.21.

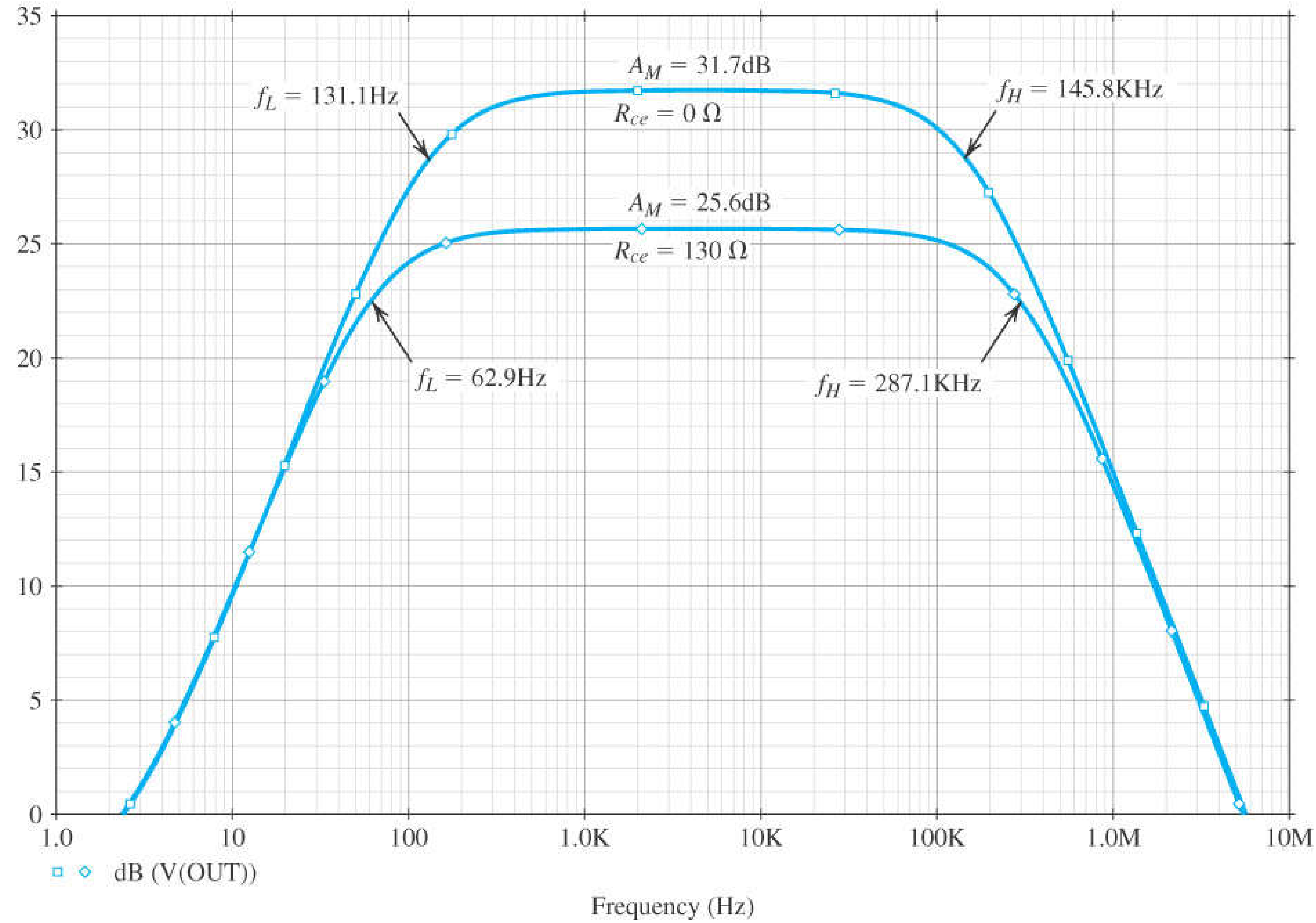

Figure 5.82 Frequency response of the CE amplifier in Example 5.21 with $R_{ce} = 0$ and $R_{ce} = 130\ \Omega$.

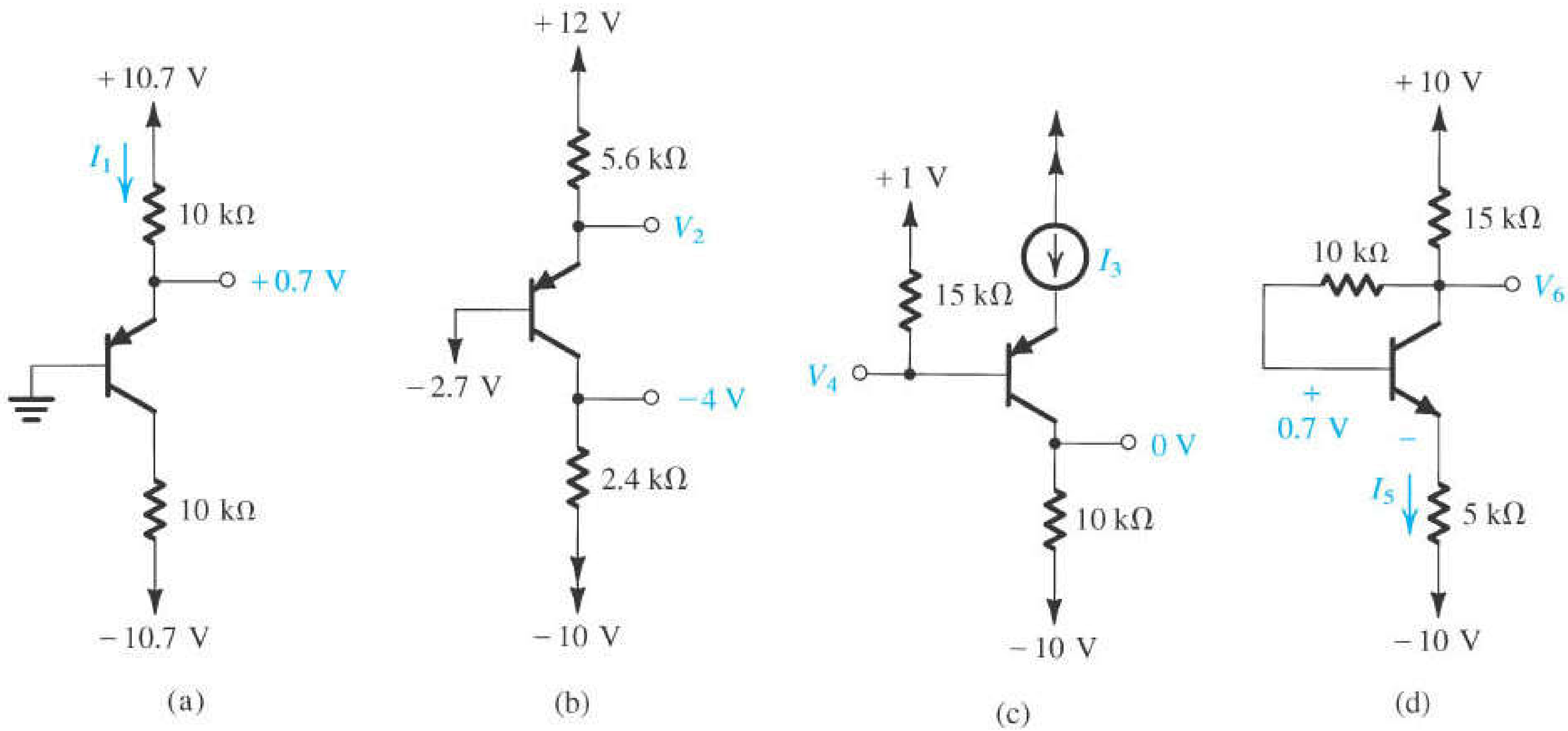
+10.7 V
I_1
10 kΩ
+0.7 V
10 kΩ
−10.7 V
(a)
+12 V
5.6 kΩ
V_2
−2.7 V
−4 V
2.4 kΩ
−10 V
(b)
+1 V
15 kΩ
I_3
V_4
0 V
10 kΩ
−10 V
(c)
+10 V
15 kΩ
10 kΩ
V_6
+
0.7 V
−
I_5
5 kΩ
−10 V
(d)

Figure P5.20

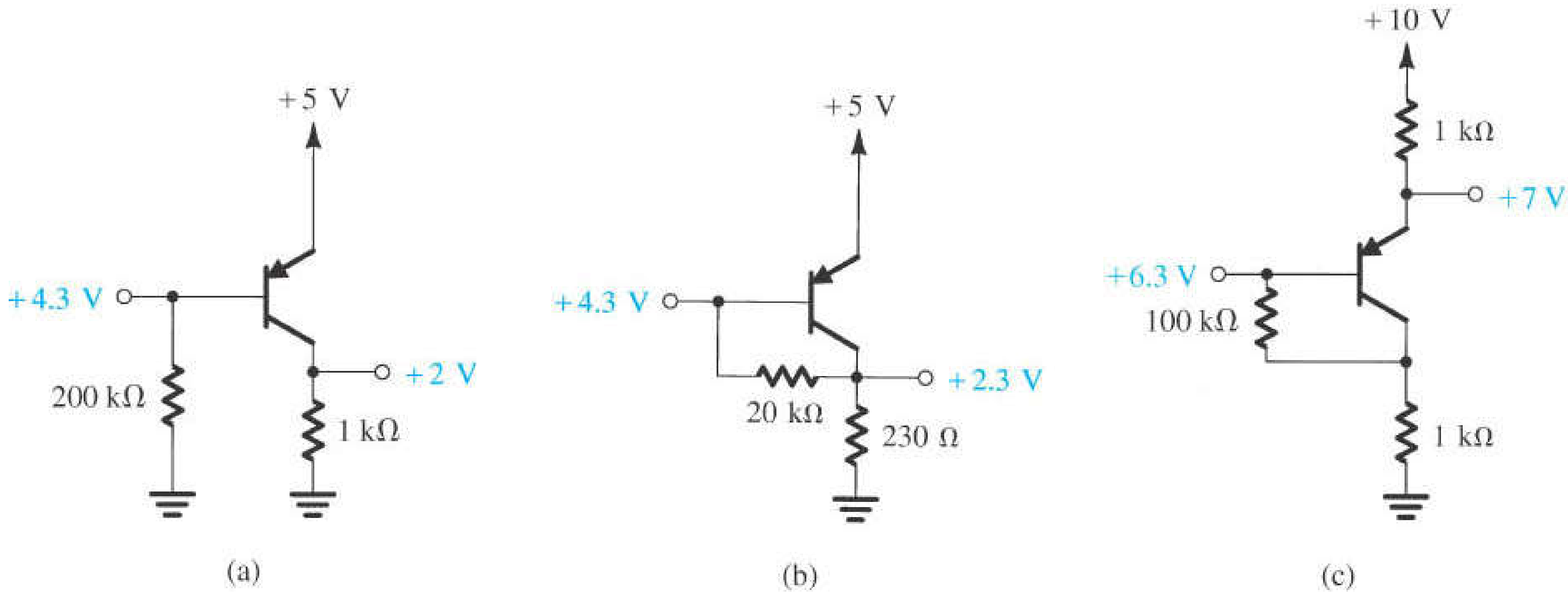
+5 V
+4.3 V
200 kΩ
+2 V
1 kΩ
(a)
+5 V
+4.3 V
20 kΩ
+2.3 V
230 Ω
(b)
+10 V
1 kΩ
+7 V
+6.3 V
100 kΩ
1 kΩ
(c)

Figure P5.21

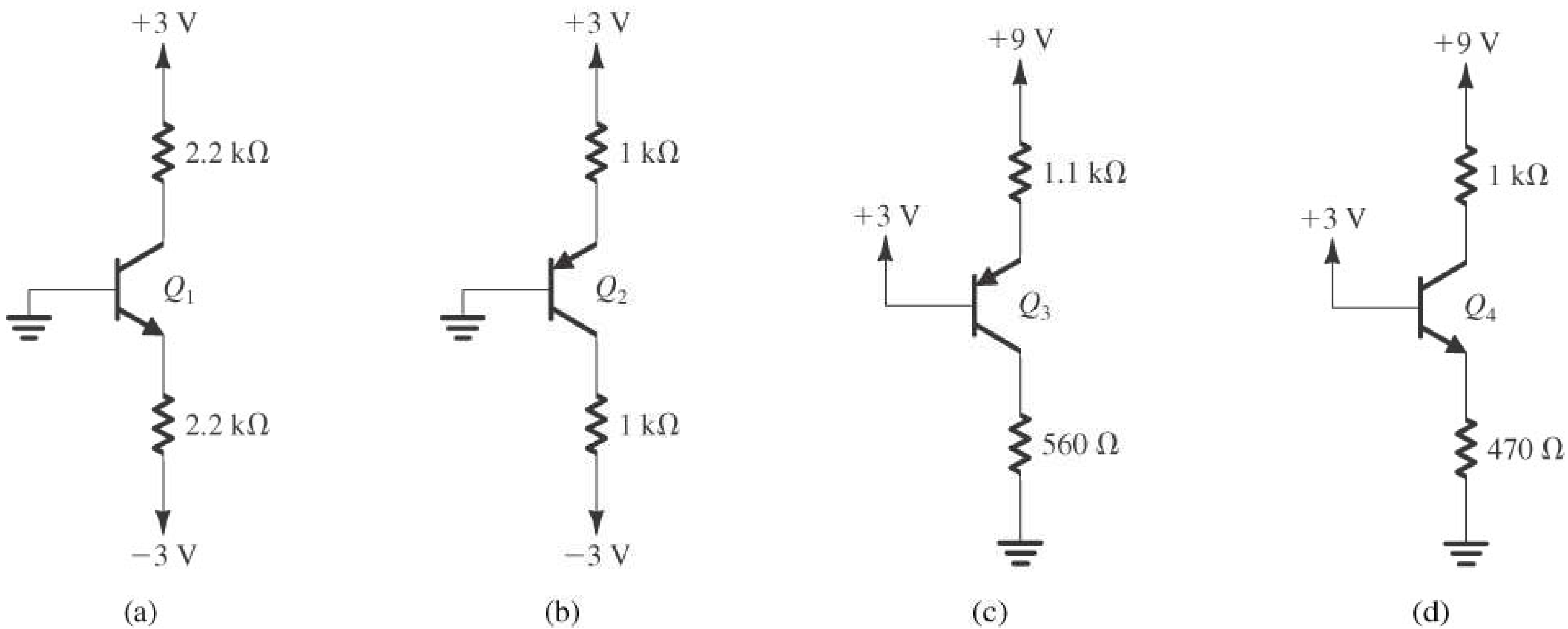
+3 V
2.2 kΩ
Q_1
2.2 kΩ
−3 V
(a)
+3 V
1 kΩ
Q_2
1 kΩ
−3 V
(b)
+9 V
1.1 kΩ
+3 V
Q_3
560 Ω
(c)
+9 V
1 kΩ
+3 V
Q_4
470 Ω
(d)

Figure P5.24

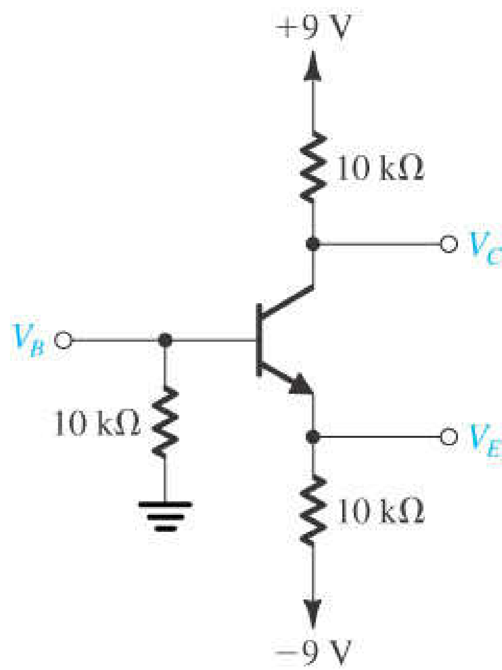

Figure P5.26

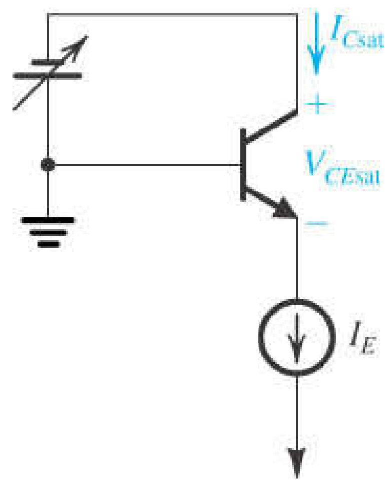

Figure P5.36

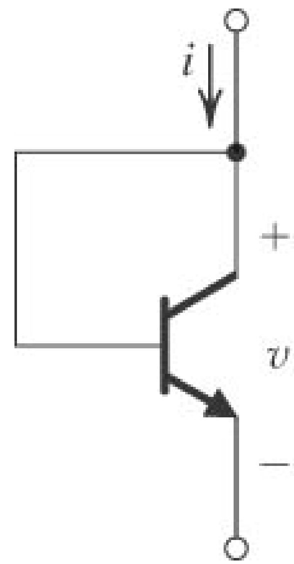

Figure P5.44

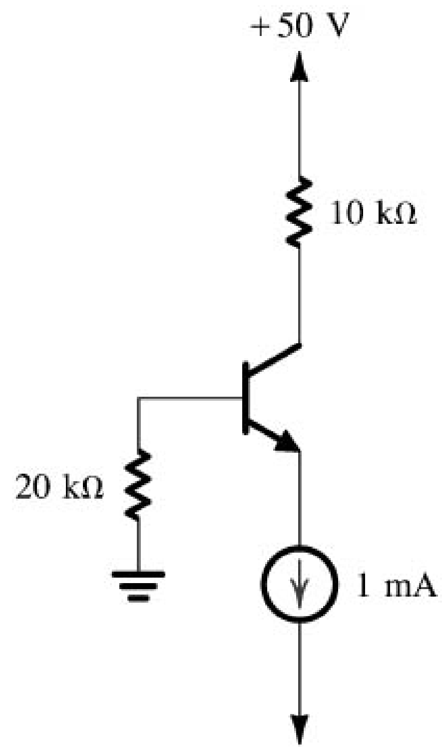

Figure P5.53

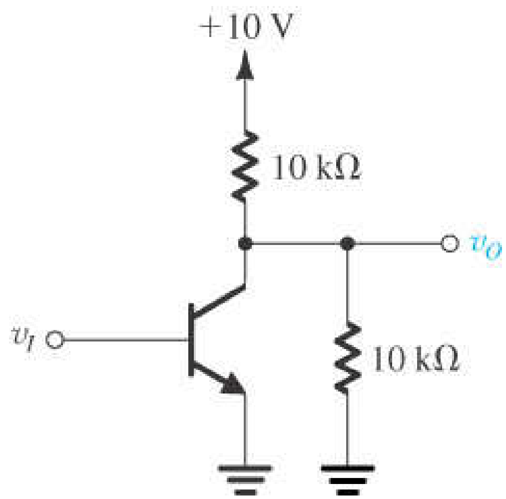

Figure P5.57

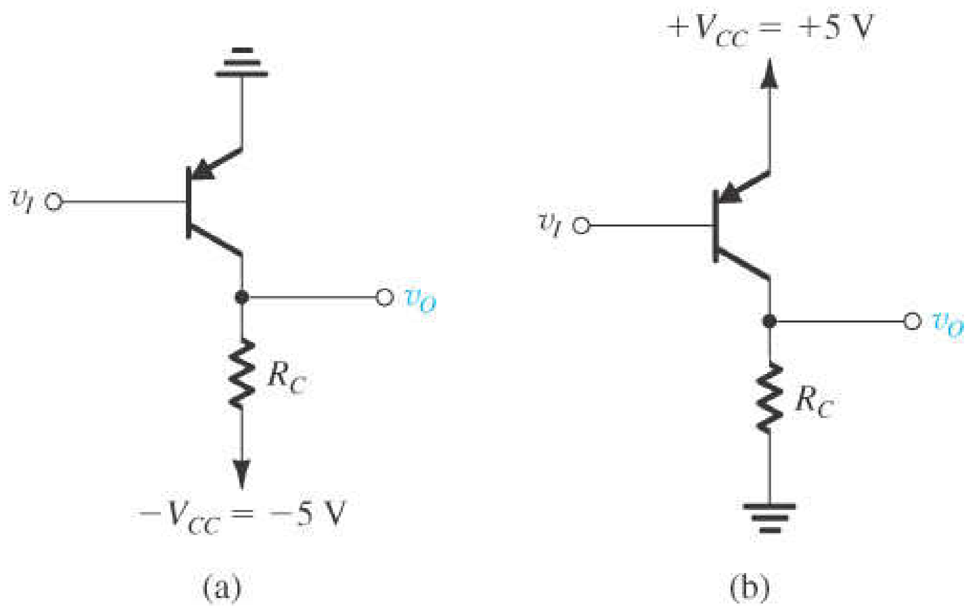

Figure P5.58

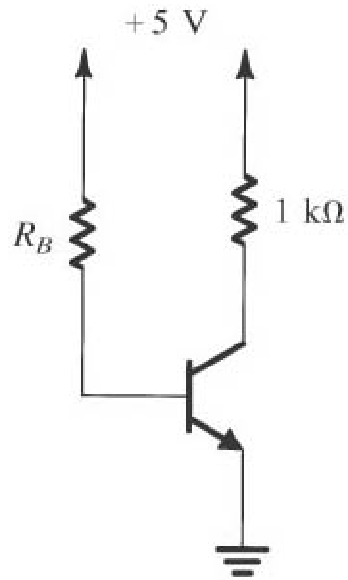

Figure P5.65

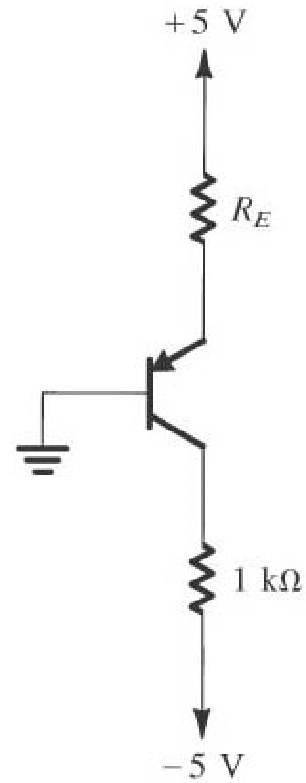

Figure P5.66

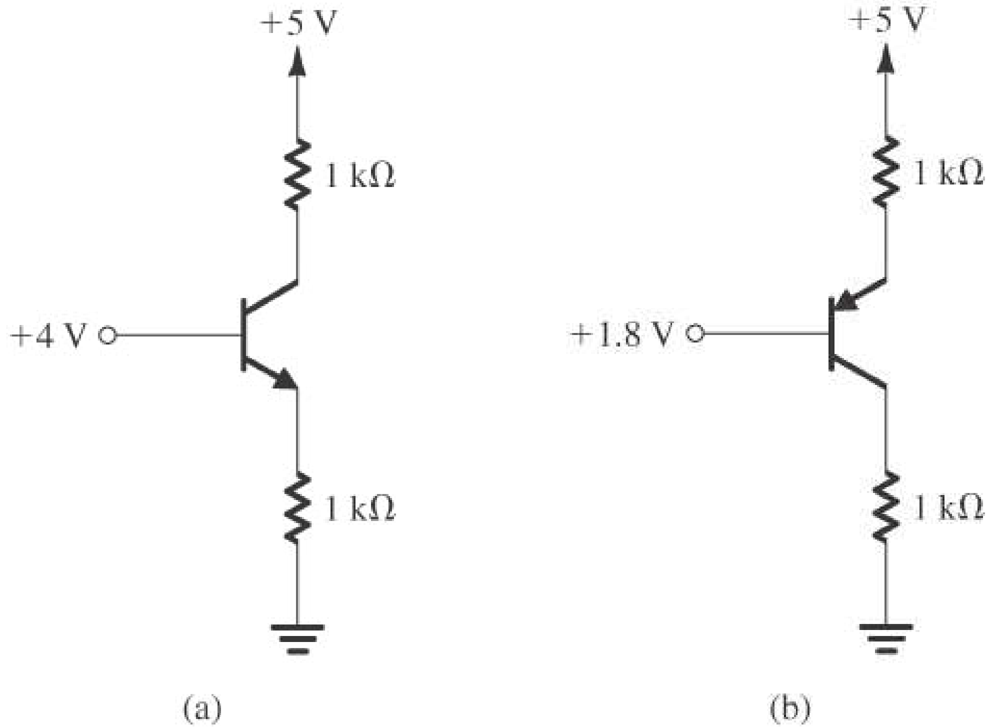

Figure P5.67

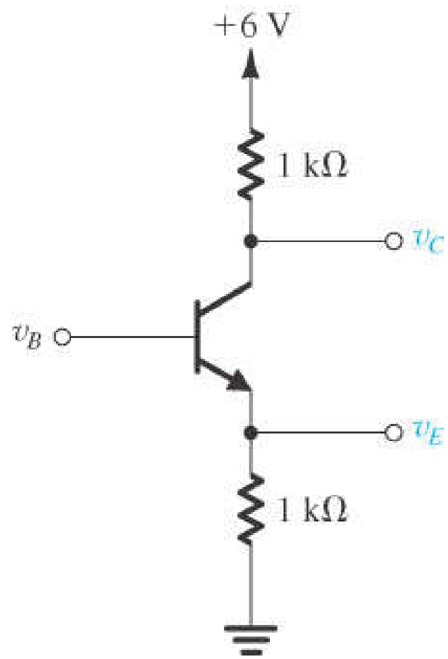

Figure P5.68

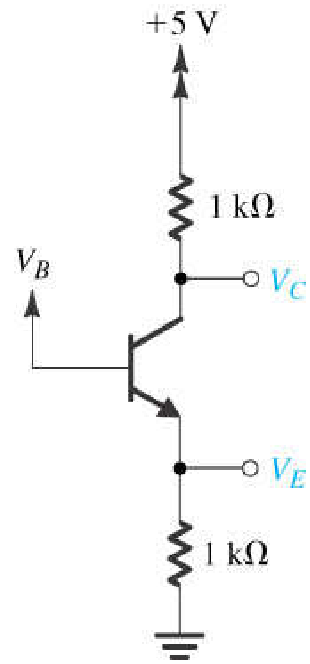

Figure P5.69

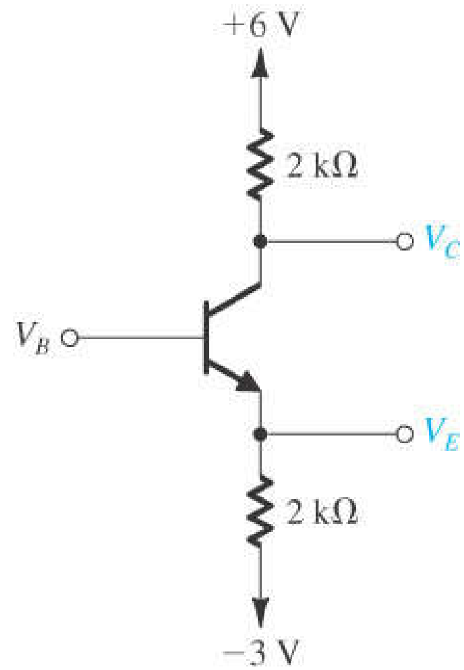

Figure P5.71

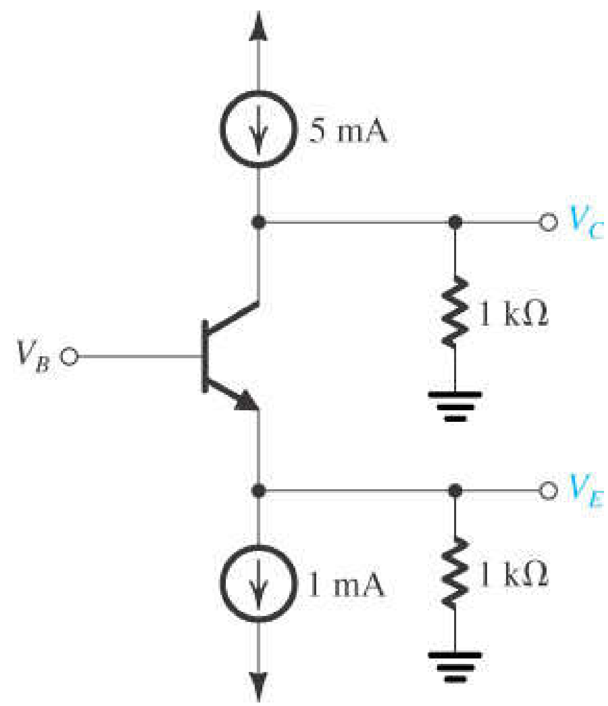

Figure P5.72

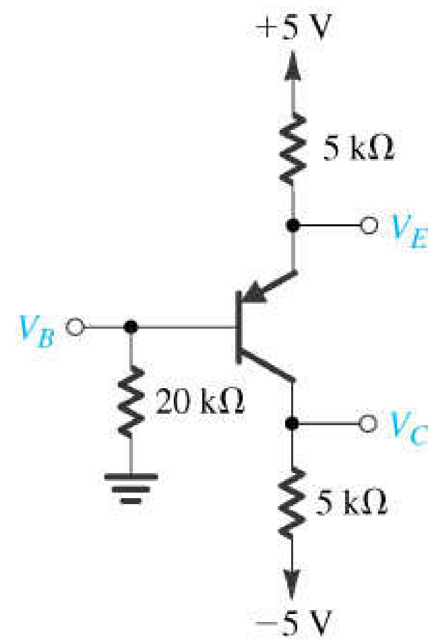

Figure P5.74

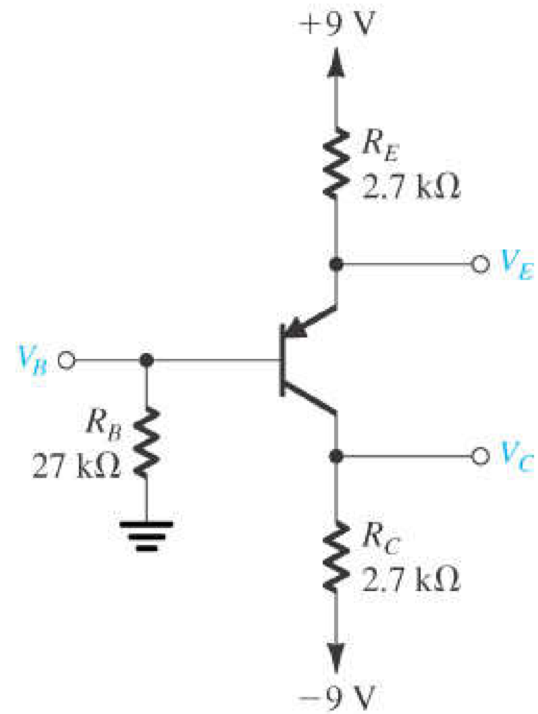

Figure P5.76

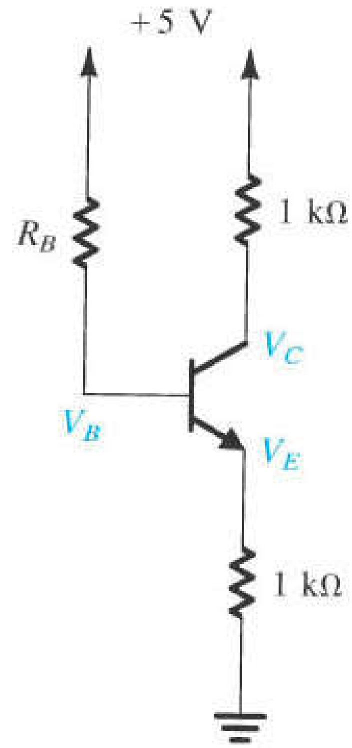

Figure P5.78

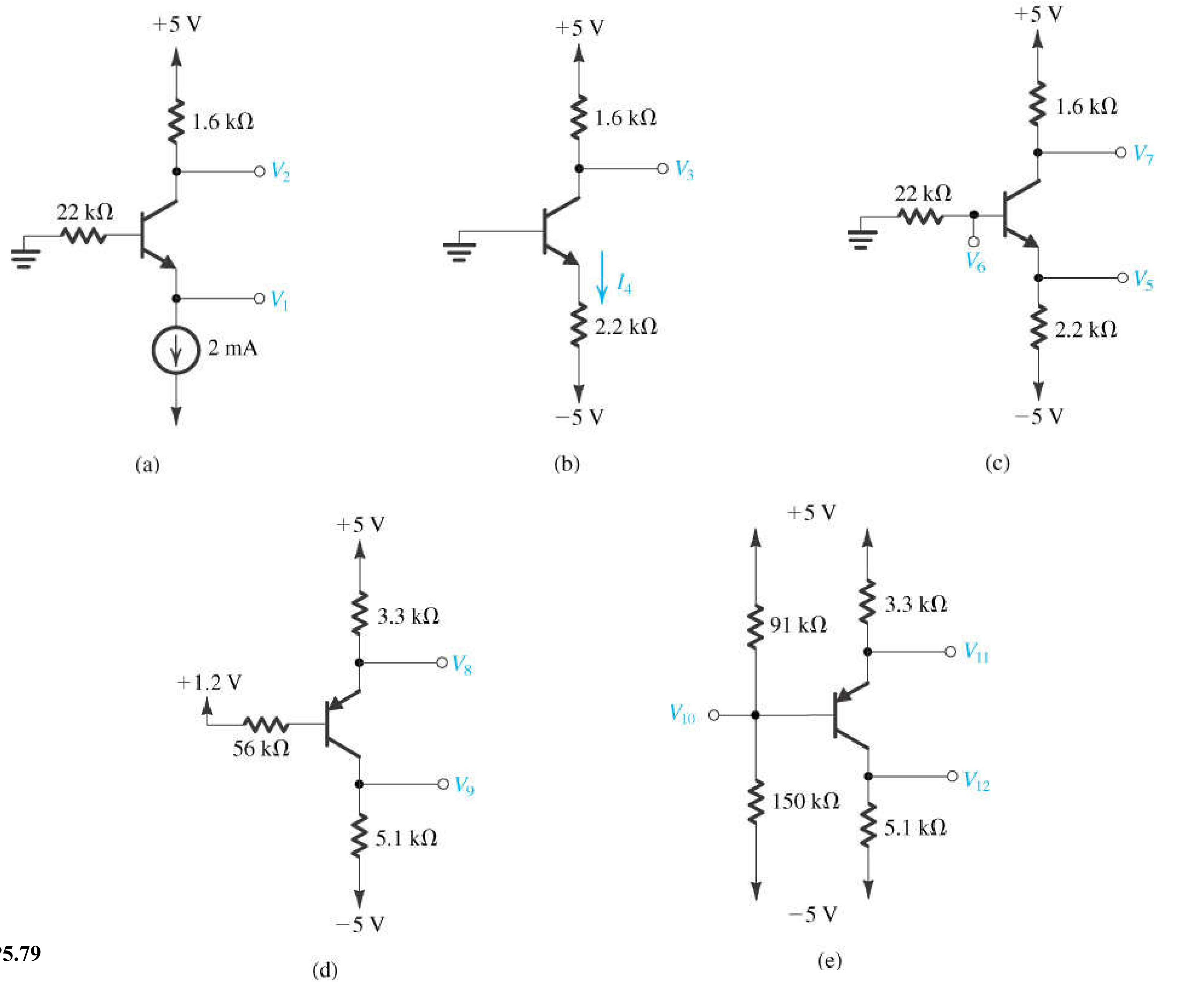
+5 V
1.6 kΩ
V2
22 kΩ
V1
2 mA
(a)
+5 V
1.6 kΩ
V3
I4
2.2 kΩ
−5 V
(b)
+5 V
1.6 kΩ
V7
22 kΩ
V6
V5
2.2 kΩ
−5 V
(c)
+5 V
3.3 kΩ
V8
+1.2 V
56 kΩ
V9
5.1 kΩ
−5 V
(d)
+5 V
91 kΩ
3.3 kΩ
V11
V10
V12
150 kΩ
5.1 kΩ
−5 V
(e)

Figure P5.79

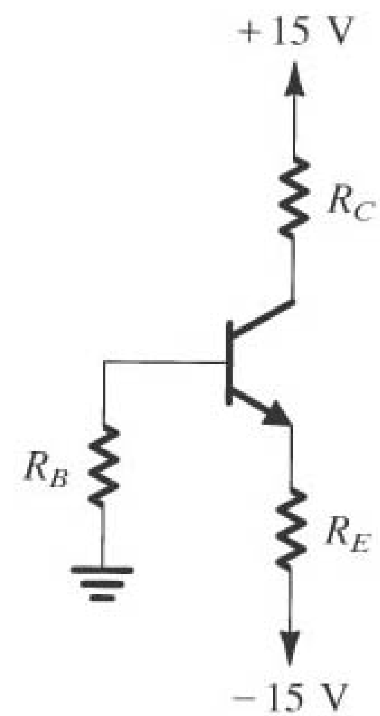

Figure P5.81

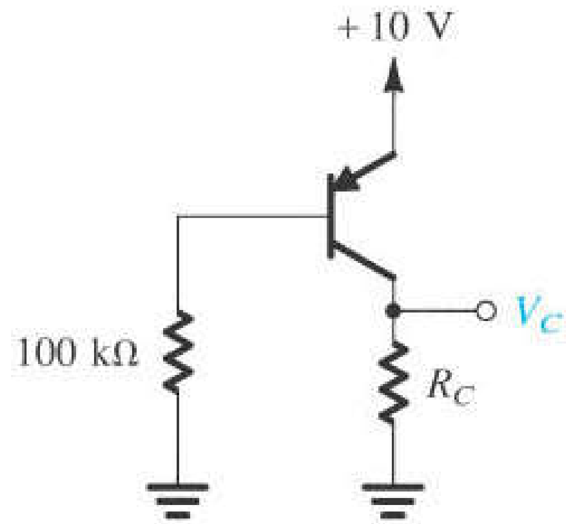

Figure P5.82

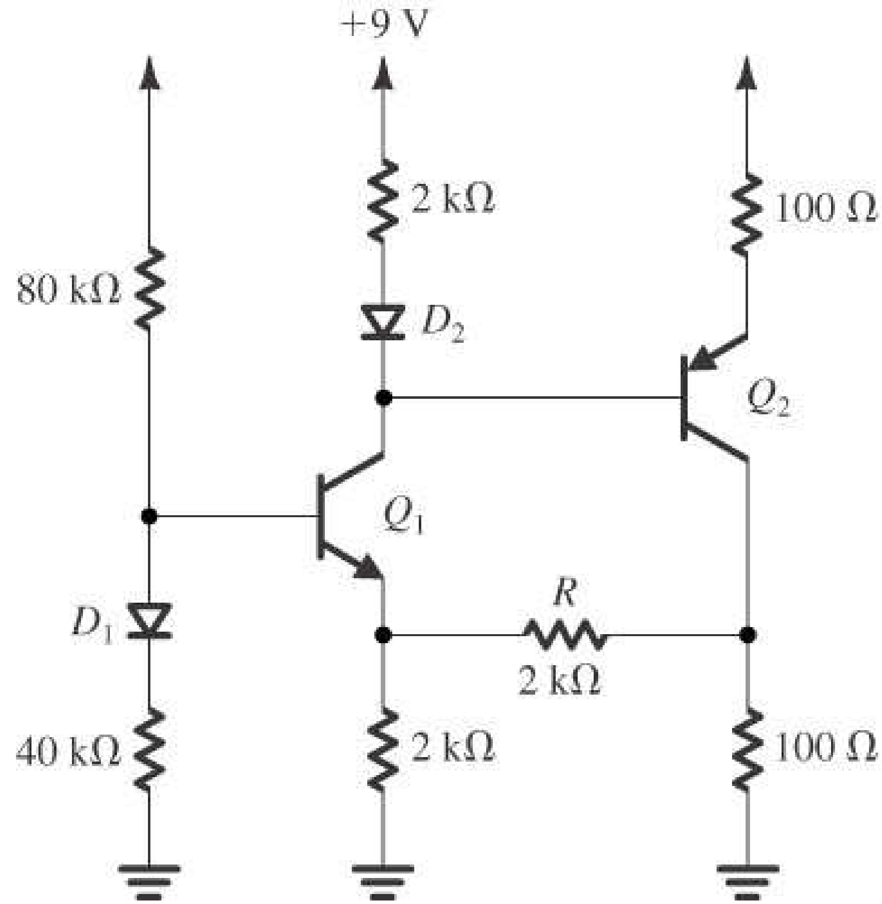

Figure P5.83

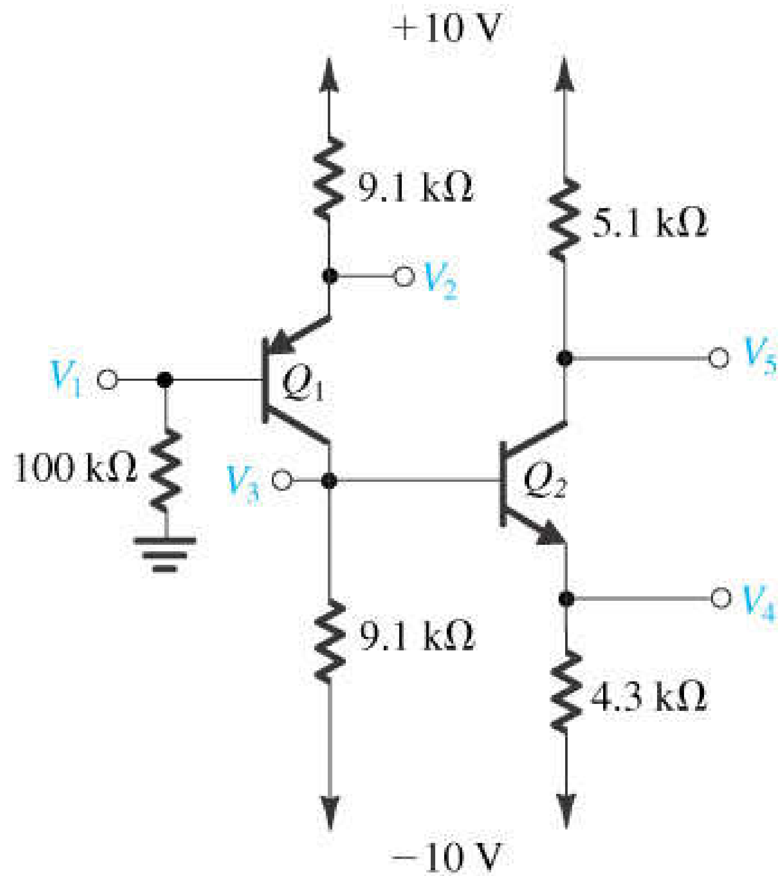

Figure P5.84

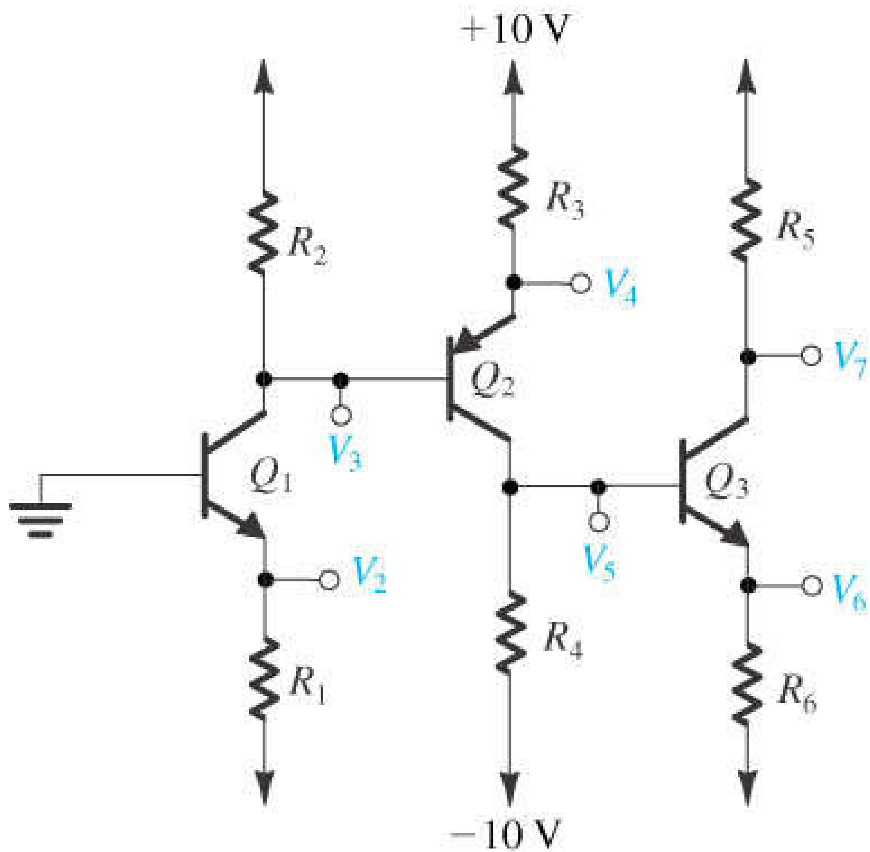

Figure P5.85

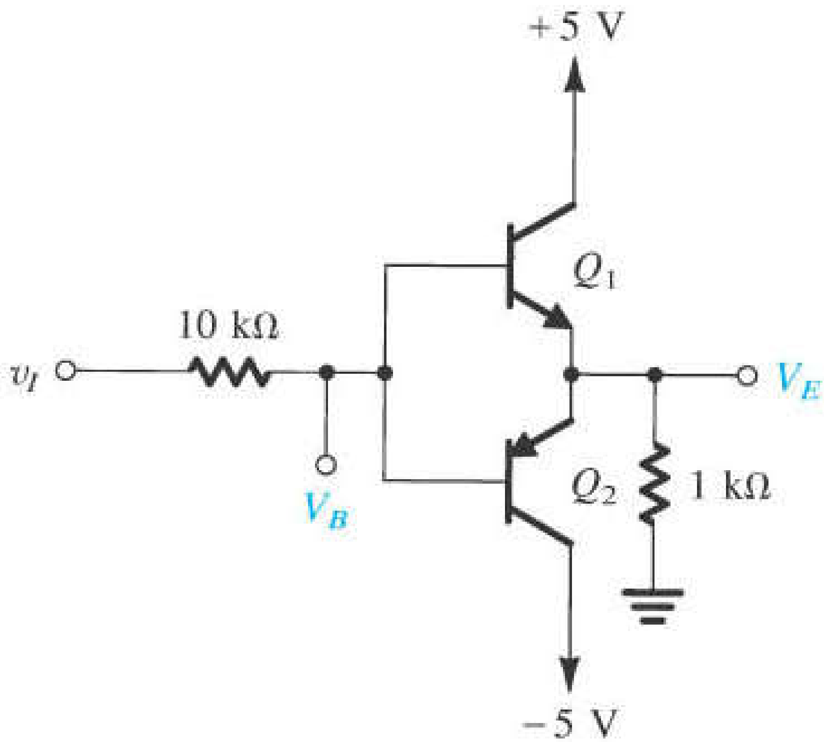

Figure P5.86

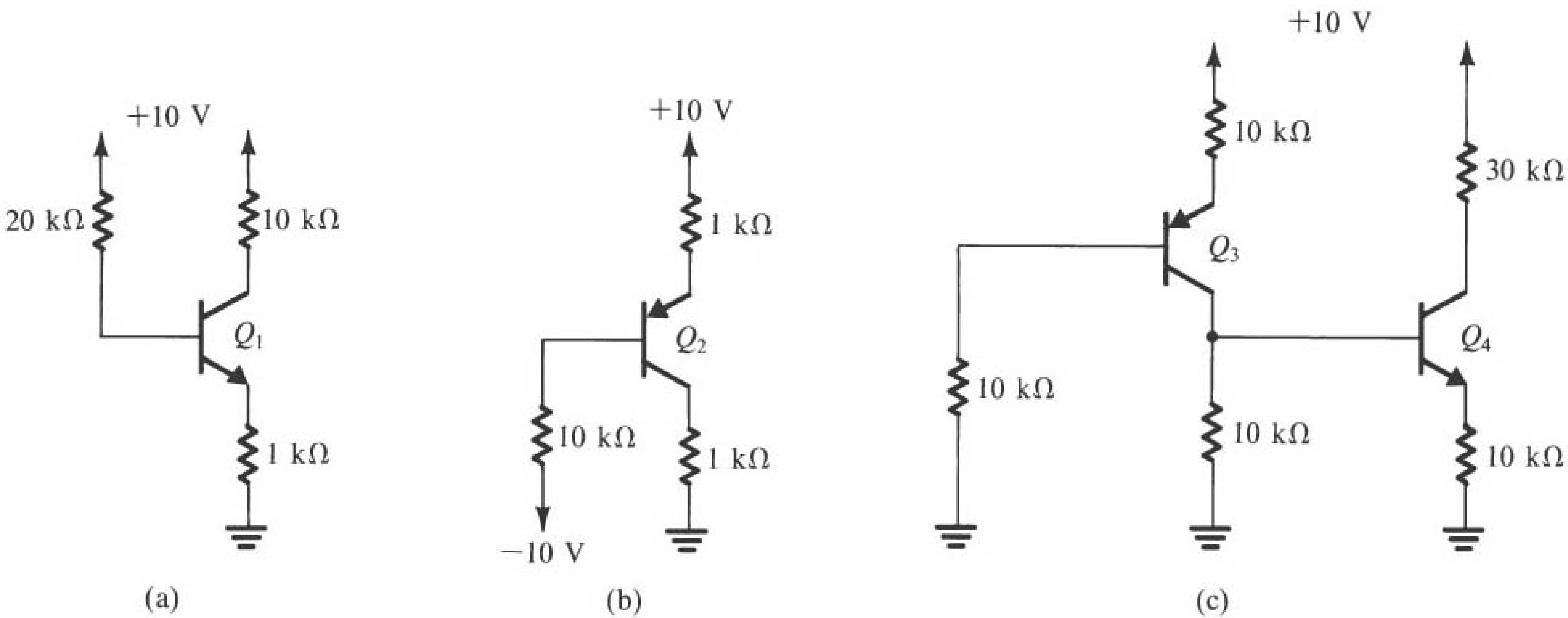
+10 V
20 kΩ
10 kΩ
Q_1
1 kΩ
(a)
+10 V
1 kΩ
Q_2
10 kΩ
1 kΩ
−10 V
(b)
+10 V
10 kΩ
30 kΩ
Q_3
10 kΩ
Q_4
10 kΩ
10 kΩ
(c)

Figure P5.87

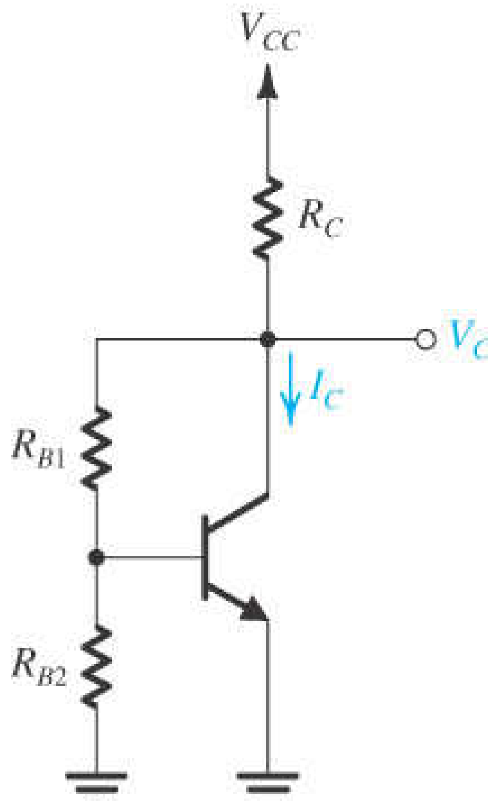

Figure P5.96

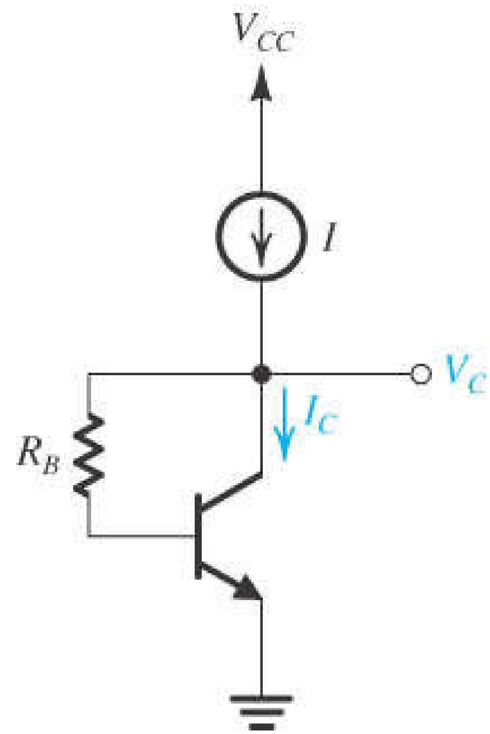

Figure P5.97

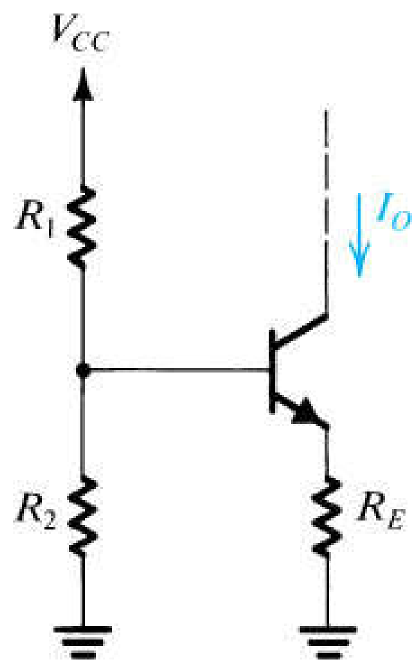

Figure P5.98

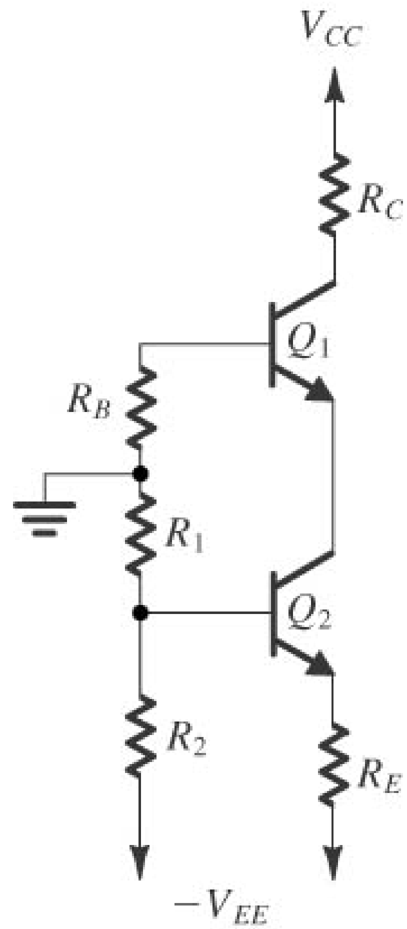

Figure P5.99

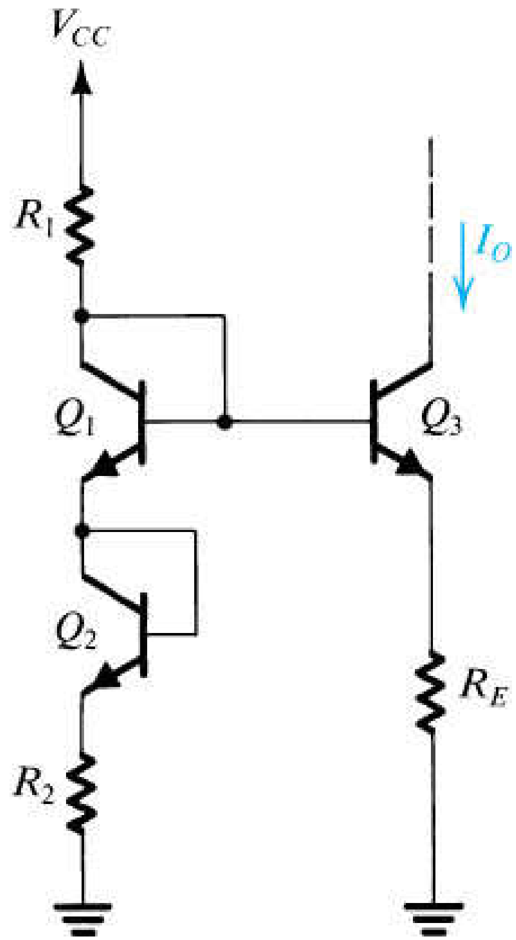

Figure P5.100

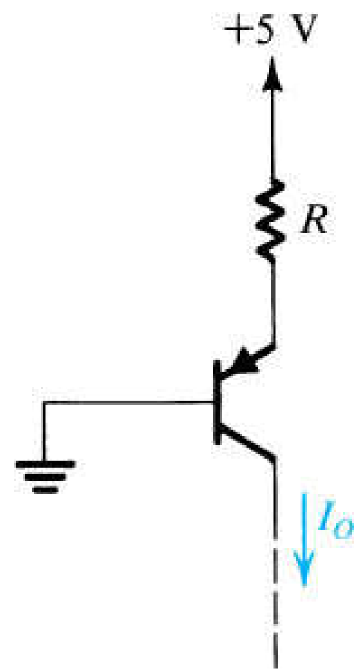

Figure P5.101

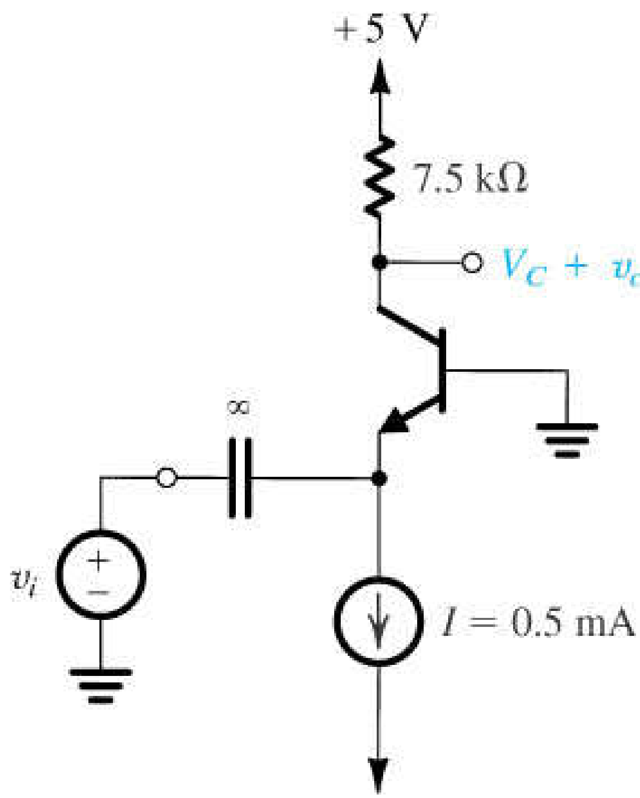

Figure P5.112

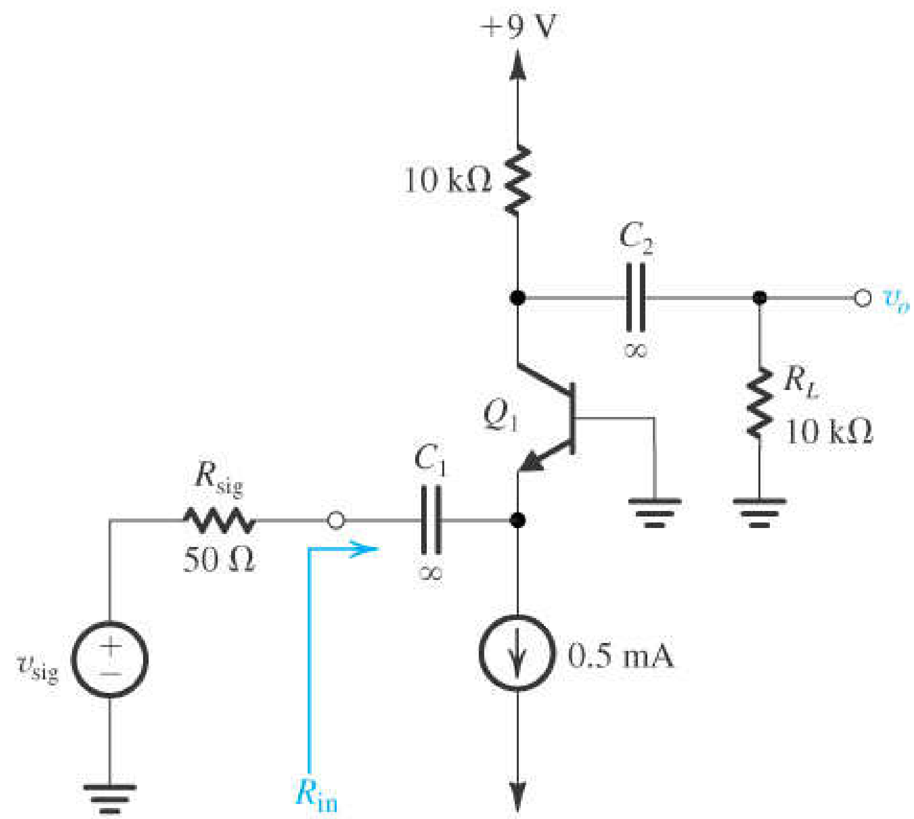

Figure P5.115

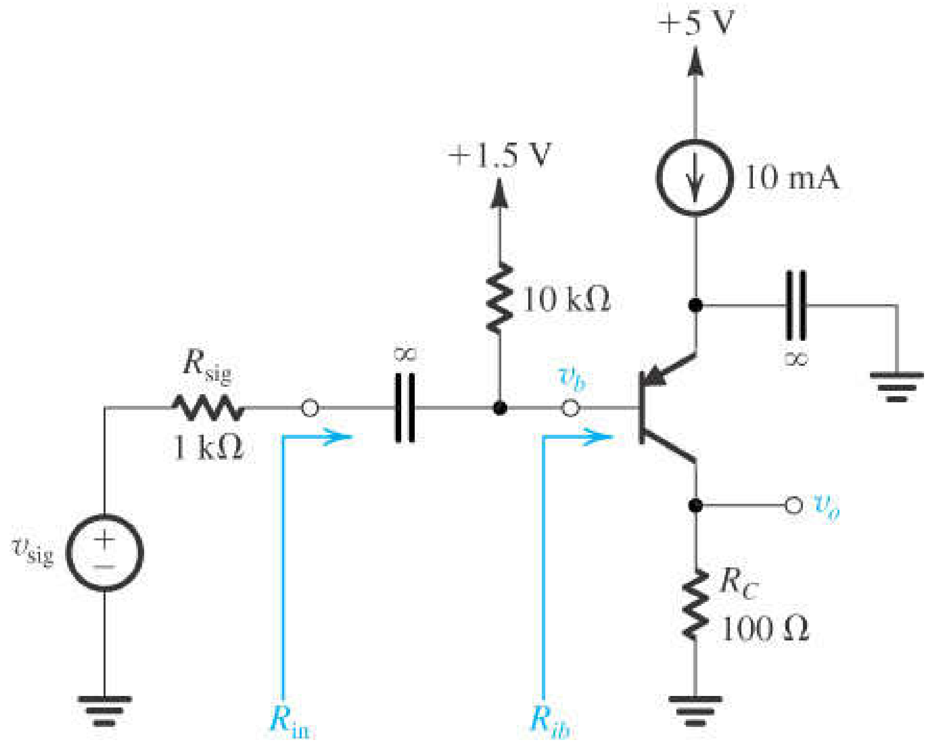

Figure P5.116

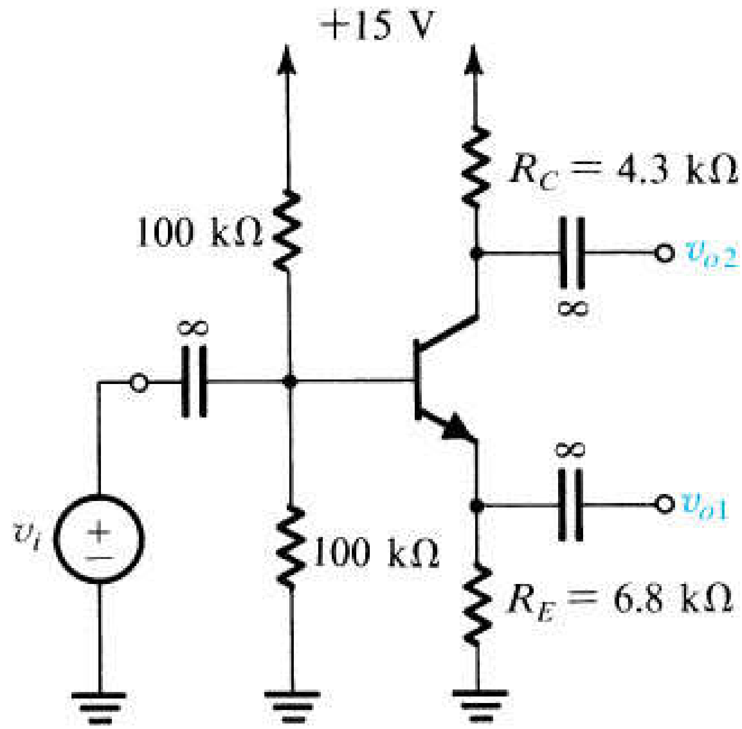

Figure P5.124

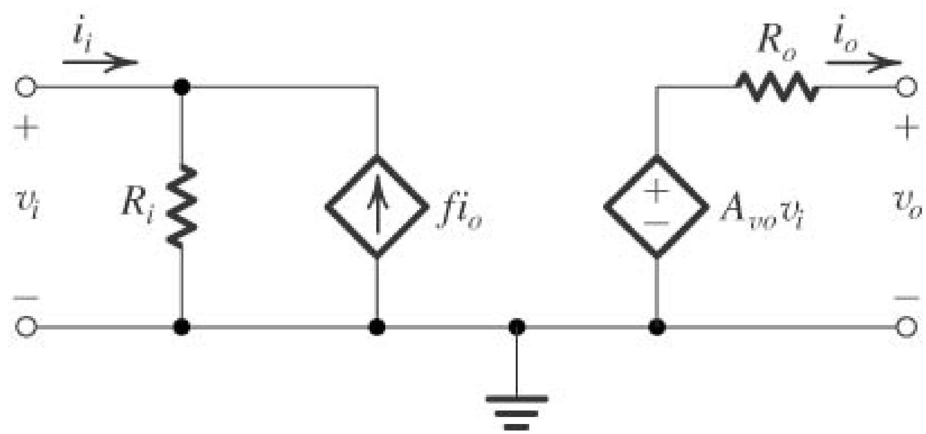

Figure P5.126

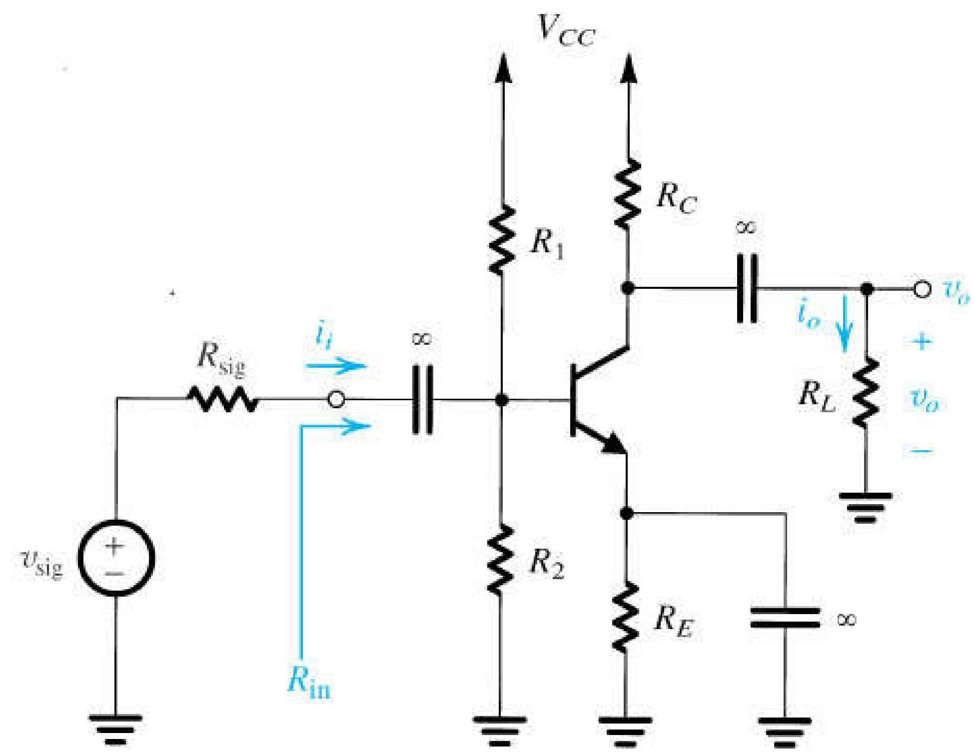

Figure P5.130

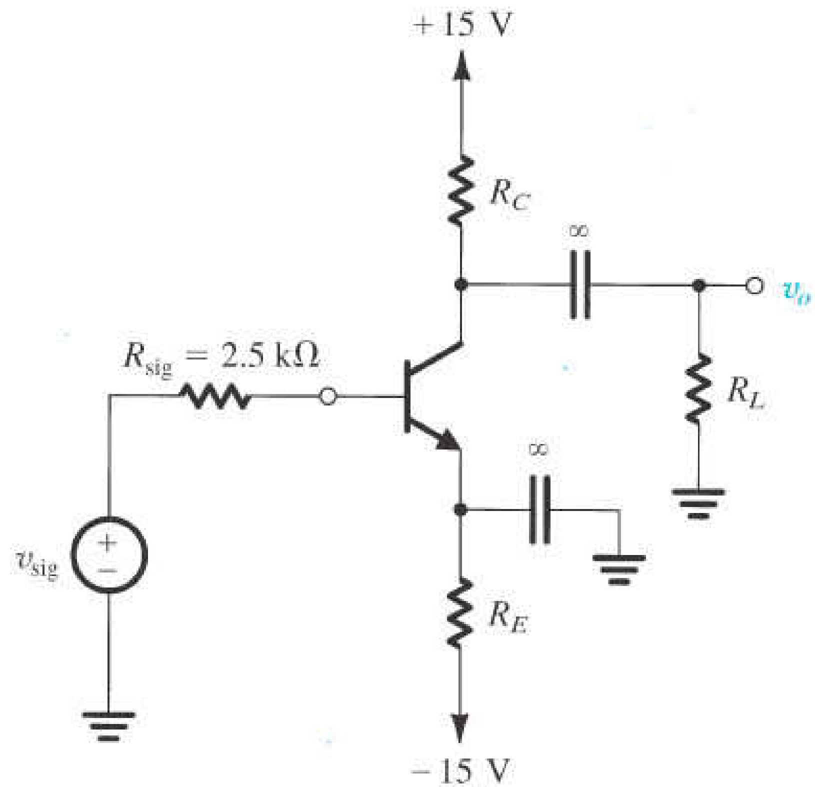

Figure P5.134

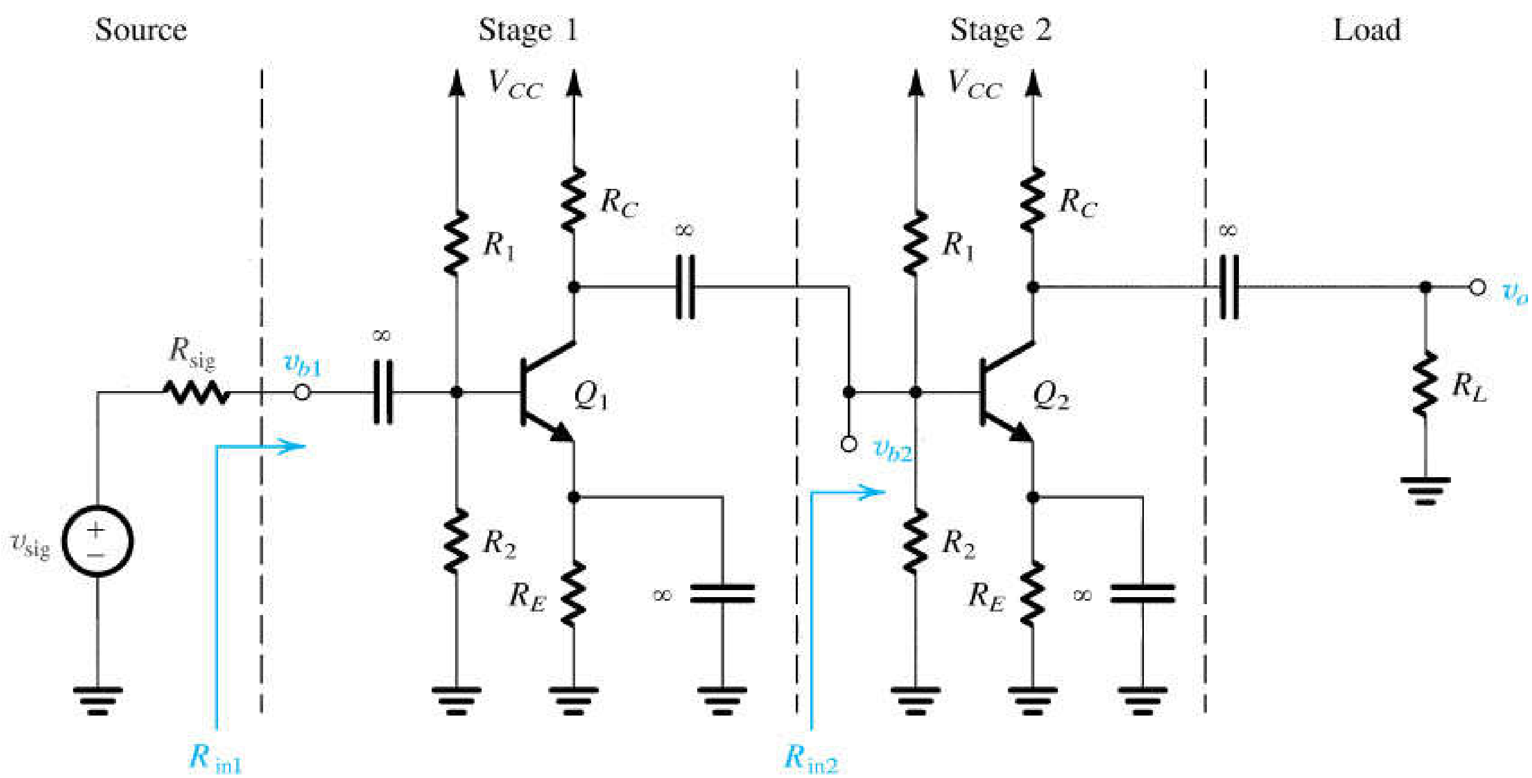

Figure P5.135

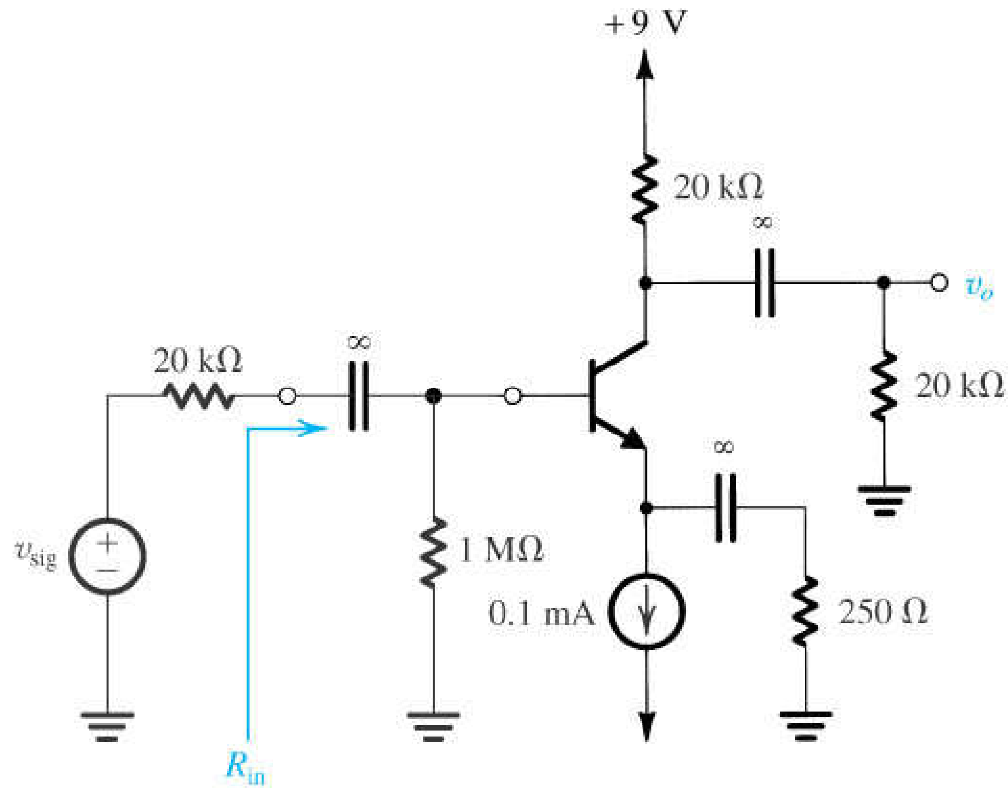

Figure P5.136

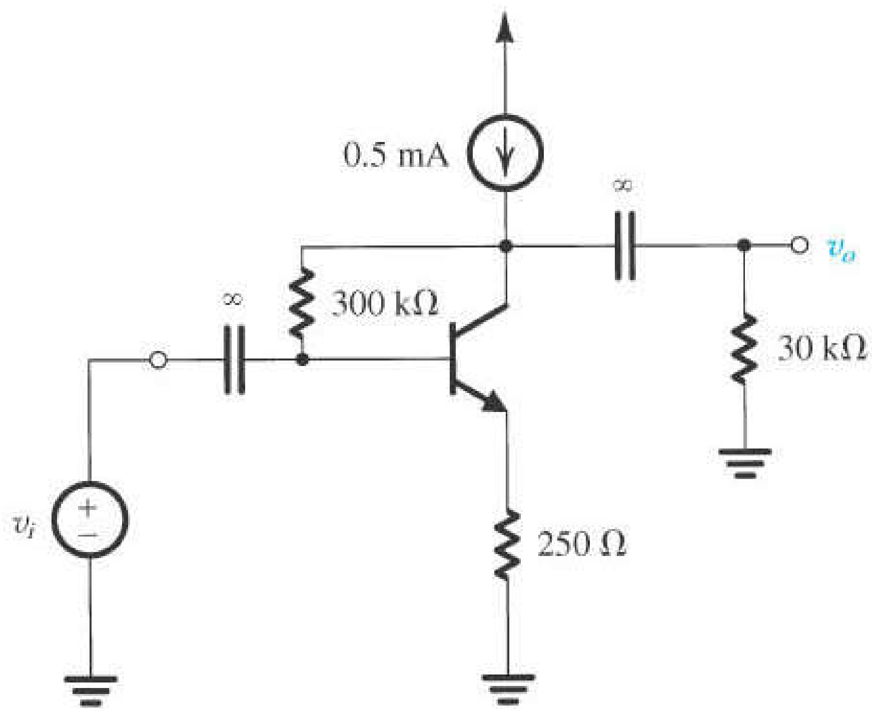

Figure P5.137

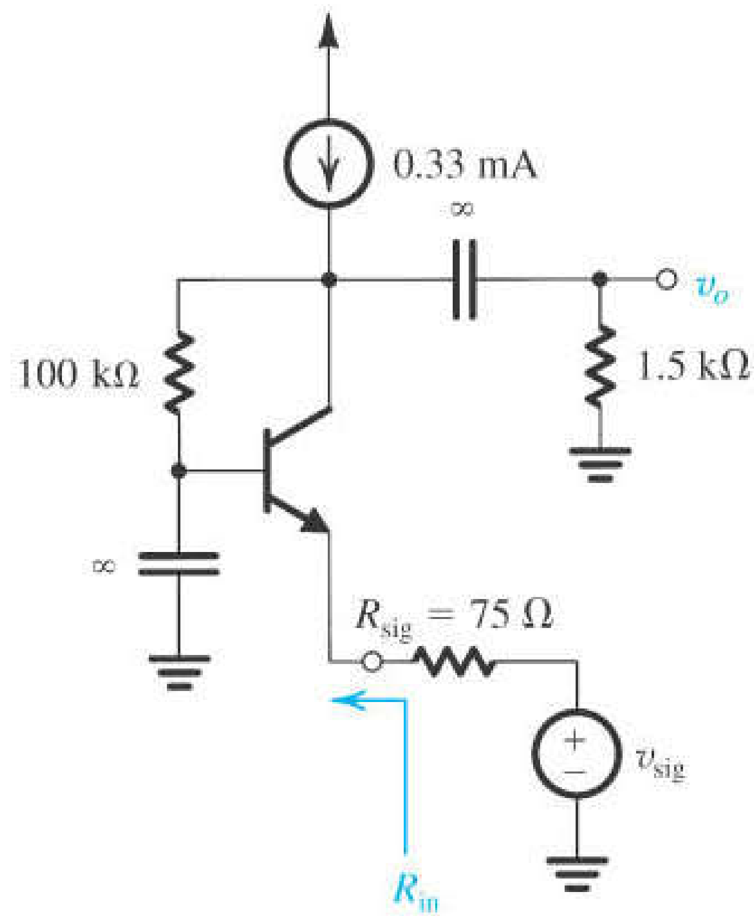

Figure P5.141

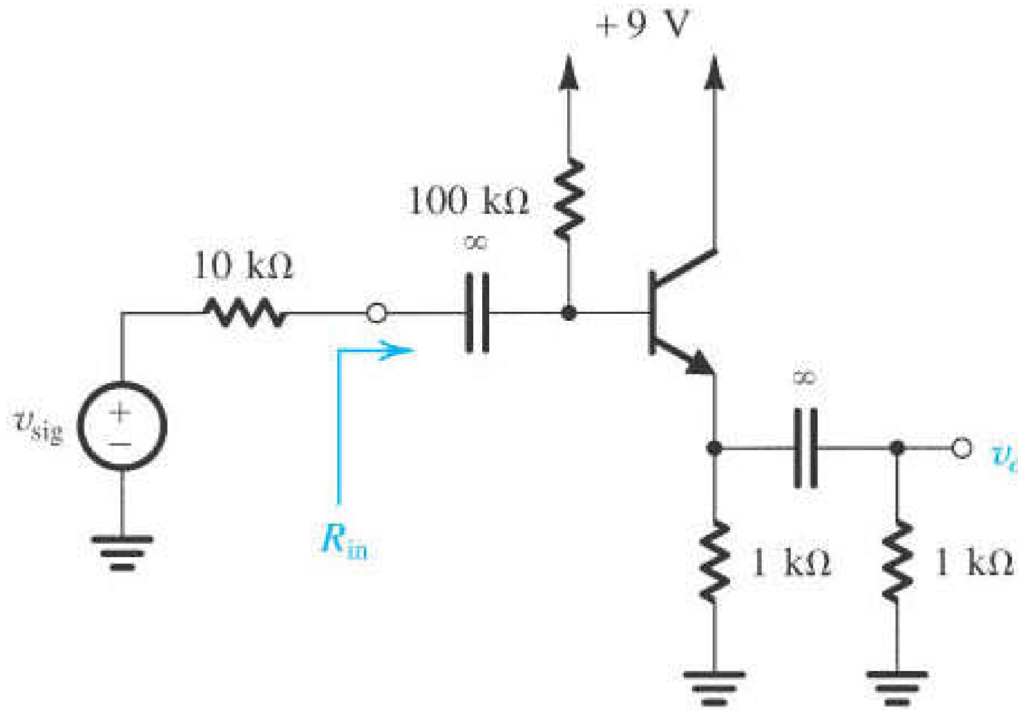

Figure P5.143

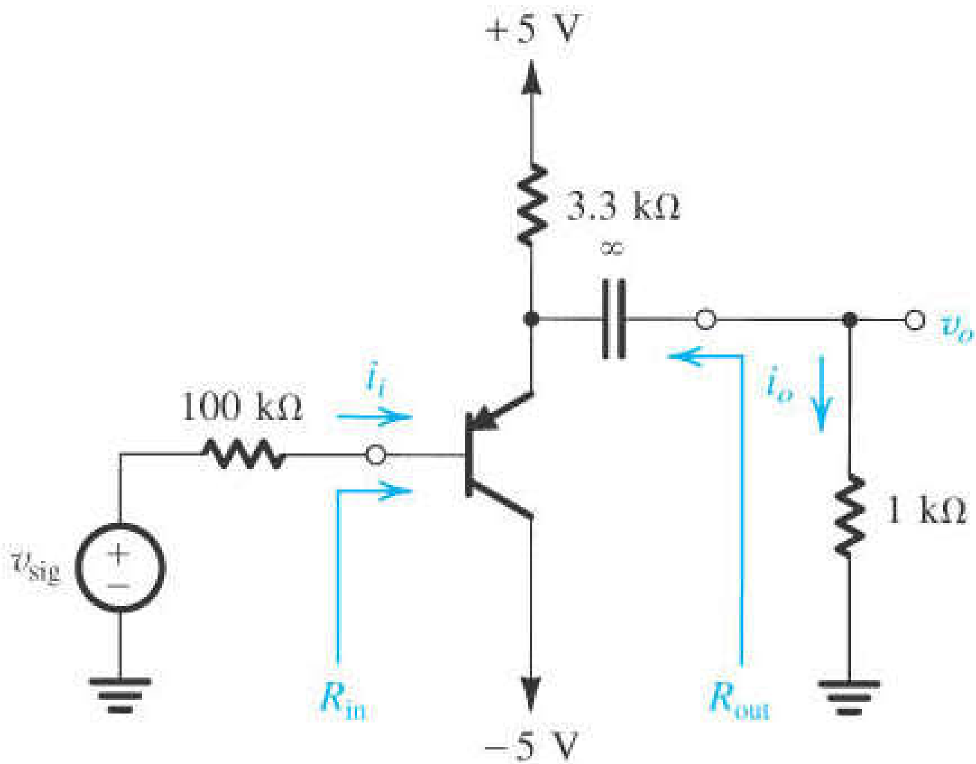

Figure P5.144

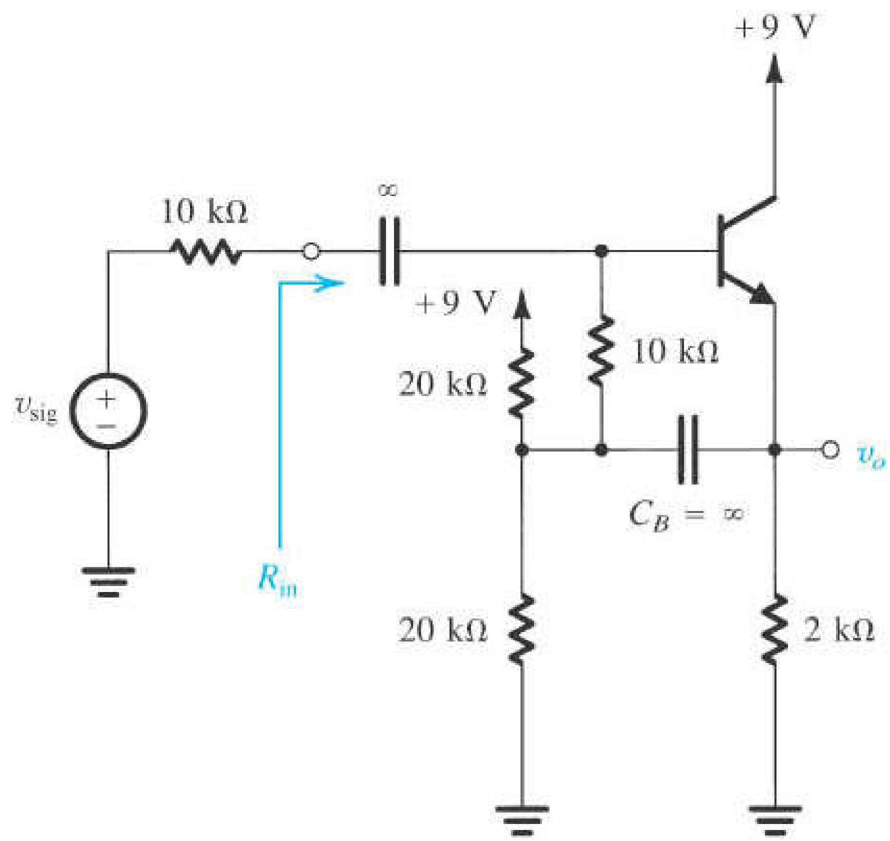

Figure P5.147

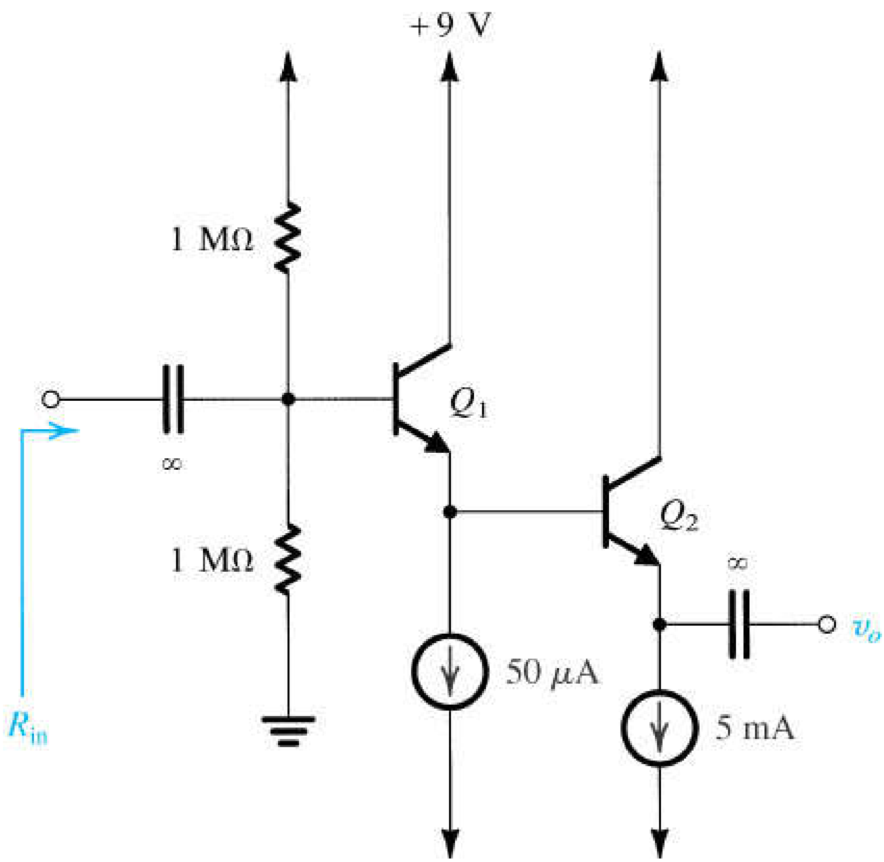

Figure P5.148

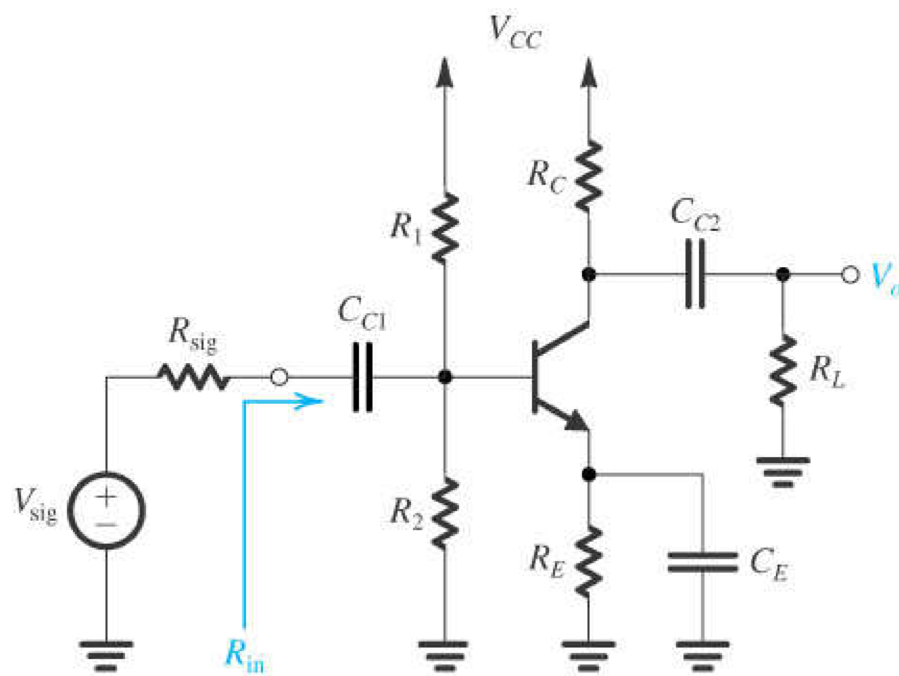

Figure P5.159

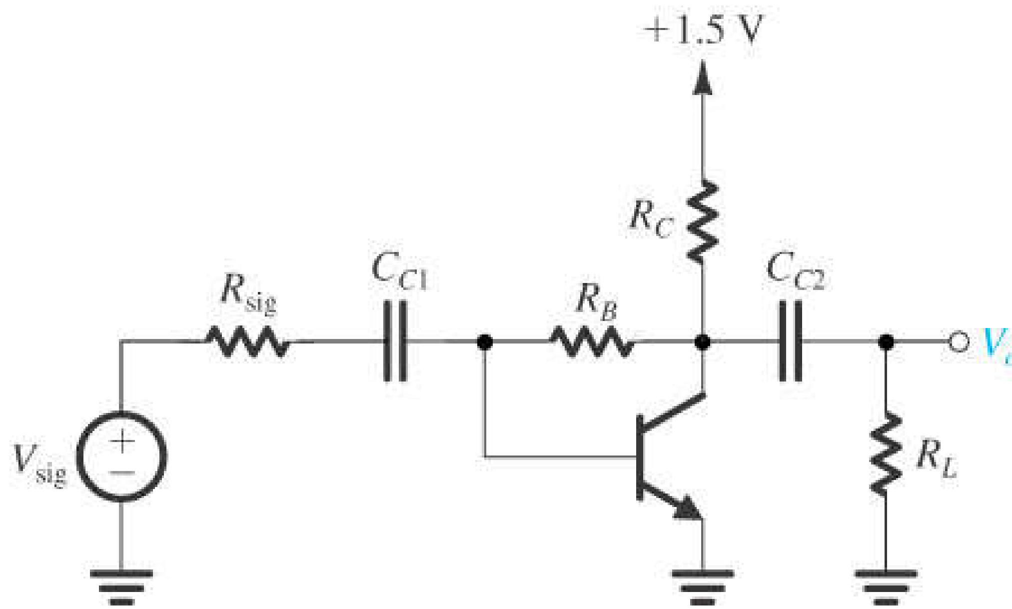

Figure P5.161

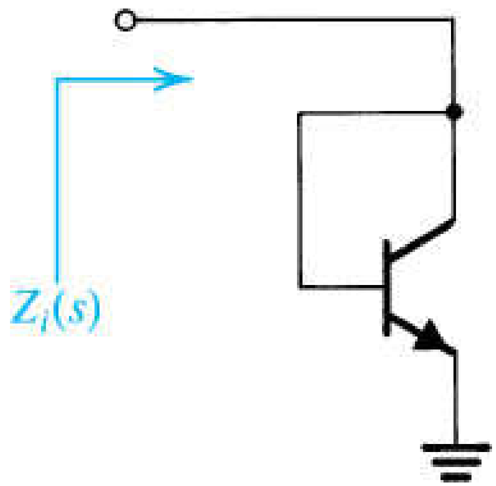

Figure P5.162

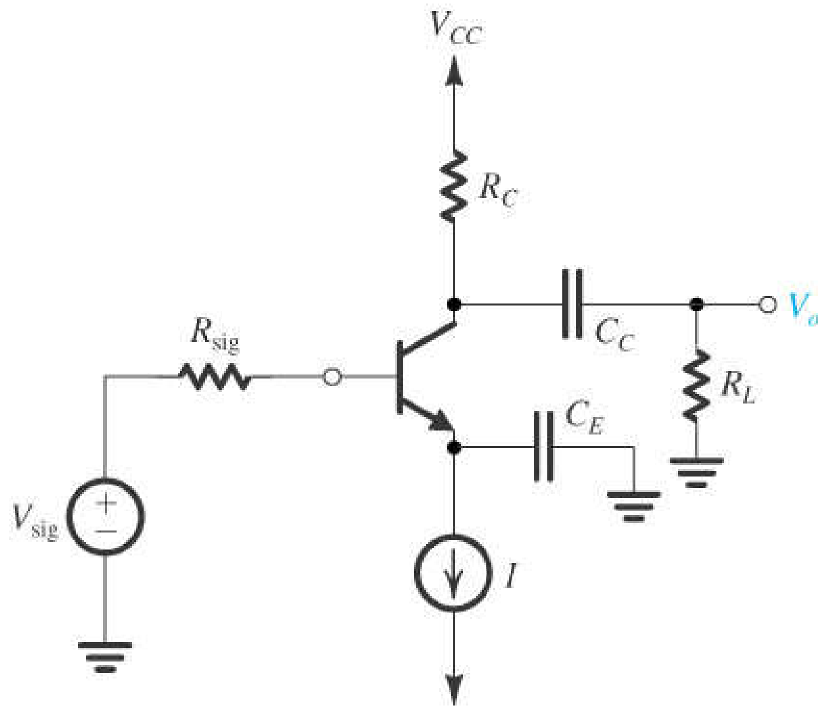

Figure P5.166

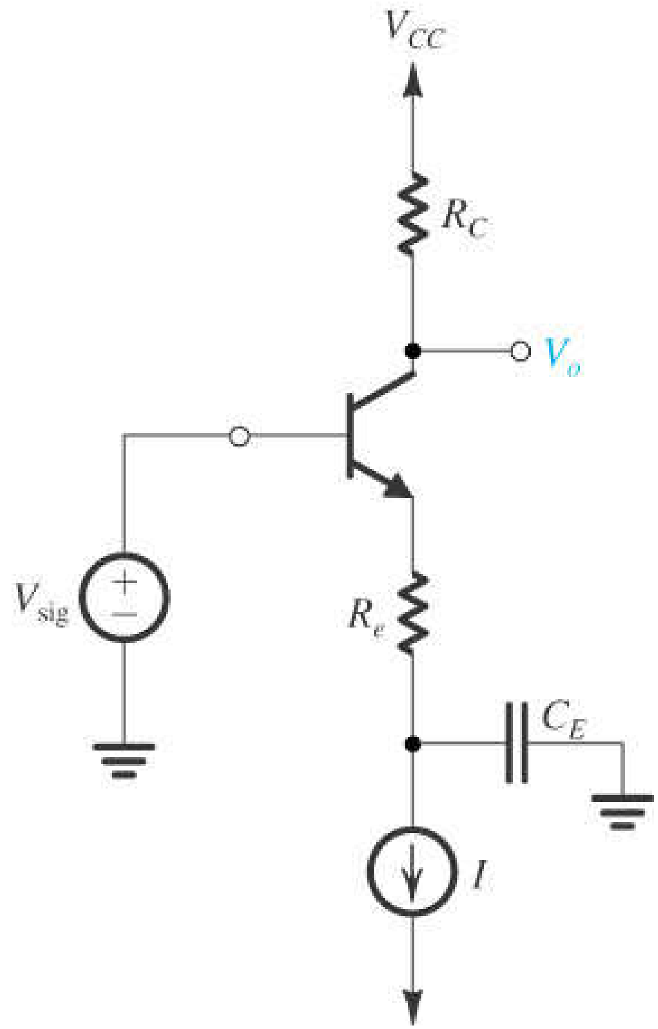

Figure P5.167

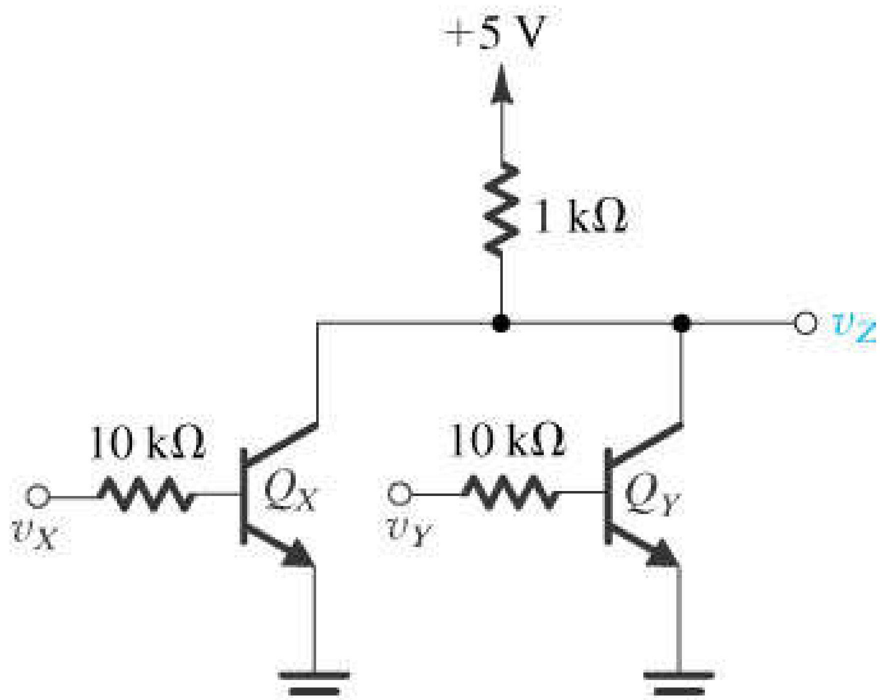

Figure P5.171

